STATUS OF THESIS

Title of thesis | **Evaluation and Modeling of Fouling Characteristics of Petroleum Crude Oils and Crude Blends**

I, **MOHAMMAD SYAMZARI BIN RAFEEN**
(CAPITAL LETTERS)

hereby allow my thesis to be placed at the Information Resource Centre (IRC) of Universiti Teknologi PETRONAS (UTP) with the following conditions:

1. The thesis becomes the property of UTP,
2. The IRC of UTP may make copies of the thesis for academic purposes only,
3. The thesis is classified as

☐ Confidential

☐ Non-confidential

If the thesis is confidential, please state the reason:
_____
_____
_____

The contents of the thesis will remain confidential for _____ years.

Remarks on disclosure:
_____
_____
_____

Endorsed by

_____
Signature of Author

Permanent address:_____
_____
_____
_____

Date:_____

_____
Signature of Supervisor

Name of Supervisor
_____

Date:_____

UNIVERSITI TEKNOLOGI PETRONAS

EVALUATION AND MODELING OF FOULING CHARACTERISTICS OF

PETROLEUM CRUDE OILS AND CRUDE BLENDS

by

MOHAMMAD SYAMZARI BIN RAFEEN

The undersigned certify that they have read, and recommend to the Postgraduate Studies Programme for acceptance this thesis for the fulfilment of the requirements for the degree stated.

Signature: _____

Main Supervisor: _____

Signature: _____

Head of Department: _____

Date: _____

EVALUATION AND MODELING OF FOULING CHARACTERISTICS OF PETROLEUM CRUDE OILS AND CRUDE BLENDS

by

MOHAMMAD SYAMZARI BIN RAFEEN

A Thesis
Submitted to the Postgraduate Studies Programme
as a Requirement for the Degree of

MASTER OF SCIENCE

CHEMICAL ENGINEERING

UNIVERSITI TEKNOLOGI PETRONAS

BANDAR SERI ISKANDAR,

PERAK

FEBRUARY 2011

DECLARATION OF THESIS

Title of thesis **Evaluation and Modeling of Fouling Characteristics of Petroleum Crude Oils and Crude Blends**

I, **MOHAMMAD SYAMZARI BIN RAFEEN**_____
(CAPITAL LETTERS)

hereby declare that the thesis is based on my original work except for quotations and citations which have been duly acknowledged. I also declare that it has not been previously or concurrently submitted for any other degree at Universiti Teknologi PETRONAS or other institutions.

Witnessed by

_____ _____
Signature of Author Signature of Supervisor

Permanent address:_____ Name of Supervisor
_____ _____
_____
_____

Date:_____ Date:_____

ACKNOWLEDGEMENT

In the name of Allah, The Most Gracious, The Most Merciful. Praised be to Allah, Lord of the World and Universe. May His Blessings be upon Prophet Muhammad s.a.w., his family and his companions.

First and foremost, I am deeply grateful to Allah the Almighty for blessing me with health, patience and endurance throughout the wonderful and colourful journey in accomplishing my research work. This work would not be possible without Allah permission.

I would like to express my deep and sincere gratitude to all the individuals who have made this thesis possible.

My deepest appreciation goes to the management of PETRONAS Research Sdn Bhd (PRSB) for giving me such a big opportunity to pursue with my research work. This work would not be possible without the full support of Dr Shahidah M Shariff, General Manager of Novel Process and Advanced Engineering who has encouraged me to enroll and persistence in supporting me throughout my research work in UTP. My special thanks also to Pn Rohani A Rahman, Program Head for Fouling project, who was always being positive and supportive in ensuring the research work progressing smoothly and successfully.

I am heartily thankful to my supervisor, Associate Professor Dr Marappagounder Ramasamy who is very dedicated and helpful throughout my research work. His wisdom and excellent guidance has been of great value for me in maneuvering my research work direction to the right and successful path. His extensive discussion and excellent comments has transformed this thesis into a better shape and it is greatly appreciated and acknowledged.

I owe my loving thanks to my wife, Atie and my son, Iman for their love, understanding and support. Thanks a lot for enduring the moment of me being a

weekend husband and father. To Atie, special thanks for being an excellent mother to Iman and stout-hearted during the difficult moments of raising Iman when I was away.

I am also indebted to the Fouling project team members; Dr Chandra, Zamidi, Pak Totok, Umesh, Mohanad, Husna, Yatie, Marziah, the two Ros and others. To Dr Chandra, thanks for the constructive comments and suggestions given to improve the quality of my research work. To Zamidi, thanks a lot for being such a good officemate and housemate. My life in UTP will be much dull without your presence. To Umesh, thanks for being a nice friend and for the fruitful discussion that we always had regarding crude oil fouling. To Pak Totok, thanks for being a wonderful friend and your kindness in teaching me advanced programming in Excel which is very much appreciated. To Mohanad, Husna, Yatie, Marziah, the two Ros and others, thanks a lot for the friendship and assistance.

I would like to show my gratitude to the Chemical Engineering Department and Postgraduate Office of UTP for providing me all the necessary support and guidance. Special thanks go to Dr Lau, Pn Suhana and Pn Kamaliah for being supportive and helpful.

Finally, my thanks are for my colleague and housemate, Idzham for his friendship and assistance during my stay in UTP. My life in UTP would have been much dreary without him as a good friend.

To all the above mentioned individuals and to those that I could not list by the names here, all of you have played an important role toward the completion of my research work. Your kind support and assistance is very much appreciated.

May Allah in His Infinite Mercy makes us among those who give thanks to Him for all His Bounty and Provisions.

ABSTRACT

Fouling of preheat exchangers in refinery crude distillation unit is a complex phenomena and identified to be the major energy consuming source in petroleum refineries. The cost of fouling could be substantial where it comprises the economics and environmental aspect. In this research work, four Malaysian crude oils and a condensate were selected for fouling experiments using Hot Liquid Process Simulator (HLPS). The experiments were conducted to determine the effect of surface temperature and crude blending on the fouling characteristics of the selected crudes and crude blends. A method published in the literature is used to analyze the raw data into a meaningful fouling resistance data. Initial fouling rates are then determined by taking the slope for the linear portion of the fouling resistance versus time curve. Arrhenius plot was used to obtain the true activation energy, *E* so that the fouling propensity could be determined. Crude ranking in term of fouling propensity for the neat crude is in the order of Crude C > Crude D > Crude B > Crude A and for the crude blend, it is in the order of A-C blend > A-D blend > A-B blend. The effect of adding Condensate E to Crude C has resulted in the lowest activation energy in comparison with the other crudes and crude blends.

Four threshold fouling models were validated with the experimental data established. The models evaluated are Ebert and Panchal model, Panchal *et al.* model, Polley *et al.* model and Nasr and Givi model. Furthermore, three estimation methods were used for each model which are (i) estimation method 1 - physical properties estimated at inlet bulk temperature, (ii) estimation method 2 - physical properties estimated at film temperature or surface temperature (for Polley *et al.* model only) and (iii) estimation method 3 – physical properties estimated at film temperature or surface temperature (for Polley *et al.* model only) plus the exclusion of removal term. Model parameters were estimated using least square technique to minimize the error between the predicted and experimental data.

There are three model parameters that need to be determined which are α, γ and E where E values are fixed to the values obtained using Arrhenius plot whilst the other two parameters, α and γ are determined using least square technique by maximizing the coefficient of determination, R^2. Practical operating condition range for model prediction applicability was also defined where the upper range limit is demarcated by the boiling point for the crudes or crude blends and the lower range limit is demarcated by the operational inlet bulk temperature of HLPS.

Model prediction using estimation method 1 was found to give better prediction in comparison with the prediction using estimation methods 2 and 3 for all crudes, crude blends and condensate – crude blend. This is based on (i) better R^2 values obtained during the model parameter estimation, (ii) fouling rates approaching zero at lower temperature without going to negative value and (iii) reasonably good and consistent prediction trend over the defined practical operating condition range. All threshold models prediction using estimation method 1 gave a reasonably good prediction where R^2 is more than 0.9 for all models. This suggests that physical properties for threshold models need to be estimated at inlet bulk temperature and the removal term for the models is required even though the crude velocity and the fluid shearing effect is low for experiment in HLPS.

ABSTRAK

Penempelan bendasing di permukaan penukar haba di dalam unit penyulingan bagi kilang penapisan minyak adalah satu fenomena yang begitu kompleks dan ianya dianggap sebagai penyumbang utama kepada penggunaan tenaga di dalam kilang penapisan minyak. Kesan daripada penempelan penempelan bendasing boleh menjadi begitu besar di mana ia merangkumi aspek ekonomi dan alam sekitar. Bagi penyelidikan ini, empat jenis minyak mentah dan kondensat dari Malaysia telah dipilih untuk menjalani eksperimen menggunakan *Hot Liquid Process Simulator* (HLPS). Eksperimen-eksperimen dijalankan untuk menentukan impak suhu permukaan dan campuran minyak ke atas karakteristik penempelan bendasing bagi minyak mentah dan campuran minyak yang telah dipilih. Satu kaedah yang telah diterbitkan sebagai bahan rujukan telah digunakan untuk menganalisa data awal menjadi data yang lebih bermakna iaitu rintangan terhadap penempelan (*fouling resistance*). Selepas itu, kadar awal penempelan ditentukan berdasarkan data *fouling resistance* untuk setiap eksperimen dengan mengambil kira kecerunan bagi bahagian yang linear untuk graf *fouling resistance* melawan masa. Plot Arrhenius telah digunakan untuk mendapatkan tenaga pengaktifan benar, *E* untuk setiap minyak mentah dan campuran minyak supaya kecendurungan penempelan dapat ditentukan. Kedudukan berdasarkan kecenderungan penempelan untuk minyak mentah adalah seperti berikut; Minyak mentah C > Minyak mentah D > Minyak mentah B > Minyak mentah A, dan untuk campuran minyak pula; Campuran A-C > Campuran A-D > Campuran A-B. Kesan penambahan Kondensat E kepada Minyak mentah C telah mengakibatkan tenaga pengaktifan yang terendah diperoleh berbanding minyak mentah dan campuran minyak yang lain.

Empat model penempelan '*threshold*' telah digunakan untuk divalidasi dengan data eksperimen dari HLPS. Model-model yang telah digunakan adalah model Ebert dan Panchal, model Panchal *et al.,* model Polley *et al.* dan model Nasr dan Givi.

Tambahan lagi, tiga kaedah perkiraan telah digunakan untuk setiap model iaitu (i) kaedah perkiraan 1 - sifat fizikal dianggar pada suhu masuk umum, (ii) kaedah perkiraan 2 – sifat fizikal dianggar pada suhu filem atau suhu permukaan (bagi model Polley *et al.* sahaja) dan (iii) kaedah perkiraan 3 – sifat fizikal dianggar pada suhu filem atau suhu permukaan (bagi Polley et *al.* model sahaja) ditambah dengan pengecualian istilah penyingkiran. Parameter bagi model dianggar menggunakan teknik kuasa dua terendah bagi meminimumkan jurang antara ramalan dan data eksperimen. Terdapat tiga parameter bagi model yang perlu ditentukan iaitu α, γ dan E dimana E ditetapkan kepada nilai yang diperolehi menggunakan plot Arrhenius manakala α dan γ ditentukan menggunakan teknik kuasa dua terendah dengan memaksimumkan angkali penentuan, R^2. Julat keadaan operasi yang praktikal bagi pengaplikasian ramalan yang dibuat oleh model didefinasikan dengan batas atas julat yang disempadani oleh takat didih bagi minyak mentah dan campuran minyak yang diujikaji dan batas bawah julat yang disempadani oleh suhu masuk umum bagi HLPS.

Ramalan model menggunakan kaedah perkiraan 1 dilihat memberi ramalan yang lebih baik berbanding ramalan menggunakan kaedah perkiraan 2 dan 3 bagi semua minyak mentah, campuran minyak dan campuran kondensat – minyak. Ini berdasarkan kepada (i) R^2 yang lebih baik diperolehi melalui kaedah anggaran parameter trend ramalan yang cukup baik diantara julat keadaan operasi yang praktikal dan (ii) kadar penempelan menjurus kepada angka sifar pada suhu yang rendah tanpa melangkaui angka negatif dan (iii) trend ramalan yang cukup baik dan konsisten diantara julat keadaan operasi yang praktikal. Kesemua model ramalan '*threshold*' menggunakan kaedah perkiraan 1 memberikan ramalan yang cukup baik dimana nilai R^2 melebihi 0.9 bagi semua model. Ini menunjukkan bahawa sifat fizikal bagi model 'threshold' hendaklah dianggar pada suhu masuk umum dan istilah penyingkiran bagi model sangat diperlukan walaupun halaju minyak dan kesan ricih bendalir adalah kecil bagi eksperimen menggunakan HLPS.

TABLE OF CONTENT

LIST OF TABLES

LIST OF FIGURES AND ILLUSTRATIONS

LIST OF PLATES

NOMENCLATURE

Symbol	Description	Units
	Symbols	
A	Pre-exponential factor	s^{-1}
A, B, C	Groups of parameters in Eq. (2.40)	
A_1, A_2	Constants in Eq. (2.16)	
$B_1 - B_5$	Constants in Eq. (2.31)	
C'	Foulant concentration in Eq. (2.13)	kg/m^3
C_b	Concentration of precursor in bulk fluid in Eq. (2.16)	kg/m^3
c_b	Bulk concentration of precursor in Eq. (2.15)	kg/m^3
c_b	Concentration at bulk in Eq. (2.36)	kg/m^3
C_{Di}	Deposit concentration at the interface in Eq. (2.23)	kg/m^3
C_p	Mean specific heat capacity	kJ/kgK
C_{rb}	Concentration of precursor in the bulk in Eq. (2.21) and (2.23)	kg/m^3
C_{ri}	Concentration of precursor at the interface in Eq. (2.21)	kg/m^3
c_s	Concentration at surface in Eq. (2.36)	kg/m^3
C_w	Concentration of precursor at solid wall in Eq. (2.16)	kg/m^3
D	Diffusion coefficient for precursor in Eq. (2.15)	m^2/s
D	Diffusivity in Eq. (2.25)	m^2/s
D	Tube diameter in Eq. (2.18) and (2.31)	m

Symbol	Description	Units
d	Tube diameter in Eq. (2.15)	m
D_1, D_2, D_3	Constants in Eq. (2.31)	
E	Activation energy	kJ/mol
E_c	Activation energy corresponding to coke in Eq. (2.31)	kJ/mol
E_t	Activation energy corresponding to tar in Eq. (2.31)	kJ/mol
f	Friction factor in Eq. (2.16)	(-)
G	Mass flowrate	kg/hr
I_N	Insolubility number	(-)
k	Reaction rate constant in Eq. (2.17)	s^{-1}
k	Velocity constant in Eq. (2.22)	s^{-1}
k_c	Mass transfer coefficient of reactant in Eq. (2.17)	m/s
K_D	Mass transfer coefficient of deposit in Eq. (2.21)	m/s
k_f	Thermal conductivity of foulant in Eq. (2.16) and (2.35)	W/mK
K_r	Mass transfer coefficient of precursor in Eq. (2.21)	m/s
K_1, K_2	Constants in Eq. (2.13)	
k', k''	Constants in Eq. (2.36)	
K^*	Constant, a function of feedstock in Eq. (2.18)	
M	Mass flowrate in Eq. (2.13)	kg/hr
m	Stoichiometric factor (mass of fouling deposit per mass of precursor transported to and reacted at the wall) in Eq. (2.35)	(-)
m	Mass flowrate in Eq. (3.2)	kg/hr
n	Reaction order	(-)
N_r	Mass flux of foulant precursor / reactant to the reaction zone in Eq. (2.19)	kg/m^2s
N_D	Mass flux of foulant away from the zone or	kg/m^2s

Symbol	Description	Units
	foulant mass flux back to the bulk fluid in Eq. (2.19)	
Pr	Prandtl number	(-)
P	Total pressure in Eq. (2.17)	Pa
q	Heat flux	W/m^2
R	Universal gas constant	kJ/molK
Re	Reynolds number	(-)
R_f	Fouling resistance	m^2K/W
r_i	Initial fouling rate in Eq. (2.34)	s^{-1}
R_{ft}	Thermal fouling resistance at time t in Eq. (2.12)	m^2K/W
$R_{f\infty}$	Thermal fouling resistance at infinite time – asymptotic value in Eq. (2.12)	m^2K/W
R^2	Coefficient of determination	(-)
S_{BN}	Solubility blending number	(-)
Sc	Schmidt number	(-)
Sc_r	Schmidt number of precursors in Eq. (2.25)	(-)
Sc_D	Schmidt number of deposit in Eq. (2.25)	(-)
Sh	Sherwood number	(-)
St	Stanton number	(-)
T_b	Bulk temperature	^oC
T_c	Heater rod temperature	^oC
T_c	Temperature at interface between tar-like and coke layers in Eq. (2.31)	^oC
T_f	Film temperature	^oC
T_s	Surface temperature	^oC
T_{so}	Initial surface temperature	^oC
T_t	Temperature at interface between tar-like deposit and fluid in Eq. (2.31)	^oC
T_o	Wall temperature in Eq. (2.34)	^oC
T_1	Inlet bulk temperature	^oC
T_2	Outlet bulk temperature	^oC

Symbol	Description	Units
u	Fluid velocity in Eq. (2.34)	m/s
u	Tubeside mean velocity in Eq. (2.40)	m/s
U_t	Overall heat transfer coefficients at time t in Eq. (3.4)	W/m^2K
U_0	Overall heat transfer coefficients at time zero in Eq. (3.4)	W/m^2K
v	Bulk fluid velocity in Eq. (2.16)	m/s
x	Deposit thickness in Eq. (2.25) and (2.31)	m
x_f	Foulant thickness in Eq. (2.16) and (2.23)	m
x_{ft}	Foulant thickness at time t in Eq. (2.13)	m
y	Mole fraction of coke precursor in bulk fluid in Eq. (2.17)	(-)
z	Axial location along the heater rod in Eq. (2.31)	m

Greek symbols

α	Deposition constant	m^2K/Whr
β	Constant dependent on system properties in Eq. (2.12)	
β	Constant for a given system in Eq. (2.34)	ms^{-2}
γ	Removal constant	$m^2K/WhrPa$
λ_1	A function of surface roughness in Eq. (2.25)	
λ_f	Thermal conductivity of deposit in Eq. (2.23)	W/mK
μ	Fluid viscosity	m^2/s
η	Dynamic viscosity	Pa.s
ρ	Fluid density	kg/m^3
ρ_f	Deposit density in Eq. (2.19) and (2.31)	kg/m^3
τ	Shear stress	Pa
τ_w	Wall shear stress	Pa
ϕ_{Td}	Rate of depositon of tar-like layer in Eq. (2.27)	

Symbol	Description	Units
ϕ_{Tr}	Rate of back convection of tar-like products to the bulk in Eq. (2.27)	
ϕ_{CT}	Net rate of conversion from tar-like product to coke product in Eq. (2.27)	
ϕ_{Fr}	Rate of deposit removal by shear forces in Eq. (2.27)	
ϕ	Deposition mass flux in Eq. (2.35)	kg/m^2s

Abbreviations

HLPS	Hot Liquid Process Simulator	(-)
TEMA	Tubular Exchanger Manufacturers Association	(-)
WAT	Wax appearing temperature	^oC

CHAPTER 1

INTRODUCTION

Continuous improvement on the current practices of the petroleum industry has always been in the mind of the industry players. The future visions for petroleum industry are outlined to be energy and operational efficient, environmental friendly and reliable and safe plant operation (API, 1999a, b). Petroleum refining is known to be one of the most energy-intensive manufacturing industries that lead to the demand of energy-efficient operation. Some practices has been introduced to the industry in order to improve the overall energy efficiency such as plant heat integration, recovery of waste heat and implementation of improved housekeeping and maintenance programs (API, 2000).

Plant heat integration or also known as process integration has become a very important tool to devise a network that uses as little external energy as possible and as few duty matches as possible. The main objective of process integration is to analyze the heat flows in a process and thus minimize the overall capital and operating cost of the plant (ESDU, 2000a). Crude preheat exchanger network in crude distillation unit is an example of process integration implementation in the petroleum refinery. Alas, heat exchanger operation will always result in the undesired fouling process. Current process integration approach always assumes that the fouling is a time-independent process whilst in reality the dynamic behavior of fouling hindered the proper application of process integration technique (Yeap *et al.*, 2004).

Fouling of heat exchanger is a process which results in the accumulation of dirt or the growth of deposits on the heated surfaces. This phenomenon is undesirable for heat exchanger operation since it reduces exchanger effectiveness and often leads to other operating difficulties such as high pressure drop or reduced flow rates. The presence of deposits results in extra thermal resistance and therefore reduces the

efficiency of a particular heat exchanger. The problem of heat exchanger fouling has become a challenge to designers, technologists and scientists, not only in terms of heat transfer technology but also in the wider aspects of economics and environmental impacts (Bott, 1992).

Attempts have been made to estimate the overall costs of fouling in terms of particular processes or in particular countries. Muller-Steinhagen (1995) estimated that the total cost of all heat exchanger fouling in the UK is of the order of USD 2.5 billion and the cost in the USA is USD 14 billion. In a very extensive study of refinery fouling costs published by van Nostrand *et al.* (1981), it is estimated that the cost of fouling is USD 10 million per annum for a refinery processing 100,000 barrels of crude oil per day.

Heat exchanger fouling has led to an increase in capital expenditure. This is due to the excess heat transfer area provided to allow for potential fouling. The cost will definitely escalate for a bigger size heat exchanger and additional cost will also be required for stronger foundation, provisions for extra space, increased transport and installation cost. In terms of fouling mitigation, extra cost should be allocated for anti-fouling equipment and installation of on-line cleaning devices (Muller-Steinhagen, 1995). Furthermore, if the fouling problem is so severe it might be necessary to install a standby heat exchanger with all associated pipe works, foundations and supports (Bott, 1995).

Energy costs and environmental issues are also some of the significant impacts caused by heat exchanger fouling. In the case of crude distillation unit, this corresponds to the additional fuel required for the furnace due to the failure of the pre-heat train to raise the crude temperature for the separation process. In principle, energy losses due to increased pressure drop may also be significant but the normal practices are to oversize the pump and control the flow using valves. Furthermore, the use of more fuel at the furnace leads to additional emission of CO_2 with the associated impact (Muller-Steinhagen, 1995).

Production losses during shutdowns due to fouling are often considered to be one of the significant costs. During a planned shutdown, the interruptions to production may be minimized but if it is an unscheduled shutdown the consequences will be

much more expensive. The unscheduled shutdown will happen if the severity of fouling problem is not recognized during the design stage resulting in fouling to happen faster than expected (Bott, 1995).

Maintenance cost is another significant impact caused by heat exchanger fouling. It includes manpower cost and the cost of chemicals or anti-fouling devices in removing fouling deposits. There is also an economic and ecological cost associated with disposal of cleaning chemicals after cleaning exercise (Muller-Steinhagen, 1995).

With respect to fouling consideration in heat exchanger design, the conventional method is to consider the potential fouling problem and assign fixed values of fouling resistance such as those specified by the Tubular Exchanger Manufacturers Association (TEMA). TEMA issues a table of fouling resistances for different types of applications. A fundamental flaw in the use of fixed values for fouling resistance is that they consider a static condition to the dynamic nature of fouling (Bott, 1995).

Most TEMA fouling resistances are for flow of water or hydrocarbons and majority of other fouling problems are not represented. The TEMA tables do not provide any information on the effect of operating parameters such as flow velocity, fluid temperature, heat flux and fluid composition on the deposition rate, even though these parameters often have dominant effects. Furthermore, the TEMA tables do not indicate after which operating time the given fouling resistances are reached. In fact, designing using these TEMA fouling resistance values will tend to oversize the heat exchangers significantly. For the liquid/liquid exchanger the selected fouling resistance requires a significant increase in the surface area in comparison with clean conditions and hence substantial amount of extra capital cost. The same fouling resistance for a gas/gas heat exchanger results in negligible additional capital cost (Bott, 1995).

The complex nature of crude oils, insufficient knowledge of fouling mechanism and the lack of validated predictive model make it difficult to reasonably predict the fouling rates and also develop an effective mitigation method for fouling (Asomaning *et al.*, 2000). It implies that reliable fouling data need to be obtained and the ability to accurately predict the fouling rates should be established. Fouling data

obtained from laboratory experiments is considered to be reliable since the fouling experiment is conducted under controlled condition. Semi-empirical modeling such as threshold fouling model looks a very promising concept in the absence of a thorough understanding of the fouling mechanism and the key fouling precursor that makes mechanistic modeling a better choice.

1.1. Problem Statement

Fouling of heat exchangers is considered to be an unsolved problem in the process industry where it results in an increase in the thermal resistance that will eventually reduces exchanger effectiveness. The impact of fouling is substantial in the way it significantly affect capital, operational, economics and environmental aspect. Fouling of heat transfer surfaces in contact with hydrocarbon streams is a complex physico-chemical process that hinders the development of effective mitigation methods. The fouling process is basically dynamic in nature but the design of heat transfer equipment is generally based on the time-independent resistances to heat transfer. This has triggered the need for accurate predictive model that could reasonably predict the fouling rates. Accurate model could be obtained through validation of the model prediction to reliable fouling data. Fouling experiment conducted under controlled conditions is one of the important criteria in producing reliable fouling data.

1.2. Objectives

The following are the specific objectives to address the above-stated hypothesis:

1. To experimentally study the effect of surface temperature, crude – crude blend and crude – condensate blend on the fouling characteristics of selected Malaysian crude oils; and

2. To compare different fouling threshold models reported in the literature for predicting fouling characteristics of selected crude and crude blends

1.3. Scope of Work

Four crude oils and a condensate originated from Malaysia will be used to study the fouling characteristics of the oils and its blends. Fouling experiments will be conducted in a fouling rig, namely Hot Liquid Process Simulator (HLPS) where each experiment is performed at constant surface temperature and crude velocity and fouling occurrence is indicated by the reduction in outlet bulk temperature over time. The effect of surface temperature variation and crude blending on the fouling characteristics will be investigated further in this study whilst the bulk temperature and crude velocity will be fixed to the operational value of HLPS. Four threshold models will be evaluated for their predictive capability using the experimental data obtained.

CHAPTER 2

LITERATURE REVIEW

2.1. Introduction

Studies on fouling mechanisms and the effect of design and operating conditions are required for planning suitable fouling mitigation strategies. There are several studies carried out by researchers related to fouling mechanisms (Bott, 1995; Bott, 1997; Melo and Bott, 1997; Panchal and Watkinson, 1993; Somerscales, 1997). In this chapter, a brief review of the available literature will be made. Fouling process will be discussed in detail in terms of its mechanisms and important factors that govern fouling in crude oil system. Attempts in predicting fouling will also be discussed especially for the fouling models related to crude oil system where it involves mechanistic and semi-empirical modeling.

2.2. Overview of fouling process

2.2.1. Fouling mechanisms

2.2.1.1. Chemical reaction fouling

Chemical reaction fouling is usually associated with organic chemicals rather than reactions of metals with aggressive agents (Bott, 1995). Furthermore, Epstein (1983a) defines chemical reaction fouling as the formation of deposit at the heat transfer surface through chemical reaction, in which surface itself is not a reactant. Panchal and Watkinson (1993) presented an idea that chemical reaction fouling generally involves the following multistep process:

Reactants (A) (soluble) → Precursors (B) (sparingly soluble) → Foulant (C) (insoluble)

Various possible steps in the process are shown in Fig. 2.1.

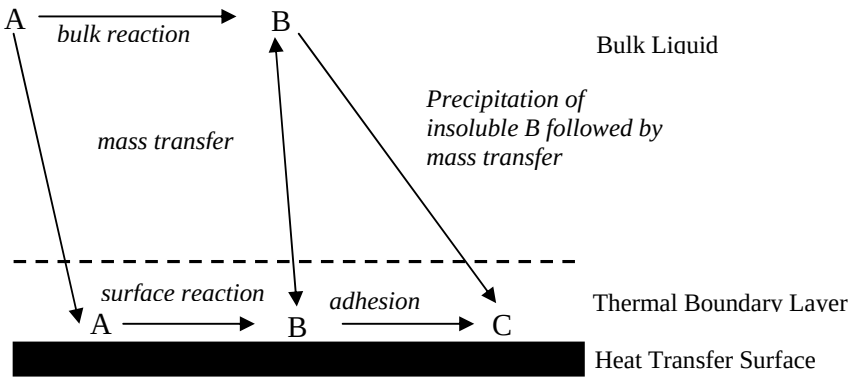

Fig. 2.1: Possible steps for fouling process (Panchal and Watkinson 1993)

In the simplest case, the fouling precursors enter the exchanger with the fluid, for instance, from a feed tank and then form the deposit by reaction on the wall. Alternatively, the reactants enter the exchanger and the precursors and foulants form in the exchanger, either in the bulk fluid, in the thermal boundary layer, or on the wall itself. Hence, not only reaction, but also transport of reactants, soluble precursors, or insoluble foulant may be important (Watkinson and Wilson, 1997). Chemical reaction fouling for organic fluids could be classified into three common classes of reactions which are autoxidation, polymerization and thermal decomposition (Watkinson, 1988).

Panchal and Watkinson (1993) envisaged a number of different reaction mechanisms that are possible for the fouling process, but dependent on where the reactions takes place with regard to the surface that is subject to fouling deposits. The reactions can take place in the bulk fluid, within the thermal boundary layer, or on the surface itself. They suggested three possible mechanisms:

Table 2.1: Possible mechanisms for fouling process

Case 1	Precursor generation in the bulk liquid
Case 1a	A→ B molecular transport to wall where B → C
Case 1b	B → C particle transport to wall
Case 2	Precursor generation in the boundary layer A → B molecular transport to wall A → B → C particle transport to the wall
Case 3	Precursor generation at the surface A → B → C occurs on the wall

In cases 2 and 3 it is possible for precursor B to "back diffuse" into the bulk.

2.2.1.2. Corrosion fouling

Corrosion fouling differs from chemical reaction fouling because the metal surface itself plays a part in the chemical reaction that results in corrosion products (Oufer, 1990). Corrosion involves two electrochemical reactions that occur simultaneously in which one of the reactions takes place at the so-called anode and the other at the cathode. At the anode, which is assumed to be made of a metal *M* of valence *z*, the electrochemical reaction is:

$$M \rightarrow M^{z^+} + ze^- \tag{2.1}$$

At the cathode, the electrochemical reaction involves the reduction of the oxygen to dissolve in water according to the following:

$$\frac{z}{4}O_2 + \frac{z}{2}H_2O + ze^- \rightarrow z\left(OH^-\right) \tag{2.2}$$

Both anode and the cathode are connected electrically through the water and by some external metallic conductor. Charge is transported by the electrons, e^- (current flow), through the external metallic conductor and also by the ionized species in the water. In addition to Eqs. (2.1) and (2.2), a secondary reaction can occur at the

cathodic parts of the surface when, as is the case here, the corroding medium is water. The reaction will be as follows:

$$M^{z^+} + z\left(OH^-\right) \rightarrow M\left(OH\right)_z \tag{2.3}$$

When Eqs. (2.1), (2.2) and (2.3) are combined; it results in the following overall reaction:

$$O_2 + 2H_2O + \frac{4}{z}M \rightarrow \frac{4}{z}M\left(OH\right)_z \tag{2.4}$$

The metal hydroxide loses its constituent water on removal from the water and drying resulting in the deposit that consists of metal oxides. These oxides and hydroxides form the fouling deposit (Somerscales, 1997). This is shown schematically in Fig. 2.2.

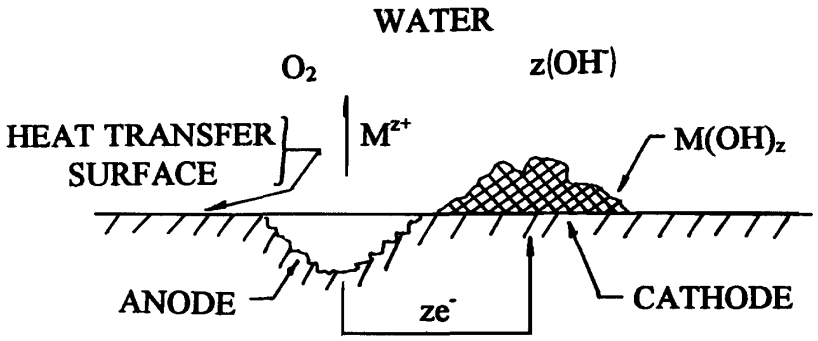

Fig. 2.2: Mechanism for corrosion fouling (Somerscales, 1997)

2.2.1.3. Particulate fouling

Particulate fouling can occur in both liquid and gas systems. In liquids, the particulate matters could be the corrosion products, particles from the processed fluid, silt or decomposing organic matter. In gas system, it could be originated from dust particle carried forward in the air and incombustible mineral matter arises from combustion process. The arrival of a particle at a surface can be by two mechanisms:

1. Gravitational settling

2. Particle transport within a fluid as it moves across the surface onto which particle deposits

Settling is usually associated with near stationary fluids. When considering heat exchanger where the fluid is moving through it, particle transport is always assumed to be more significant to describe particulate fouling in heat exchanger. Two important steps must occur before a particle in suspension in fluid deposits on a surface to become part of the foulant layer. Firstly, the particle has to be transported to the surface by one or combination of mechanisms including Brownian motion, turbulent diffusion or by virtue of the momentum possessed by the particle. The second step is that the particle must stick if it is to be regarded as part of the foulant layer residing on the surface (Bott, 1995).

2.2.1.4. Crystallization fouling

The deposition of crystals on heat exchanger surfaces is a common occurrence in aqueous systems. The problem might arise in cooling water circuits where deposition of hardness salts is normally encountered on heat transfer surfaces (Bott, 1995). Nevertheless, crystallization fouling is not exclusive only to aqueous systems. This phenomenon could also occur for waxy hydrocarbons that are being cooled where there is a strong possibility wax crystals to be deposited on the cold heat transfer surface. In general, the extent of the prevailing supersaturation will govern the crystallization rate. The sequence of events that leads to deposit formation on the surface may be visualized as (Bott, 1997):

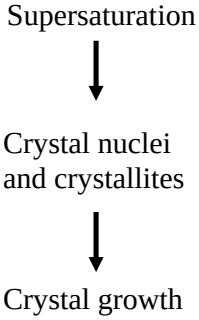

The region for supersaturation could either be at the surface-liquid interface or remote from the surface. If it occurs at the surface-liquid interface, precipitation on the surface is likely to happen. In contrast, if the supersaturation is remote from the surface, crystals form in the bulk solution and then migrate to the surface as particles to form a solid deposit. The formation of crystals is usually assisted by the presence of suitable nuclei that could be either solid impurities in suspension in the solution or sites on the heat exchanger surface. Crystal growth follows the formation of stable nuclei within the region where supersaturation occurs (Bott, 1997).

Mullin (1972) suggested a number of processes that takes place simultaneously for an ionized solute to be crystallized from an aqueous solution:

1. Bulk diffusion of solvated ions through the diffusion boundary layer
2. Bulk diffusion of solvated ions through an adsorption layer
3. Surface diffusion of solvated and unsolvated ions
4. Partial or total desolvation of ions
5. Integration of ions into the crystal lattice
6. Counterdiffusion of released water through the adsorption layer
7. Counterdiffusion of water through the boundary layer

2.2.1.5. Biological fouling

Biological fouling is the fouling process where nature plays a vital role. It may be caused by strong adhesion of marine macro or microorganisms to any surface such as that of a boat, oil platform, or any part of a cooling system in a plant using sea water as a coolant. Biological organisms that lead to biological fouling can also be present in fresh water exposed to any extent to the surrounding environment (Oufer, 1990).

The general development of a biofilm with time is shown in Fig. 2.3.

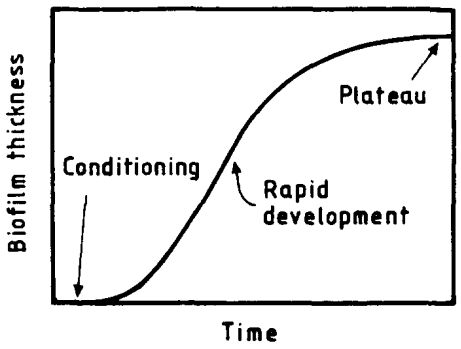

Fig. 2.3: Typical boifilm growth with time (Melo and Bott, 1997)

After the conditioning and initiating of biofilm growth, there is a rapid development in biofilm thickness for a certain period of time followed by the period when the thickness becomes stabilized known as plateau. At the plateau, it is considered that the factors that enhance growth such as nutrient availability are offset by the removal forces owing to the fluid shear.

In summary, the sequences of events in biofilm formation are (Melo and Bott, 1997):

1. Mass transfer of macromolecules to the surface and the formation of an adsorbed layer
2. Transport of microorganisms to the adsorbed layer
3. Irreversible adhesion of the cells or clusters to the surface
4. Possible removal of cells from the surface
5. Establishment of a stronger bond between the microorganisms and the surface layers
6. Mass transfer of nutrients to the surface and through the biofilm together with transport away from the surface
7. Cell metabolism, including the production of new cells and extracellular polymers

8. Possible sloughing of the biofilm when it has attained a critical thickness

2.2.2. Fundamental steps in fouling

There are a series of sequential event that occurs as the fouling process proceeds. Fundamental steps in fouling are categorized as follows including brief explanation of each step:

1. Initiation
2. Transport
3. Attachment
4. Removal/Auto-retardation
5. Ageing

2.2.2.1. Initiation

During the initial period of stable operation for the new or cleaned heat exchanger, the high transfer coefficients may remain unchanged for a certain period of time. This is considered to be the time in which nuclei for crystallization are formed or nutrients for biological growth are deposited. This delay period may last anytime from few seconds to several days. No delay period is required for particulate fouling but for crystallization and chemical reaction fouling, the initiation period decreases with increasing surface temperature as supersaturation and/or reaction rate increase. In general, it is reported that the delay time which is the time before deposition starts, decreases with increasing roughness of the heat transfer surface (Muller-Steinhagen, 2000).

2.2.2.2. Transport

For deposit formation, at least one key component (such as suspended particles, dissolved ions or oxygen for corrosion) must be transported from the bulk flow to the heat transfer surface. This is achieved by diffusion process for most of the cases. Local diffusing mass flux is calculated from:

$$M_{diffusion} = \beta A (C_b - C_w) \quad (2.5)$$

with C_b and C_w being the concentrations of the key components in the bulk flow and the region close to the heat transfer surface and β being the mass transfer coefficient. The mass transfer coefficient may be calculated for the existing flow conditions using the appropriate *Sh-Re-Sc-d/L* correlation (Muller-Steinhagen, 2000).

2.2.2.3. Attachment

After being transported to the heat transfer surface, the fouling species must attach (particulate) or react to form the deposit (crystallization/chemical reaction) based on the following relationship (Muller-Steinhagen, 2000):

$$M_{reaction} = k_r A (C_w - C^*)^n \quad (2.6)$$

the reaction rate constant, k_r is proportional to an Arrhenius term:

$$k_r = K \exp(-E/RT) \quad (2.7)$$

2.2.2.4. Removal/Auto-retardation

Depending on the strength of the deposited layer, it may be susceptible to erosion as early as the beginning of the deposition process. There are several possible mechanisms for removal process (Muller-Steinhagen, 2000):

1. Fracture of relatively large section due to irregularities in the deposit
2. The shear force of the fluid
3. Turbulent bursts from the flow

Additionally, there are several mechanisms which do not cause removal of existing deposit, but instead slowing down the deposition process and this is known as suppression. This may be due to:

1. The reduction of the interface temperature to the fluid
2. Reduced oxygen transfer for increasing corrosion layer thickness
3. Changing electric double layer intensity
4. The reduced surface roughness as deposition proceeds

2.2.2.5. Ageing

Ageing process is common to almost all types of deposit. Ageing may increase the strength of the deposit by polymerization, re-crystallisation, dehydration etc. For biological deposit, it may get poisoned by metal ions and may wash away by the bulk flow. Ageing is the least investigated and understood step and it is usually ignored in the attempt to model fouling process (Muller-Steinhagen, 2000). Dickakian (1989) has shown how the fraction of coke in a deposit from crude oil increases over time, whereas the fraction of asphaltenes decreases. An initial deposit contained 30% asphaltenes and no coke. After 3 hours of heating and further fouling, the coke content of the deposit was 60% and the asphaltene content about 14%. The thermal resistance of the deposit will change owing both to the chemical reactions and to the further deposition. This aging reaction must be understood if the mechanisms of fouling are to be deduced from deposits taken from industrial exchangers that may have been on stream for many months.

2.2.3. Factors influencing fouling

2.2.3.1. Effect of surface temperature

A widely known relationship for the dependency of reaction rate on the temperature is represented by Arrhenius relationship. Surface temperature effect in processing crude oil fouling has always been considered to follow the Arrhenius relationship which is expressed as follows:

$$\frac{dR_f}{dt} = A\exp\left(-E/RT_s\right) \tag{2.8}$$

The above equation implies that a plot of *ln* (dR_f/dt) versus $1/T_s$ gives a straight line from which the values of *A* and *E* are determined. In applying this equation the factors such as velocity, fluid composition and geometry should be kept constant. Crittenden *et al.* (1992) fitted this equation to fouling data for light crude oil and obtained *A* and *E* values of 4.9 x 10^{-7} and 33 kJmol^{-1}, respectively. Crittenden *et al.* obtained the activation energy value for heavy crude oils as 21 kJ/mol. Crittenden *et al.* mentioned that the activation energy below 40 kJ/mol indicates that both chemical and physical mechanism are important. Scarborough *et al.* (1979) and Eaton and Lux (1984) obtained values of 53 and 36 kJ/mol, respectively for crude oil feed stocks. It should be noted that these values are based on the wall/surface temperature, T_s. Ebert and Panchal (1995) used the film temperature, T_f, in their analysis of fouling rates and obtained value for activation energy of 68 kJ/mol using Scarborough *et al.* (1979) data sets. T_f value was obtained using the following relationship:

$$T_f = T_b + 0.55\left(T_s - T_b\right) \tag{2.9}$$

Asomaning (1997) studied the effect of surface temperature by using fuel oil at an inlet bulk temperature of 85^{o}C and fluid velocity of 0.6 m/s. He observed that at an initial surface temperature of 185^{o}C, deposition was negligible and final fouling resistance was 0.0085 m^{2}K/kW. When the initial surface temperature was raised to 215^{o}C, the final fouling resistance was increased to 0.04 m^{2}K/kW which is a five-fold

increase. A further increase in initial surface temperature to 240^{o}C and 320^{o}C resulted in final fouling resistance that increased to 0.05 and 0.085 m^{2}K/kW, respectively which is a six and ten-fold increase respectively over that at 185^{o}C. Increase in initial surface temperature resulted in an increase in fouling propensities of the fuel oil. The fouling rate was expressed by Arrhenius equation. The initial fouling rate doubled for every 60^{o}C increase in surface temperature.

Saleh *et al.* (2004) conducted fouling experiment using Gippsland crude oil heated at moderate temperature. The experiments were run for periods up to 90 hours at constant heat flux. Initial surface temperature was varied over the range of 180 to 260^{o}C, at a fixed velocity of 0.25 m/s. At an initial surface temperature of 180^{o}C, the probe surface temperature increases with time by about 12^{o}C over the 90 hours of the test. At an initial surface temperature of 260^{o}C, the increase in probe surface temperature with time is about 48^{o}C over the 90 hours test. The calculated fouling rates show that it ranged from 1.94x10^{-7} m^{2}K/kJ at initial surface temperature of 180^{o}C to 5.89x10^{-7} m^{2}K/kJ at initial surface temperature of 260^{o}C. Surface temperature was found to have a major impact on fouling rates where an increase of roughly 80^{o}C resulted in tripling of initial fouling rates. The activation energy determined using the Arrhenius plot were 42 kJ/mol and 28.5 kJ/mol based on the film and surface temperature, respectively.

Srinivasan *et al.* (2004) carried out experiments using Light Sour Blend oil (LSB) to study the effect of surface temperature. Experiments were carried out in a recirculation fouling loop, equipped with an annular electrically heated probe. Experiments were carried out at a fixed bulk temperature of 275^{o}C, velocity of 0.75 m/s and surface temperatures ranging from 335 to 370^{o}C. They observed sharp increase in fouling rates with initial surface temperature with fouling activation energy of 54.2 kJ/mol. They calculated activation energy based on the film temperature T_f, and obtained a value of 77.2 kJ/mol. The film temperature, T_f, was calculated as:

$$T_f = 0.3T_b + 0.7T_{so} \tag{2.10}$$

Crittenden *et al.* (2007) studied the effect of surface temperature on fouling rates using pilot-scale parallel twin –tube apparatus. Maya crude oil was selected for the test because it was expected to foul under pilot-plant conditions. Experimental results showed a seemingly straight dependency of the initial fouling rate on the surface temperature where the fouling rates increased with the surface temperature at a constant crude velocity.

2.2.3.2. Effect of crude oil composition and blending

Crude oil by itself is an extremely a complex mixture of various component. One of the crucial factors governing fouling is the amount of asphaltenes present in the crude. Heavy crudes tend to have higher asphaltene contents and are more prone to fouling. Asphaltene is the highly condensed aromatic material that causes many crude oils to be black in colour (ESDU, 2000b). Asphaltenes are defined as a class of crude oil constituents insoluble in non-polar solvents such as pentane, hexane or heptane but soluble in solvents such as pyridine, carbon disulphide, carbon tetrachloride, toluene or benzene (Watkinson, 1992). Dickakian and Seay (1988) studied the effect of asphaltenes on fouling due to thermal effect and the characterization of the deposits formed on the heated surfaces at various times showed that the deposits were initially asphaltene which were then carbonised on the surface into an infusible coke. The asphaltenes is known to have the highest thermal reactivity of any constituents of a crude oil. Asphaltenes react to form lower molecular weight products when it is soluble but the major thermal reaction product is coke when it is insoluble (Wiehe, 1993). Other than asphaltenes, traces of metal are always present in petroleum streams as natural compounds and as corrosion products. Vanadium, nickel and some iron exist naturally in petroleum as metal chelates known as porphyrins. Besides, iron sulphide as a corrosion product is second only to asphaltenes as the most common foulant found in crude pre-heat trains (Wiehe, 1997b). It is always being mistaken for coke due to the fact that it is a black and granulated solid.

Another important factor which influences crude oil fouling is crude blending. Blending of crudes can cause unstable mixes which precipitate species such as

asphaltene and result in rapid fouling, which is described as acute fouling (Wilson and Polley, 2001). Mixing typical paraffinic crudes or condensate and asphaltenic crudes can cause asphaltene to precipitate out and subsequently resulted in high fouling factor. This has led to the idea of limiting the amount of condensate that can be mixed with the crude oil to mitigate fouling (ESDU, 2000b). In a series of papers, Wiehe (1999a, b, c) and Wiehe and Kennedy (1999) demonstrated a simple laboratory measurement to determine crude oils incompatibility by introducing two parameters that can be defined to characterise a crude blend, namely the Insolubility Number, I_N and the Solubility Blending Number, S_{BN}. The importance of the blending order is also stressed since it is an important factor that causes crude blends to become incompatible. This procedure has been verified in commercial crude preheat application. Saleh *et al.* (2005) studied the effect of mixing and blending crude oils at certain operating conditions with the intention of using the results to guide a fouling mitigation strategy.

2.3. Crude oil fouling prediction model

2.3.1. Fouling models

Modeling crude oil fouling has always been a very challenging task due to the complexity of the fouling phenomenon. The complex nature of the fouling process is due to the different mechanisms and different types of precursors involved. Having a generalized fouling model that can accurately predict this complex physico-chemical process has been an ultimate motivation for the research work in this area. The complexity of the fouling process almost makes it impossible to link the various factors involved in order to predict what would happen to a heat transfer surface exposed to a fluid under harsh operating conditions. Such a problem is evidently clear as no fouling model that could predict entirely the fouling process of a hydrocarbon stream (Fryer, 1988). Most of the fouling models available in the literature come with

the assumptions that some are invalid in reality. So the predictive accuracy of the models is limited (Asomaning, 1997).

Attempts in predicting fouling phenomenon has started long time ago. As early as 1934, Nelson (1934) has come out with the idea that the rate of coking is directly dependent upon the volume of fluid in the film which is at temperature higher than that of bulk temperature. Such a theory can account for the widely held view that a fouling rate can be reduced by increasing the fluid velocity, thereby reducing the thermal boundary layer thickness.

Kern and Seaton (1959) proposed a very simple and useful concept in an attempt to model fouling process involving chemical reactions. They came out with the idea that fouling mechanism involves two terms which are deposition and removal term. The proposed concept by Kern and Seaton is based on the following assumptions:

1. No chemical reaction is involved
2. Net deposition is the result of deposition minus fouling removal
3. Fouling removal increases with mass of deposit
4. Rate of deposition is independent of mass of deposit

The well-known Kern and Seaton model is represented by the following equation:

$$\frac{dm}{dt} = \dot{m}_d - \dot{m}_r \tag{2.11}$$

Kern and Seaton proposed a mathematical restatement of Eq. (2.11) with tubular flow in mind as:

$$\frac{dx_f}{dt} = K_1 C' M - K_2 \tau x_{ft} \tag{2.12}$$

$K_1C'M$ in the equation above refers to the rate of deposition term similar to the first order reaction whilst $K_2 \tau x_{ft}$ refers to the rate of removal term. Integrating the

above equation assuming *C'* and *M* are constants for a steady flow heat exchanger results in:

$$x_f = \frac{K_1 C' M}{K_2 \tau}\left(1 - e^{-K_2 \pi}\right) \tag{2.13}$$

The simplest form of the above equation could be represented by Eq. (2.14) with $K_1 C' M$ a constant that is equivalent to R_{fo} whilst $K_2 \tau$ is also a constant that is equivalent to β:

$$R_{ft} = R_{f\infty}\left(1 - e^{-\beta t}\right) \tag{2.14}$$

The model is considered to be impractical for the heat exchanger designer unless values for R_{fo} and β are in hand. The actual values of these constants will depend upon the type of fouling and operating conditions. In general, there are no ways of predicting these values unless some detailed experimental work has been performed.

The model which Kern and Seaton proposed is an attempt to provide a generalized equation for fouling. The equation is general where it does not specifically refer to the mechanism of deposition and it assumed that the mechanism of removal is similar in most situations since it depends on the conditions at the fluid/foulant interface. The basic Kern and Seaton equation has been modified to incorporate an appropriate term for fouling–film removal (Watkinson and Epstein, 1970; Taborek *et al.*, 1972).

Atkins (1962) made an important observation in fired heater tubes that the fouling deposits appeared as two layers which are an outer porous (or tarry layer) and a hard crust of deposit next to the wall. This introduces another phenomenon of the fouling process where primary tarry deposit was subjected to further chemical reaction (or decomposition) resulting in the hard coke layer and it is also known as deposit ageing process. Heat would then have to flow through the first layer which is formed by coke and then through the second layer which is softer since it is built up by recent material deposition.

Another interesting concept was proposed by Nijsing (1964) while dealing with fouling originating from deposition of organic coolants in nuclear reactors. He outlined probably the first systematic study of fouling where the foulant products are allowed to diffuse back into the bulk stream. Assuming instantaneous first order reaction of foulant precursor, the rate of foulant deposition was found to be controlled by diffusion of precursor to the wall. By applying simplifying assumptions, the equations for flow and diffusion were solved to give average rate of deposition:

$$\phi_D \alpha \frac{\left(c_b D(\mathrm{Re})\right)^{0.875} (Sc)^{0.33}}{d} \tag{2.15}$$

Another mathematical model of fouling process was introduced by Watkinson and Epstein (1970). They proposed a transfer-adhesion-release model adopting the Kern and Seaton removal term to which they added a deposition term involving a particle sticking probability, *S*. Watkinson and Epstein developed this equation based on the following basic assumptions:

1. Precursors are present in the bulk fluid
2. Insoluble foulant are formed in the bulk fluid
3. Sticking probability is inversely proportional to shear forces
4. Sticking probability is proportional to the Arrhenius factor
5. First order function of deposit thickness for removal/release term

Their final equation for the rate of fouling was given by:

$$\frac{dR_f}{dt} = \frac{d\left(x_f / k_f\right)}{dt} = \frac{A_1 (C_b - C_w) \exp(-E / RT_s)}{v f^{1/2}} - A_2 f v^2 x_f \tag{2.16}$$

Although Eq. (2.16) was derived for sand/water slurries, it was found to agree well with the experimental data obtained for gas oil fouling when correlating the initial fouling rate. However, it did not predict accurately the asymptotic fouling resistance values. The authors cautioned regarding the use of the removal term of Eq.

(2.16) which is the term on the right hand side of equation if hard deposits are obtained in a given fouling process such as coking.

A few attempts had been made to model fouling process with no consideration of removal term due to the strong nature of the deposit where one of the efforts was made by Jackman and Aris (1971) who tried to model coke deposition occurring in pyrolytic reactors. The general picture was simplified to two single reactions:

1. A first order reaction that describes the decomposition of the reactant in the tube to produce coke

2. A zero order reaction that describes the deposition on the tube walls where no mass transfer effects were included in the analysis

Fernandez-Baujin and Solomon (1976) proposed another model without any removal term where they considered a two-step mechanism by which the reactant first diffuses to the wall then reacts by a first-order reaction. The overall rate of coke formation was then found to be:

$$\frac{dx_f}{dt} = k_c y \left(1 - \frac{k_c}{\frac{kP}{RT} + k_c} \right) \tag{2.17}$$

Eq. (2.17) may be simplified as in the case of pyrolysis where the temperature of the coil is so high compared to the temperature of the bulk fluid that mass transfer becomes the rate limiting step. In that case, the rate of coke deposition was given by:

$$\frac{dm_f}{dt} = \frac{K^* G^{0.8}}{\left(D - 2x_f\right)^{1.8}} \tag{2.18}$$

The transport-reaction model by Fernandez-Baujin and Solomon were developed to consider chemical reaction as well as the transport of fouling precursor to and from heated surface. Neither Kern and Seaton nor Watkinson and Epstein incorporated chemical reaction effects to describe the common case where the foulant precursors are generated *in situ*.

Sundaram and Froment (1979) also came out with another model without any consideration of removal term and it was developed for the cracking of propane. The model was applied to various consecutive mechanisms leading to coke formation from propane and was found to agree with experimental data. In all cases, the overall coke deposition rate was assumed to be controlled by kinetics. In other words, diffusion problems were not taken into account because the study was made in a mixed flow reactor.

Taborek *et al.* (1972) presented a model which although mainly directed toward fouling of cooling tower water could be also used for chemical reaction fouling since the factors introduced may be determined. The main development introduced by these researchers is in the expression of the deposit removal mechanism which they suggested:

1. Proportional to the fluid shear stress
2. Inversely proportional to a new quantity called deposit bond resistance, R_b.

R_b was defined as the adhesive strength of the deposit per unit area at the plane of weakest adhesion. It is therefore expected to be high for uniform and strong deposits such as polymers and coke and low for weaker deposits.

The simple concepts of Nelson (1934) and Atkins (1962), the analysis provided by Kern and Seaton (1959) together with the use of film mass transfer and simple chemical kinetics led Crittenden and Kolaczkowski (1979a) to develop a comprehensive fouling model that allows chemical reaction and transport to and from a surface to be considered. Crittenden and Kolaczkowski (1979a) published a more general study to model hydrocarbon fouling. They considered a single chemical reaction of first order occurring at the deposit-fluid interface. The deposition term included both kinetics and mass transfer of reactants while the removal term was formed by two terms: one related to shear forces and the other to back diffusion of the foulant into the bulk fluid. In order to make the mathematics manageable, the following simplifying assumptions were considered:

1. The heat flux and mass transfer are maintained constant
2. Foulant material is formed by an irreversible reaction
3. The precursor concentration in the bulk fluid, C_{pb}, may be considered constant in view of the relatively low ratio of deposition flux to the flow through the exchanger
4. The precursor diffuses to the reaction zone but the foulant may diffuse away from the zone into the main flow as well as to the heating surface on which it deposits
5. There is no induction or initiation period
6. The properties of the foulant do not alter as the fouling process proceeds and the properties of the fluid are constant over the temperature range covered by the conditions
7. In the first instance it may be assumed that the reaction zone is the clean wall/fluid interface
8. Mass transfer of light products (other than foulant) away from the reaction zone is not likely to be deposition rate limiting owing to the relatively high diffusion rates of these relatively small molecules and the existence of potentially high driving forces

The rate of fouling layer build up is given by the following equation:

$$\frac{dx_f}{dt} = \frac{1}{\rho_f}\left(N_r - N_D\right) \tag{2.19}$$

Applying the film theory of mass transfer, the mass fluxes may be written down in terms of mass transfer coefficient, *K*, and a concentration driving force:

$$N_r = K_r\left(C_{rb} - C_{ri}\right) \tag{2.20}$$

and

$$N_D = K_D\left(C_{Di} - C_{Db}\right) \tag{2.21}$$

The mass flux of precursors can be balanced by the rate of reaction to get an expression for N_r without having an unknown C_{ri} in the equation:

$$N_r = kC_{ri}^{\ n} \tag{2.22}$$

By assuming first order reaction and C_{Db} equal to zero, Eq. (2.19) can be expanded as follows:

$$\frac{dR_f}{dt} = \frac{d\left(x_f / \lambda_f\right)}{dt} = \frac{1}{\rho_f \lambda_f}\left(\frac{C_{rb}}{\frac{1}{K_{tr}} + \frac{1}{k}} - K_{tD}C_{Di}\right) \tag{2.23}$$

In general, mass transfer coefficients of precursor and foulant will be unknown but they may be estimated from flowrate and physical properties by the application of the Chilton and Colburn analogy (1934). The Chilton and Colburn analogy suggested the use of more published information on heat transfer to give a meaningful and useful estimate for mass transfer coefficient. Results of experimental studies of heat transfer may be conveniently represented by means of the *j*-factor method developed by Chilton and Colburn for representing data on heat transfer between a turbulent fluid and the wall of a pipe. The *j*-factor equation for heat transfer is represented by:

$$j_h = St\,\mathrm{Pr}^{0.67} = 0.023\,\mathrm{Re}^{-0.2} \tag{2.24}$$

Chilton and Colburn found out that the use of the Eq. (2.24) for heat transfer gave a good estimate for the mass transfer coefficient at the same flowrate and physical properties of the *Re* term.

By applying Chilton and Colburn analogy, Eq. (2.23) is expanded to give an equation which showed a complex dependency of fouling rate on mass flowrate. The reaction velocity constant increases exponentially with absolute temperature according to Arrhenius equation and could be represented by the Arrhenius equation.

Crittenden and Kolaczkowski arrive at an extremely complex equation taking these factors into accounts:

$$\frac{dR_f}{dt} = \frac{1}{\rho_f \lambda_f}\left\{\frac{C_{rb}}{\dfrac{p(d-2x)^{1.8}(Sc_r)^{0.67}}{1.213\lambda_1\eta^{0.2}G^{0.8}} + \dfrac{1}{Ae^{\frac{-E}{RT}}}} - \frac{1.213\lambda_1\eta^{0.2}G^{0.8}C_{Di}}{p(d-2x)^{1.8}(Sc_r)^{0.67}}\right\} \qquad (2.25)$$

$$T = T_b + \left\{\frac{q}{0.023(\mathrm{Re})^{0.8}(\mathrm{Pr})^{0.4}}\right\}$$

Eq. (2.25) is an extremely complex and difficult to use in design or in the analysis of an operating system due to too many unknowns. This model also contains foulant back diffusion term which is a function of foulant/deposit concentration at solid-liquid interface which is very difficult to determine practically. At very high temperatures severe thermal degradation to hard coke occurs and thus foulant/deposit concentration at the interface, C_{Di}, is assumed to be zero and Eq. (2.25) can be written as:

$$\frac{dR_f}{dt} = \left[\frac{1.213\lambda_1\eta^{0.2}G^{0.8}C_{rb}}{k_f\rho_f\rho(d-2x)^{1.8}(Sc_r)^{0.67}}\right]. \qquad (2.26)$$

Crittenden *et al.* (1987) used data obtained during the polymerization of 1% styrene in kerosene to test three-step model, Eq. (2.25). Mass transfer of precursor to the wall, reaction at the wall and back convection of foulant to the bulk stream forms the three-step model. The order of reaction for this system is 5/2 rather than 1, assumed in Eq. (2.25). With no back convection considered, the predicted values of the initial fouling rate were much higher than the experimental values as the temperature is increased. Again, the relationship between initial fouling rate and flow rate appears to be of a complex nature. The foulant interfacial concentration was found to be independent of flow rate but it increases sharply with temperature.

Oufer (1990) formulated a transport and reaction model to describe fouling from solutions of styrene in heptane under boiling conditions. Back convection of the

polystyrene product was considered to be negligible. The polymerization of styrene was found to be 2nd order with respect to styrene. The model did not give good agreement with the observed initial fouling rate, which was attributed to errors in estimating mass transfer coefficient. This model and Crittenden *et al.* (1987) emphasized the need to understand the order and mechanism of chemical reaction before attempting any mechanistic modeling.

Later in the year 1979, Crittenden and Kolacazkowski (1979b) further extended their model to the two-layer concept first described by Atkins (1962). The assumption made was that a mobile tarry layer would thermally degrade with time to produce a hard coke, the thermal conductivity of which was greater than the tarry layer. In this case, the final equation was given by:

$$\frac{dR_f}{dt} = \phi_{Td} - \phi_{Tr} - \phi_{CT} - \phi_{Fr} \tag{2.27}$$

The four terms forming the right hand side of Eq. (2.27) were as follows:

$$\phi_{Td} = \frac{1}{\frac{B_1\left(D-2x_f\right)^{1.8}}{G^{0.8}} + B_2 e^{(E_t/RT_t)}} \tag{2.28}$$

$$\phi_{Tr} = \frac{B_3 G^{0.8}}{\left(D-2x_f\right)^{1.8}} \tag{2.29}$$

$$\phi_{CT} = \frac{B_4}{e^{(E_C/RT_C)}} \tag{2.30}$$

$$\phi_{Fr} = \frac{B_5 G^{1.8} R_f}{\left(D-2x_f\right)^{3.8}} \tag{2.31}$$

The initial fouling rate can then be easily obtained as

$$\dot{R}_{f0} = \frac{1}{\frac{D_1 D^{1.8}}{G^{0.8}} + \frac{e^{(E_t/RT_t)}}{D_2}} - \frac{D_3 G^{0.8}}{D^{1.8}} \tag{2.32}$$

This model was tested using the gas oil fouling data obtained by Watkinson and Epstein (1969). Good agreement seems to have been obtained. The overall fouling rate was determined for that specific fluid to be:

$$\frac{dR_f}{dt} = \dot{R}_{f0} - 4.63 \times 10^{-5} G^{1.8} R_f \tag{2.33}$$

Paterson and Fryer (1988) adopted a reaction engineering approach to explain the decrease in initial fouling rate with increasing velocity which they previously observed experimentally with fouling of skimmed milk. Paterson and Fryer proposed a model based on the following hypothesis:

1. Fouling is controlled by a single reaction

2. No mass-diffusion resistance

The proposed model which can account for a decline in fouling rate with an increase in fluid velocity is given as follows:

$$r_i = \beta \exp\left(\frac{-E_r}{RT_o}\right) \Big/ u \tag{2.34}$$

Although the original idea was proposed by Nelson (1934) the authors were able to explain that the size of the boundary layer is really the key to many fouling problems.

Panchal and Watkinson (1993) have outlined the basis for a more sophisticated and complicated model. It is based on the assumption that the key chemical reaction leading to fouling can be expressed in a two-step reaction involving the generation of a soluble precursor followed by the formation of an insoluble foulant. The scheme is:

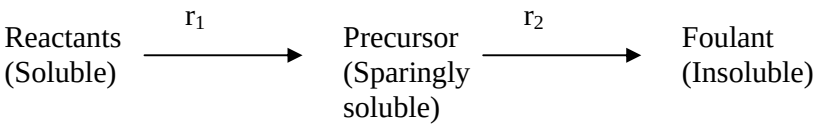

Panchal and Watkinson visualized a number of different mechanisms of chemical reaction fouling and suggested three possible cases as shown in Table 2.1.

Epstein (1994) criticized the model developed by Crittenden and Kolaczkowski (1979a) because at time zero it is fundamentally difficult to justify a finite concentration of foulant at the wall which would be required for back-diffusion to occur. Epstein then developed a model to describe the initial rate of chemical reaction fouling at a heat transfer surface in which surface attachment, treated as a process in series with mass transfer, was assumed to vary directly with the residence time of the fluid at the surface. Epstein assumed that the greater the residence time, the greater would be the opportunity for the chemical reaction to promote attachment and also to overcome the hydrodynamic forces that resist attachment. This is very crucial as the residence time at the heated surface depends strongly on the fluid mechanics and hence on the geometric design of the fouling test section. The proposed model by Epstein is as follows:

$$\left.\frac{dR_f}{dt}\right|_{t=0} = \frac{m\phi}{k_f \rho_f} \tag{2.35}$$

The deposition mass flux, ϕ is represented by the following:

$$\phi = \frac{c_b}{\left(\frac{k' Sc^{2/3}}{u}\right) + \left(\frac{k'' \rho u^2}{\mu \exp(-E/RT_{so}) c_s^{\,n-1}}\right)} \tag{2.36}$$

The first term in the denominator represents the mass transfer of foulant and/or its precursors to the heated surface. The second term in the denominator represents the reaction and attachment aspects of the fouling process. The reaction part is described by an n^{th} order process with a true activation energy, *E*. The model uses the surface temperature rather than the film temperature. Eq. (2.36) shows that fouling rate has a complex dependence on velocity. Indeed for all surface temperatures the equation shows that there would be a maximum in the fouling rate-velocity curve. Epstein was able to demonstrate the validity of his model using data published by Crittenden *et al.* (1987) for the polymerization of styrene. Epstein's model is applicable not only to chemical reaction fouling but also to particulate fouling.

2.3.2. ‘Threshold fouling’ concept

The ‘threshold fouling’ concept for crude oil fouling was introduced by Ebert and Panchal (1995) at the Engineering Foundation conference. This is an alternative and realistic approach on crude oil fouling where they proposed a semi-empirical approach to quantify the effect of crude velocity and temperature on the tube-side fouling in crude oils. Ebert and Panchal developed their correlation for predicting threshold fouling conditions based on the following assumptions:

1. The net deposition is given by formation minus removal of foulant from the thermal boundary layer.

2. Foulant is formed in the boundary layer by reactions which can be grouped as a one-step reaction.

3. Concentration gradients of reactants in the boundary layer are negligible.

4. Foulant is transported by diffusion and turbulence eddies from the boundary layer to the bulk flow.

5. The temperature profile in the boundary layer is linear.

6. An integrated reaction term can be expressed by the film temperature in the boundary layer.

The correlation proposed by Ebert and Panchal for predicting the fouling rate and the ‘threshold fouling’ is as follows:

$$\frac{dR_f}{dt} = \alpha \,\mathrm{Re}^{-\beta} \exp\left(\frac{-E}{RT_f}\right) - \gamma \tau_w \tag{2.37}$$

The deposition mechanism which is related to chemical reaction, promotes fouling while the suppression mechanism which is related to the shear stress at the tube surface acts to mitigate fouling. If the deposition mechanism dominates the suppression mechanism, deposition on the heat transfer surface will occur. The

'threshold fouling' (net rate of zero) occurs where the two mechanisms are balanced and below threshold, no significant fouling will occur. For the deposition term, $Re^{-\beta}$ term is included to represent the effective thickness for thermal boundary layer where it is assumed to be analogous to the heat transfer-like relationship proposed by Paterson and Fryer (1988). Temperature dependent reaction rate is represented by the Arrhenius-like term, where reaction is assumed to occur in the film close to the wall. For the removal term of the model, the model use wall shear stress, τ_w to represent the removal mechanism of foulant from boundary layer. The proposed model by Ebert and Panchal was based on pilot plant studies at Exxon by Scarborough *et al.* (1979). A nonlinear regression analysis was used to determine the values of α, β, γ and E of the Eq. (2.37) by using the data obtained by Scarborough *et al*.

Ebert and Panchal (1995) model ignores the effect of crude oil thermal conductivity and specific heat and only considers the effect of crude oil density and viscosity by means of Reynolds number. In 1999, Panchal and co-workers (1999) considered data sets obtained from both pilot plant tests and monitoring of plant exchangers to give revised form of original equation proposed by Ebert and Panchal in 1995 as follows:

$$\frac{dR_f}{dt} = \alpha' \mathrm{Re}^{-0.66}\, \mathrm{Pr}^{-0.33} \exp\left(\frac{-E}{RT_f}\right) - \gamma' \tau_w \qquad (2.38)$$

where the fluid flow and thermal properties are accounted by the use of Prandtl number and a fixed power on the Reynolds number. Panchal and coworkers obtained their laboratory data using a high pressure autoclave fouling unit under various conditions (Kuru *et al.*, 1997).

Polley *et al.* (2002) made simple modifications to the Ebert and Panchal threshold fouling model with the following assumptions:

1. Surface temperature is used instead of film temperature in the reaction term
2. Retain the velocity dependency for the generation term, but use $Re^{0.8}$
3. The removal term is proportional to $Re^{0.8}$ that is associated with a mass transfer process rather than wall shear stress

The reason for using $Re^{0.8}$ rather than wall shear is due to the fact that wall shear stress suggests a physical mechanism to remove the deposit from the tube wall and it is difficult to correlate this to the threshold model given that a deposit has yet to form. Polley and co-workers (2002) modeled deposition term closely related to that proposed by Paterson and Fryer (1988) and a mass transfer related suppression term analogous to that proposed by Crittenden *et al.* (1987).

$$\frac{dR_f}{dt} = \alpha'' \mathrm{Re}^{-0.8}\,\mathrm{Pr}^{-0.33} \exp\left(\frac{-E}{RT_s}\right) - \gamma'' \mathrm{Re}^{0.8} \tag{2.39}$$

This model was tested using Knudsen *et al.* (1999) data and it gives a good prediction of the threshold temperature, particularly when the errors associated with experimental measurements are considered. This model is also found to have better agreement for a number of pilot plant and exchanger monitoring data sets reported by Asomaning *et al.* (2000), although estimation has to be done for several sets due to no access to the thermophysical properties. They also discounted the high temperature data from Scarborough's study as these featured conditions unfamiliar to most preheat exchangers and were likely to feature coking reactions.

Revision of the Epstein (1994) model has been done by Yeap and co-workers (2004) where they proposed a model with a removal term and a deposition term in the form of:

$$\frac{dR_f}{dt} = \frac{AC_f u T_s^{\,2/3} \rho^{2/3} \mu^{-4/3}}{1 + Bu^3 C_f^{\,2} \rho^{-1/3} \mu^{-1/3} T_s^{\,2/3} \exp\left(E / RT_s\right)} - Cu^{0.8} \tag{2.40}$$

This model has been compared against several published sets of pilot plant and refinery data for crude oil fouling by Panchal *et al.* (1999), Scarborough *et al.* (1979), Knudsen *et al.* (1999) and Lambourn and Durrieu (1983). The model was found to describe the observed fouling trends quite close. The form of the denominator enables this model to describe data sets where mass transfer dominate fouling process and fouling increases with increasing flowrate which is encountered in a small number of data sets.

Nasr and Givi (2006) proposed a latest threshold fouling model which is independent of Prandtl number, as:

$$\frac{dR_f}{dt} = \alpha \,\mathrm{Re}^{-\beta} \exp\left(-E/RT_f\right) - \gamma \,\mathrm{Re}^{0.4} \tag{2.41}$$

The proposed model was then evaluated based on the experimental data measured by Saleh *et al.* (2004) for Australian crude oil. The model gives a fair agreement in comparison with the experimental data. Besides, the model was also tested with the experimental data from Scarborough *et al.* (1979), Knudsen *et al.* (1999) and refinery data published by Polley *et al.* (2002) and Panchal *et al.* (1999) and the model gives a better prediction in comparison with model proposed by Polley *et al.* (2002).An alternative way of determining the 'threshold fouling' conditions has been conducted by Knudsen *et al.* (1999) where they experimentally determine the 'threshold fouling' conditions. Knudsen *et al.* reported a careful laboratory study aimed at the identification of the fouling threshold for Alaskan crude oil. Their experiments featured an annular test cell with a heated inner rod, with bulk velocities in the range of 0.91 – 3.1 ms^{-1}, at two bulk temperatures of 149^{o}C and 204^{o}C and a range of surface temperatures. In order to determine the threshold surface temperature at which fouling occurred at a given velocity, the velocity was fixed and held constant. A test was initiated at a low surface temperature. If no fouling occurred in at least 24 hours, the heater surface temperature was increased by an incremental amount. This procedure was repeated until a surface temperature was reached at which fouling occurred. The threshold surface temperature for the initiation of fouling was considered to be between the surface temperature at which fouling occurred and the next lower temperature at which no fouling occurred.

2.4. Summary

In this chapter, a detail review on the fouling process has been done where discussion starts with the general overview of fouling process comprises of possible mechanism for fouling, fundamental steps involved as fouling proceeds and selected factors related to experiments in HLPS that influence fouling. Then, detail review on the fouling prediction model mostly related to crude oil system was done considering both mechanistic and empirical modeling. The interesting concept of 'threshold' condition for fouling is discussed by using available fouling threshold models and experimental data as reference.

CHAPTER 3

EXPERIMENTAL

3.1. Introduction

In this study, fouling experiments are carried out in a fouling rig called Hot Liquid Process Simulator (HLPS) using different types of crude oils. Experiments are conducted to determine the effect of surface temperature and crude blending to the fouling characteristics of selected crude oils. This chapter contains the important elements involved for the experimental work in which experimental setup, experimental procedure, methodology for fouling analysis and crude oils are discussed.

3.2. Experimental setup

Hot Liquid Process Simulator (HLPS) is used to conduct crude oil fouling experiment in this research work. This equipment is supplied by Alcor Inc. where it is specially designed for petroleum fouling research with extended flexibility and capabilities. Brons and Rudy (2002) describe the use of the Alcor Hot Liquid Process Simulator (HLPS) that is an electrically heated annular unit to determine fouling characteristics for different types of crude oils. The device was operated at fixed surface temperature with time in such that the amount of heat transferred to the liquid decreased as fouling took place. Fouling resistance is measured by the reduction in the rise of outlet bulk temperature of the oil passing through the unit. It is concluded that the HLPS unit is capable of determining relative fouling rates for different crude oils.

The snapshot of the HLPS unit used in this research work is shown in Plate 3.1 while the schematic diagram of HLPS in shown in Fig. 3.1:

Plate 3.1: Snapshot of HLPS unit

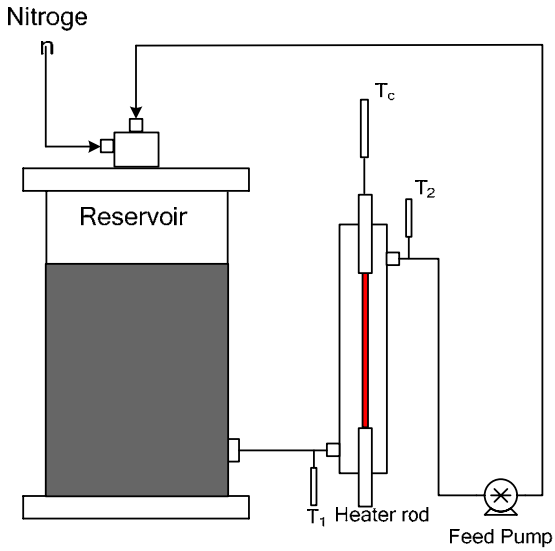

Fig. 3.1: Schematic diagram for HLPS unit

HLPS is used in this research work to study fouling characteristics for selected Malaysian crude oils. HLPS consists of several modules that have their own function and the modules are listed as follows:

1. Control Module
2. Base Assembly
3. Heated System

The controllers for HLPS unit are located in the Control Module. This module is used for flowrate and temperature control and also for temperature monitoring at different locations. The crude oil flowrate through the system is controlled using a flow rate control pot where the flowrate is controlled at 3 ml/min. A programmable digital time/temperature controller is used to control the temperature of the heater rod surface where a program scheme can be run and stop automatically according to the specified settings. Manual control fine adjust pot is provided to further refine the controller output of the digital controller. Two temperature indicators are provided for temperature monitoring purpose.

The Base Assembly is the unit where crude oil is circulated for the fouling experiment. The main components are the reservoir, bus bar tower and gear pump. The reservoir is a one litre capacity reservoir with a three way valve that is used to control the system pressure. The bus bars are the means by which the electric power is delivered to the heater rod to heat up the heater rod to a desired temperature. Modified zenith gear pump is used to circulate the crude oil through the system where it is capable of working reliably at high temperatures and pressures. The main process line is constructed using 1/8” tubing that could withstand high pressure and temperature.

Heated System comprises of two main components which are heated system tower and heated system operating components. Analog proportional relay controllers ranging from 0-200 ^{o}C are located at the heated system tower to manually control the temperature at different important locations of the system loop. Heated system operating components mainly consists of line heaters, reservoir jacket and pump jacket to electrically heat the lines, reservoir and gear pump respectively. Insulation ferrules are also provided to prevent metal to metal contact to the incoming and

outgoing lines of the pump and this will enable the electrical resistance heating to be effective in between the points where the insulation ferrules are placed.

Based on Fig. 3.1, a brief process description of the unit is explained. The unit is provided with a one litre capacity reservoir where the crude oil flows out of the reservoir through the outlet line at the lower side of the reservoir. The reservoir is equipped with a heater jacket that has velcro closure and thermocouple built into the inner wall. The crude oil then enters the most vital part of the unit which is the annular test section, at a controlled bulk temperature. The annular test section consists of heater rod that forms the annular geometry with the heater test section tube where the heater rod is electrically heated. The sketch of the annular heater test section together with its dimension is shown in Fig. 3.2. The crude flows out of the test section with a higher bulk temperature resulting from the heat being imparted to heat up the heater rod surface. A modified zenith gear pump is used to pump the oil back to the reservoir. Analog proportional relay controllers are used to control the temperature of reservoir heater jacket, pump heater jacket and line heater for the inlet line to the annular test section. Programmable digital controller is used to control the surface temperature of the heater rod. The recirculation of the crude oil through the system will continue until the experiment is finished.

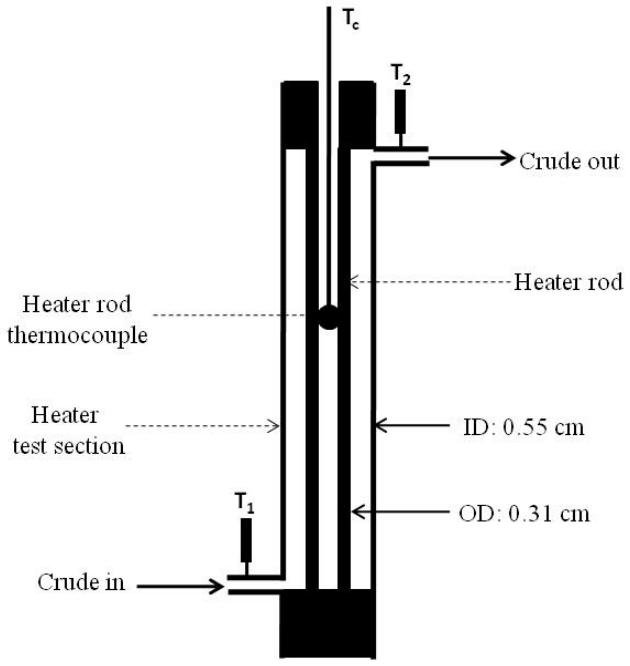

Fig. 3.2: Sketch of heater test section assembly of HLPS

The main features of HLPS can be summarized as Table 3.1.

Table 3.1: Main features for HLPS operation

Flowrate, ml/min	3
Velocity, m/s	0.003
Reynolds number	15 - 40
Operating pressure, bar	35
Mode of operation	Surface temperature control

3.3. Experimental procedure

The experimental procedure for the crude oil fouling experiment using HLPS involves sample preparation and fouling experiment.

For sample preparation, it is made sure that the crude is thoroughly mixed before a sample of required volume is taken. If crude blending is required, selected crude oils will be mixed simultaneously according to the required proportion.

For the fouling experiment, a new heater rod will be used for every experimental run. The heater rod will form the annular geometry with the heater test section and it is electrically heated to the desired temperature. Heater rod temperature is controlled at the hottest spot of the rod using programmable digital time/temperature controller. The reservoir is equipped with the magnetic stirrer to ensure that the crude oil is well-mixed throughout the experiment. Purified nitrogen gas is used to pressurize the system to the required pressure in order to suppress boiling at higher temperature operation. Gear pump is used to circulate crude oil throughout the whole process loop. Analog proportional relay controllers are used to control the inlet bulk temperature. When the system stabilizes, temperature values for bulk fluid inlet and outlet, reservoir, pump, incoming line and heater rod are recorded at different time interval. The aforementioned temperatures are recorded until the experimental duration finish. Upon completion of the experiment, the system is left for it to cool down to a reasonable temperature before disassembling the necessary parts. Toluene is then used to clean the whole system by re-circulating it through the system for several hours.

3.4. Methodology for fouling analysis

The raw data obtained from the fouling experiment is in the form of temperature variation with respect to time and space. This data need to be converted into the fouling resistance data over time where the initial fouling rate for each experiment conducted could be calculated. Method proposed by Watkinson (2004) is adopted to analyze the raw data into fouling resistance data over time.

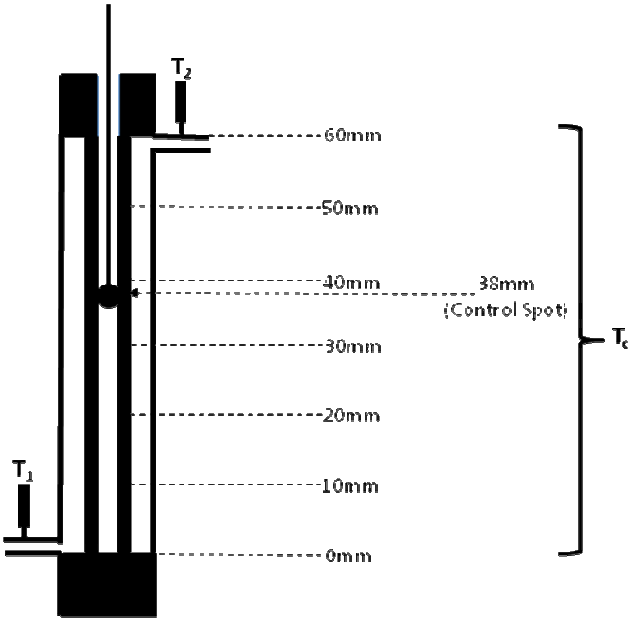

Fig. 3.3: Sketch for the location of readings taken at the heater test section assembly

Fig. 3.3 shows the readings taken for the heater test section assembly at different location where bulk (T_1 and T_2) and heater rod temperature (T_c) are taken. From the readings obtained, a plot of axial temperature profile for the heater rod temperature and the bulk fluid inlet and outlet temperature is made in order to determine the heat transfer coefficient. To determine the heat transfer coefficient under clean or fouled conditions, an appropriate driving force must be defined. As seen in Fig 3.5 below, axial surface temperatures were recorded over eight positions from z = 0 mm to z = 60 mm.

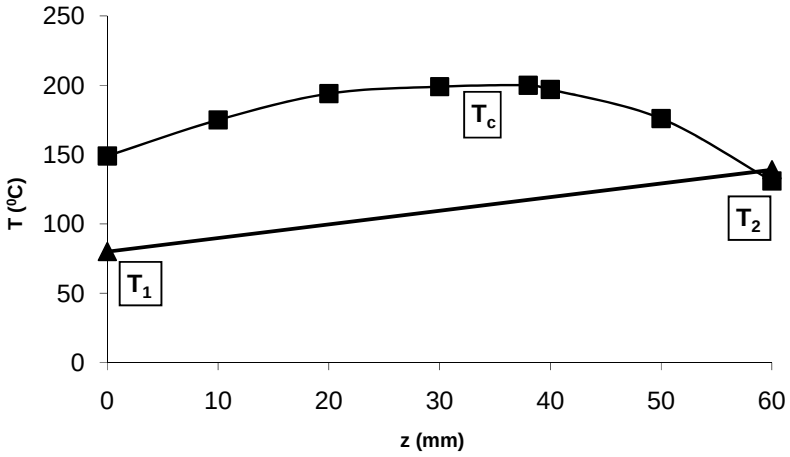

Fig. 3.4: Typical plot for HLPS experimental results at a particular time

For this research work, the average temperature driving force, ΔT_m, can be determined over the central six axial positions

$$\Delta T_m = \sum_{i=2}^{7} \left[T_c(z)_i - T_b(z)_i \right] / 6 \tag{3.1}$$

The two end sections each of 10 mm in length were eliminated from the calculations to eliminate entrance and exit effects. It is assumed that the bulk temperature varies linearly between the inlet and outlet and therefore the bulk temperature at different positions were determined using linear interpolation.

The heat flow, Q, is calculated using the following equation:

$$Q = mC_p \left(T_{b,z=50\,mm} - T_{b,z=10\,mm} \right) \tag{3.2}$$

and m is obtained by multiplying density, ρ with volumetric flow, V

Based on the known values of Q, A and ΔT_m, the overall heat transfer coefficient is given by:

$$U = Q / \left(A \times \Delta T_m \right) \tag{3.3}$$

Then the thermal fouling resistance value, R_f, at time t is calculated by:

$$R_f(t) = \frac{1}{U_t} - \frac{1}{U_0} \tag{3.4}$$

Eq. (3.4) circumvents calculating the film heat transfer coefficient and all the errors associated with each of its parameter and this implicitly assumes that the film heat transfer coefficient does not change as fouling proceeds (Bennet *et al.*, 2006). The results of this calculation will give the variation of R_f over the experimental duration. From this result, the initial fouling rate is determined based on the linear portion of the R_f versus time curve. The calculation for the initial fouling rate is illustrated in Fig. 3.5 for the experiment using Crude B at a surface temperature of 280°C.

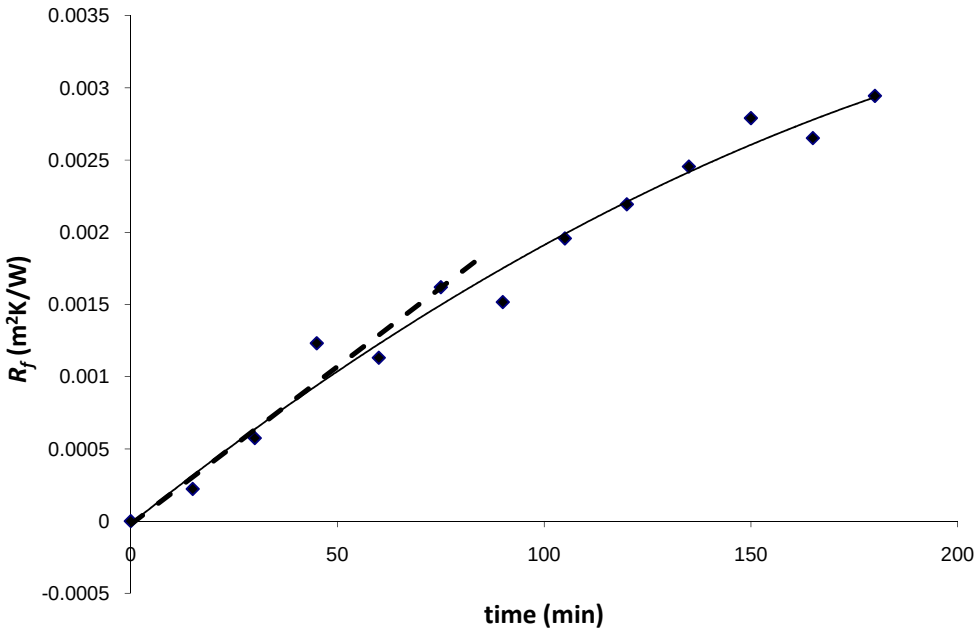

Fig. 3.5: Initial fouling rate calculation for R_f versus time plot

Based on the above plot, initial fouling rate is calculated based on the slope of the dotted line which is the slope of the linear portion of the R_f versus time curve considering no initiation period involved for the fouling process considered above. The initial fouling rate for the curve above is calculated to be 2.07 x 10^{-5} m^2K/Wmin.

In these fouling experiments, there is also possibility of an inverse response of the calculated fouling resistance plot as shown in Fig. 3.6.

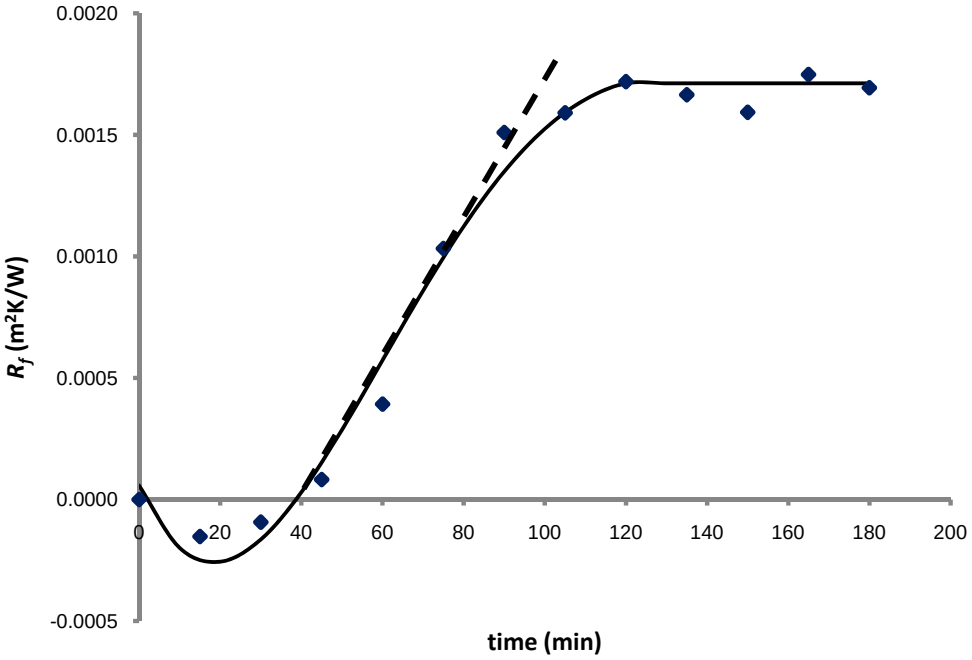

Fig. 3.6: Initial fouling rate calculation for the inverse response R_f versus time plot

An example of inverse response for R_f values is demonstrated by the experiment using Crude C at a surface temperature of 260 ^{o}C. For this plot, the initial fouling rate is determined by taking the positive linear slope of the plot shown as the dotted line in Fig. 3.6. The initial fouling rate for the curve above is calculated to be 2.68 x 10^{-5} m^2K/Wmin.

This procedure is performed for all experimental results to get the initial fouling rates for the experiment conducted at different surface temperature level for different crude and crude blends.

3.5. Crude oils

In this study, experiments are carried out with four Malaysian crude oils and a condensate. Physical properties of the selected crude and crude blends are extracted from a process simulation software where Advanced Peng-Robinson equation of state is used for properties estimation (PetroSim, version 3.1). The extracted properties are density, viscosity, thermal conductivity and mass heat capacity. The properties are taken at the operating pressure of HLPS and over a selected temperature range. In

addition to that, API Gravity is also included where the data is taken from the crude assay library. Selected physical properties are tabulated in Table 3.2.

Table 3.2: Physical properties of selected crude oils and condensate

Properties	Units	Crude A	Crude B	Crude C	Crude D	Condensate E
Crude type		Paraffinic	Naphthenic	Paraffinic	Naphthenic	Intermediate
API Gravity	-	46.5	32.7	45.2	36.2	60.4
Density @ 15^{o}C	kgm^{-3}	805.2	870.7	812.5	853.1	744.8
Viscosity @ 25^{o}C	Pas	$1.61x10^{-3}$	$3.91x10^{-3}$	$1.42x10^{-3}$	$2.27x10^{-3}$	$0.289x10^{-3}$
Thermal conductivity @ 15^{o}C	$W(m\ K)^{-1}$	$1.33x10^{-1}$	$1.46x10^{-1}$	$1.35x10^{-1}$	$1.40x10^{-1}$	$1.21x10^{-1}$
Specific heat @ 15^{o}C	$J(kg\ K)^{-1}$	1988.3	1760.4	1960.6	1802.9	2024.6

3.6. Summary

In this chapter, fouling rig used for this study which is HLPS, is discussed in detail where it includes the rig setup, experimental procedure used for fouling experiment and methodology used to analyze raw data from experiments. In addition to that, crude oils and condensate used for the experiments are listed together with selected physical properties of the crude oils and condensate.

CHAPTER 4

RESULTS AND DISCUSSIONS

4.1. Introduction

In this study, experiments are performed in HLPS using different types of crude oils to obtain experimental fouling data followed by further analysis on the experimental data. Several fouling threshold model are used to validate the experimental data. In this chapter, fouling experimental results will be reported and discussed in detail in terms of the effect of selected operating conditions on the fouling characteristics of different crude oils and crude blends. Analysis of the results will also involve the use of Arrhenius equation and different types of fouling threshold models that will be based on different methods for determination of physical properties of the flowing fluid.

4.2. Effect of surface temperature on the fouling characteristics of crudes and crude blends

Bott (1995) mentioned that chemical reaction can take place in the heat exchanger under the influence of temperature where the reaction does not involve heat transfer surface as a reactant. Crittenden (1984), who reviewed the effect of temperature on fouling, mentioned that higher the temperature the more likely for the fouling problem to be associated with chemical reactions. Crittenden (1984) also observed that there is generally a minimum temperature below which fouling will not proceed. Generally, an increase in temperature favours chemical reaction with an exponential increase in the rate constant with absolute temperature as represented by Arrhenius equation.

In order to study the surface temperature effect on the fouling characteristics, experiments were conducted at different surface temperatures for every crude oil and crude blend. The surface temperature range selected is based on the surface temperature range used in the heat exchanger post desalter in the refinery which the place where chemical reaction fouling is dominant. For each experiment, the surface temperature is maintained at a constant value and the indication of fouling process was monitored by the decrease in the outlet bulk temperature. The raw experimental data obtained is given in Appendix A. A total of 25 successful experimental runs conducted are listed in Table 4.1:

Table 4.1: Details of fouling experiments performed

Crude oil	**Blend Ratio (vol %)**	**Surface temperature tested (^{o}C)**
Crude A	100	220, 240, 260, 280
Crude B	100	220, 240, 260, 280
Crude C	100	220, 240, 260, 280
Crude D	100	220, 240, 260, 280
Crude A – Crude B	40 - 60	240, 260, 280
Crude A – Crude C	40 - 60	240, 260, 280
Crude A – Crude D	40 - 60	240, 260, 280

The experimental results for each experiment are then analyzed based on the method explained in Section 3.4. The results of the analysis will be in the form of fouling resistance, R_f variation over time and they are shown in Figs. 4.1 – 4.4 for neat crude oils. The calculated values for R_f variation over time are tabulated in Appendix B.

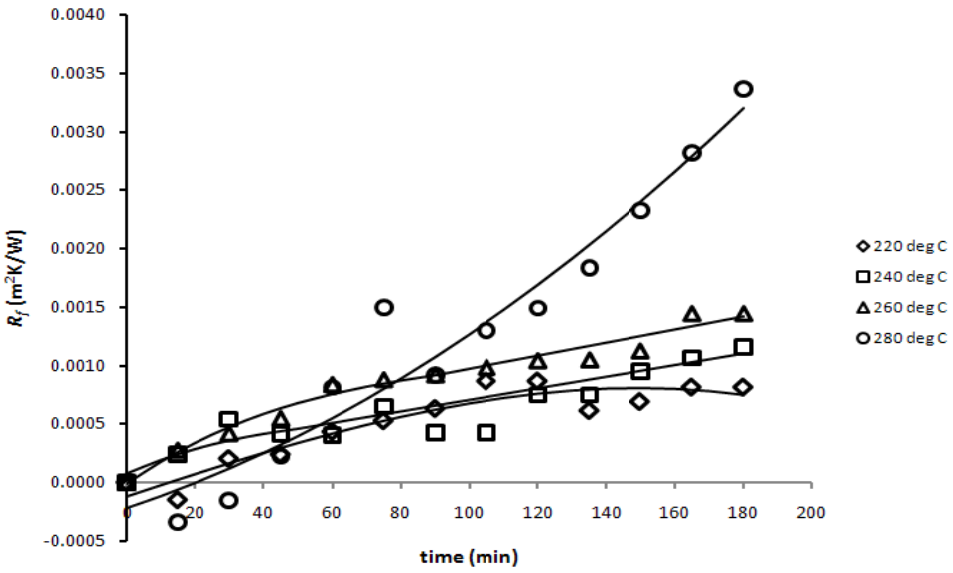

Fig. 4.1: R_f versus time graph for Crude A

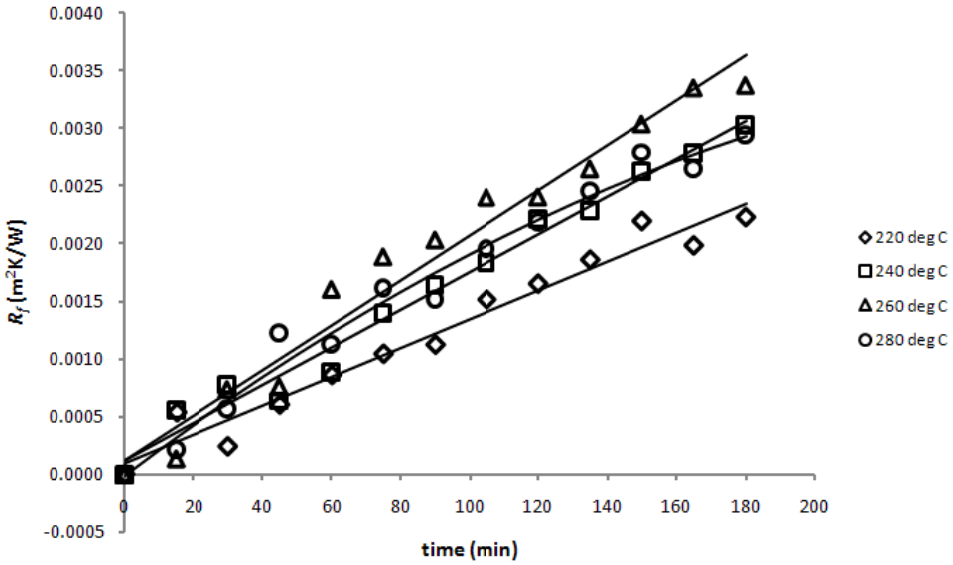

Fig. 4.2: R_f versus time graph for Crude B

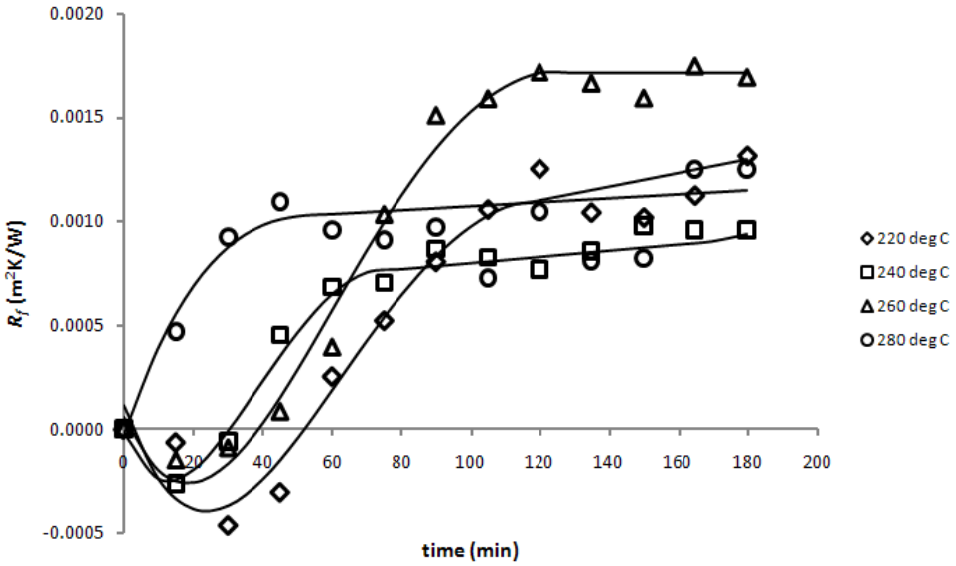

Fig. 4.3: R_f versus time graph for Crude C

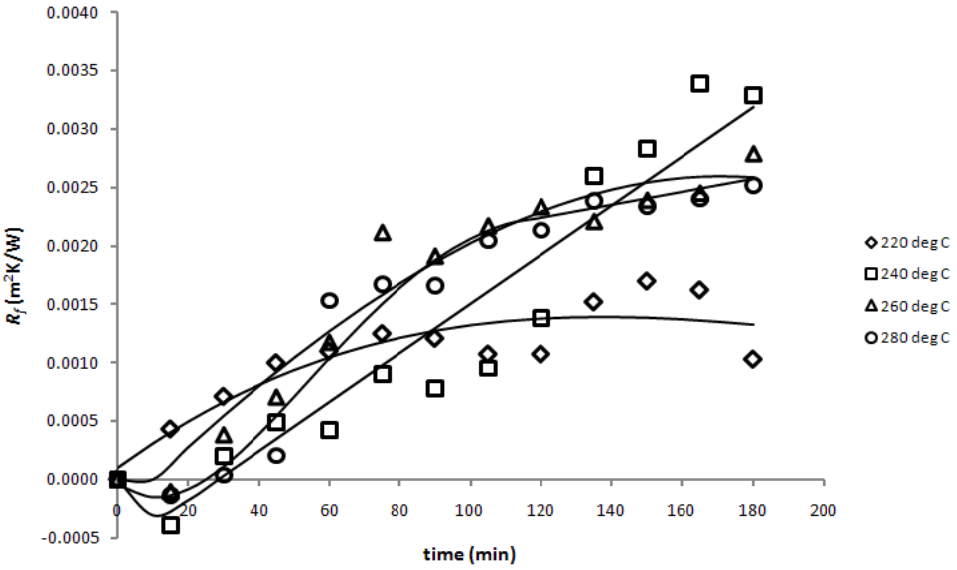

Fig. 4.4: R_f versus time graph for Crude D

Apart from the experiments conducted for neat crude oils, experiments were also carried out for the crude oil blends at different surface temperatures to see the effect of crude blending on the fouling characteristics. Mixing different types of crude is also found to be an important factor in managing crude oil fouling. Mixing typical paraffinic crude and asphaltenic crude can cause the asphaltenes to precipitate, giving rise to high fouling (ESDU, 2000b). The selection for the crude blends is based on the normal practice in the refinery processing this type of crude where Crude A is the

main diet for the refinery. Crude A will be blended with Crudes B, C and D in a ratio required to make sure that the products are within the specifications required. Results for the experiments conducted for crude blends at different surface temperatures are shown in Figs. 4.5 – 4.7.

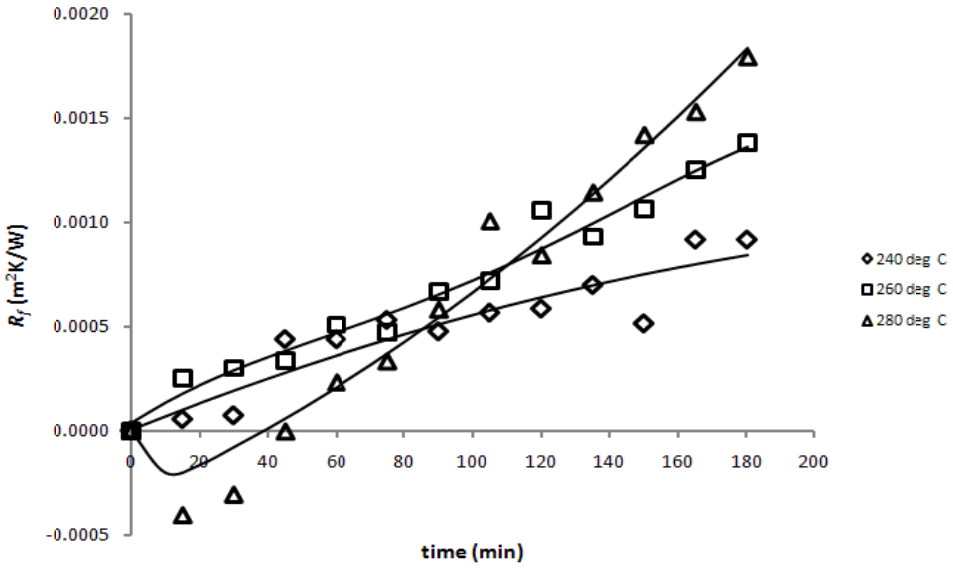

Fig. 4.5: R_f versus time graph for A-B (40-60%) blend

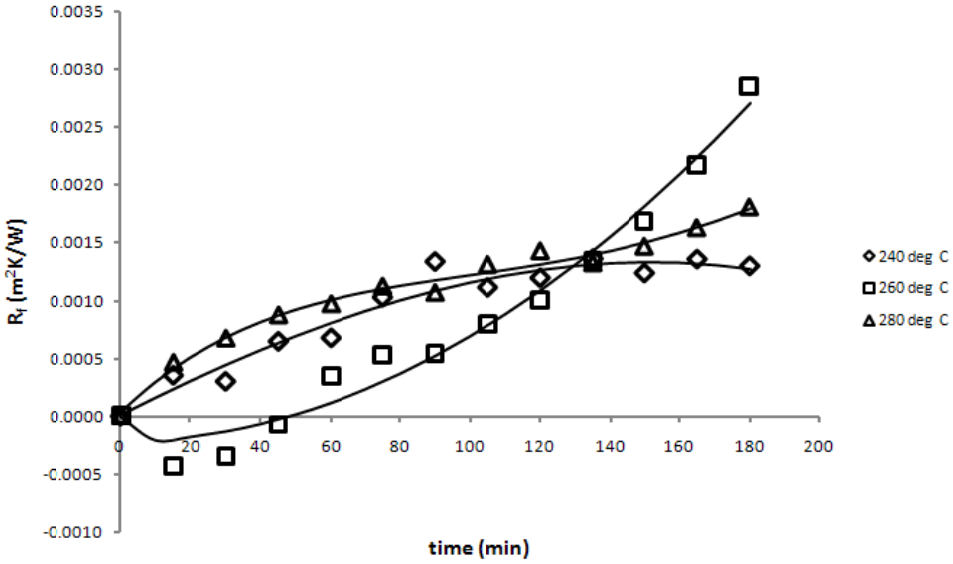

Fig. 4.6: R_f versus time graph for A-C (40-60%) blend

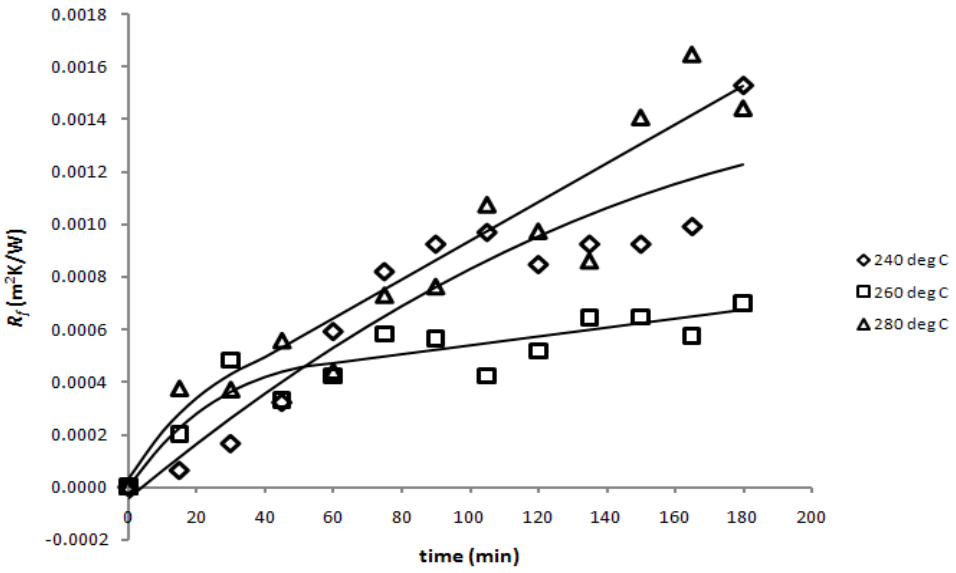

Fig. 4.7: R_f versus time graph for A-D (40-60%) blend

The initial fouling rates were determined from the slope of R_f versus time curves over the linear portion of the curve where the procedure is explained in detail in Section 3.4. For some of the data, the R_f value drop to a negative value first before it goes up again to give a positive slope. This happens due to the assumption of constant film heat transfer coefficient in the calculation of R_f values where the calculation consider the changes in overall heat transfer coefficient over time as fouling proceeds. Since fouling process typically roughen the heater rod surface, it will increase the film heat transfer coefficient and consequently negative fouling resistances are often observed until the fouling resistance surpasses the enhanced heat transfer (Bennet *et al.*, 2006). For each of the fouling resistance plots for neat crude and crude blends, it is observed that the fouling behavior of the crude is:

- Nearly linear increase in fouling resistance
- The rate of fouling, initially increases with time
- Once the fouling reaches a certain value, the rate of fouling decreases
- A decrease in the fouling rate resistance initially is observed and is due to the roughening effect of the fine deposit

The initial fouling rate is determined from the positive slope of the fouling resistance curve. The initial fouling rate values indicate the fouling tendency of crude and crude blends. The results for the initial fouling rates calculated for crude and crude blends at different surface temperatures are summarized in Tables 4.2 – 4.3.

Table 4.2: Initial fouling rates data for neat crude oils

Surface Temperature (^oC)	**Initial fouling rate, dR_f/dt (m^2K/Whr) x 10^4**			
	Crude A	**Crude B**	**Crude C**	**Crude D**
220	5.0289	7.5312	11.890	11.371
240	5.6524	9.8286	13.179	12.613
260	8.2883	11.729	16.098	15.604
280	9.2532	12.447	18.038	18.668

Table 4.3: Initial fouling rates data for crude blends

Surface Temperature (^oC)	**Initial fouling rate, dR_f/dt (m^2K/Whr) x 10^4**		
	A – B blend	**A – C blend**	**A – D blend**
240	3.6860	8.2425	5.4977
260	4.2609	9.1975	7.1705
280	5.5760	11.676	7.9492

The effect of surface temperature is clearly seen for each crude oil. In general, it is observed that the initial fouling rate increases with increasing surface temperatures and it follows the same trend for all crude oils and crude blends. For the neat crude oils, it observed that Crude D has the highest fouling tendency followed by Crude C, B and A based on the initial fouling rate values obtained for the surface temperature range tested. As for the blends, comparing with Crude A will be more sensible as Crude A being the main diet in the refinery. A-B blend shows a fouling tendency lower than the Crude A itself whilst A-C and A-D blends give a higher fouling tendency than Crude A.

By looking at the initial fouling rate range, it is shown that the values obtained are in the same magnitude as the data reported by Watkinson (2004) for experiment in HLPS using three different types of crude oils namely LSB, MDL and CLK. The reported data by Watkinson (2004) shows that the initial fouling rate values are in the range of 0.6 – 8.6 x 10^{-4} m^2K/Whr.

Epstein (1983a) stated that chemical reaction fouling mechanism for crude oil exhibit the common characteristics with other chemical reactions where the rate of reaction increases exponentially with temperature. Therefore, Arrhenius plot is used to determine the effect of temperature on the rate of fouling. The activation energy is determined by plotting the Arrhenius plot of $ln(dR_f/dt)$ versus $1/T$. For this research work, the plot is performed for film and surface temperatures to differentiate the effect of both film and surface temperatures on the initial fouling rates. The film temperature is determined by Eq. (4.1) proposed by Ebert and Panchal (1995):

$$T_f = T_b + 0.55\,(T_s - T_b) \tag{4.1}$$

The Arrhenius plots for crude and crude blends are shown in Figs. 4.8 – 4.9.

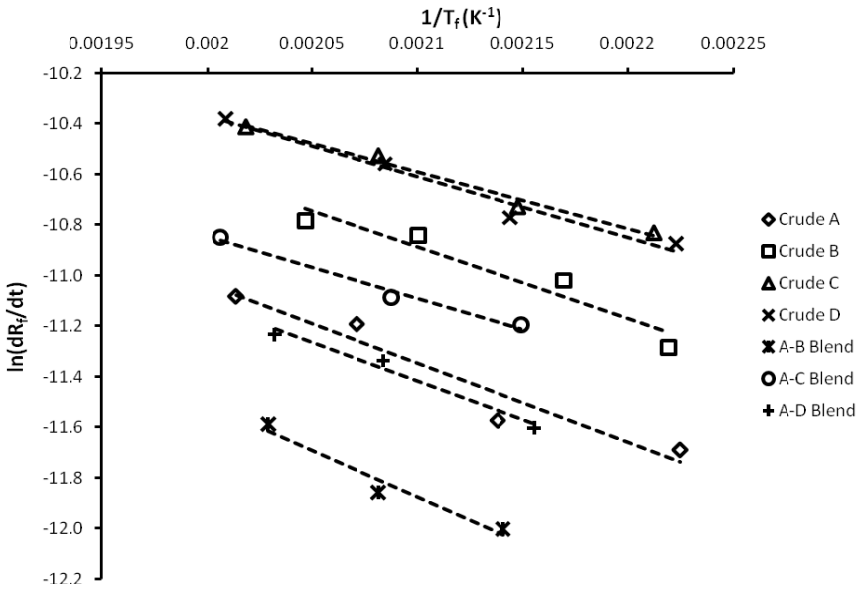

Fig. 4.8: Arrhenius plot for crude and crude blends based on film temperature

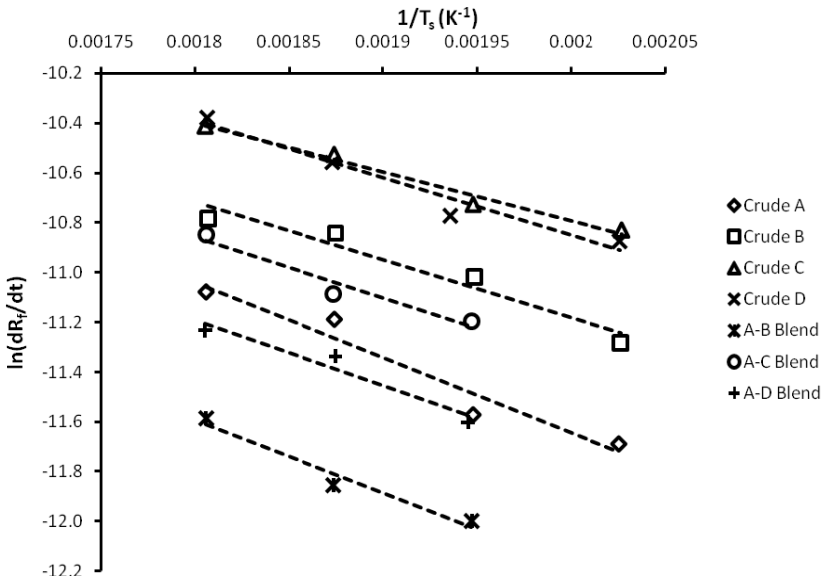

Fig. 4.9: Arrhenius plot for crude and crude blends based on surface temperature

Table 4.4: *E* values and corresponding initial fouling rates range for neat crude oils

Parameter		Crude A	Crude B	Crude C	Crude D
Initial fouling rate range (x 10^4)	m^2K/Whr	5 - 9	7 - 12	11 - 18	11 - 19
E (based on T_f)	kJ/mol	25.99	23.67	18.61	19.99
E (based on T_s)	kJ/mol	25.12	19.27	16.28	19.23

Table 4.5: *E* values and corresponding initial fouling rates range for crude blends

Parameter		A-B blend	A-C blend	A-D blend
Initial fouling rate range (x 10^4)	m^2K/Whr	3 - 6	8 - 12	5 - 8
E (based on T_f)	kJ/mol	30.68	20.48	25.28
E (based on T_s)	kJ/mol	24.26	20.39	21.97

Initial fouling rates and *E* values estimated using Arrhenius plot are tabulated in Tables 4.4 – 4.5. Based on physical justification and interpretation of the Arrhenius equation, lower *E* value contribute to the higher reaction rate due to less energy barrier to be surmounted for the molecules to react. The range of the *E* values obtained for this experiment is found to be lower than the reported *E* values in the literature for bigger scale fouling rig. Ebert and Panchal (1995) reported *E* value of 68 kJ/mol for Scarborough *et al.* (1979) data where the experiments were conducted at calculated film temperature of 370 – 400^{o}C and bulk velocity of 1.2 – 5.2 ms^{-1}. Saleh *et al.* (2004) reported *E* value of 42 kJ/mol for the experiment conducted at velocities

in the range of 0.25 to 0.65 ms^{-1} with surface temperatures from 180 – 260^{o}C and bulk temperature from 80 – 120^{o}C. For the fouling experiments conducted in same type of fouling rig, Watkinson (2004) reported *E* values for three different crude oils, namely MDL, LSB and CLK as 28, 36 and 38 kJ/mol respectively. Looking at the *E* values obtained in this experiment, it is lower than the one reported by Watkinson but it is still about the same range and magnitude. The slight difference may be due to the different type of crudes and operating conditions used for the experiments. The *E* values obtained are ranked as follows for the Arrhenius plot based on film and surface temperature.

***E* based on film temperature**

Neat crude

Crude C – 18.61 < Crude D – 19.99 < Crude B – 23.67 < Crude A – 25.99

Crude blend

A-C blend – 20.48 < A-D blend – 25.28 < A-B blend – 30.68

***E* based on surface temperature**

Neat crude

Crude C – 16.28 < Crude D – 19.23 < Crude B – 19.27 < Crude A – 25.12

Crude blend

A-C blend – 20.39 < A-D blend – 21.97 < A-B blend – 24.26

The reason for determining *E* values based on the film and surface temperatures is due to the assumption that the fouling reaction could occur at the film close to the wall or at the wall surface. This assumption is very important when considering the model prediction later because one of the basis for model prediction will be the reaction location for the fouling process where some researchers believe the reaction to be at the film close to wall while some believe it to happen at the wall surface itself. It is concluded that the crude with low values of *E* has a higher fouling

tendency than the crude with higher *E* value. The E values obtained are analyzed with the physical properties of the crude oils tabulated in Table 4.6.

Table 4.6: Crude oil properties related to crude oil fouling

Crude	E @ T_f	E @ T_s	Asphaltene	Wax	Iron	Vanadium	Nickel	Sulfur
	kJ/mol	kJ/mol	wt%	wt%	ppm	ppm	ppm	wt%
A	25.99	25.12	0.06	1.00	0.3	0.018	1.660	0.029
B	23.67	19.27	0.03	3.96	0.7	0.098	1.012	0.077
C	18.61	16.28	0.1	14.64	0.8	6.080	0.560	0.080
D	19.99	19.23	0.2	5.91	0.7	0.140	0.882	0.062

Wiehe (1997a) stated that aliphatic sulphur which is commonly found in crude oil is the most thermally reactive element in crude oil. Thus, breaking the carbon – sulphur bond will result in hydrogen sulphide and hydrocarbon free radicals that initiates the thermal cracking which also leads to the reaction with iron containing surfaces to form iron sulphide that is known to promote fouling. Vanadium, nickel and some iron can exist in crude oil as natural elements and corrosion products while corrosion products such as iron sulphide is one the most common foulant in crude preheat train (ESDU 2000b).

Crude C has been observed to contain the highest amount of iron, sulphur and vanadium and due to which the fouling tendencies of the crude is expected to be high. This is verified through the lowest E value obtained through the experiments. The wax content of Crude C has been found to be substantially higher in comparison to that in the other crude oils. This may also be a cause for the higher fouling propensity exhibited by Crude C. Crude A has been found to contain the lowest sulphur, iron, vanadium and wax which result in the least fouling tendencies with high *E* value.

For the crude blending, the *E* values obtained for the blends are compared to the *E* value of Crude A. *E* values for A-C and A-D blends are lower than the *E* value of Crude A as shown in Tables 4.4 and 4.5 and this is because the crude properties of the blends mostly resulted to be higher than the Crude A alone making it more fouling than Crude A itself. However for A-B blend, *E* value obtained is higher than Crude A and this is due to the properties of both neat crude A and B are quite balanced with B have higher amount of iron, vanadium and sulphur but lower in asphaltene and nickel. This has resulted in the blend that has lower fouling tendency than Crude A.

Furthermore, Crude B being the naphthenic type of crude when blended with Crude A that has higher asphaltene content do not promote asphaltene destabilization as compared to paraffinic crude. In terms of the compatibility of crude blending, A-B blend is observed to be the most compatible blend with the highest *E* value in comparison with the other blends that resulted in lowest fouling tendency.

Asomaning *et al.* (2000) stressed on the importance of having a model that could reasonably predict the fouling rates and the threshold conditions for the fouling process. Validation of the model with reliable experimental data is very crucial in determining the applicability of the model for certain fouling processes and conditions. In this research work, four types of threshold fouling models have been chosen to be validated with the experimental data obtained. The threshold fouling models used are all the aforementioned threshold models in Section 2.2.2 which are Ebert and Panchal model (Eq. 2.37), Panchal *et al.* model (Eq. 2.38), Polley *et al.* model (Eq. 2.39) and Nasr and Givi model (Eq. 2.41).

In addition to the above models, three different estimation methods were proposed for all the models which are (i) estimation method 1 - physical properties estimated at inlet bulk temperature, (ii) estimation method 2 - physical properties estimated at film temperature or surface temperature (for Polley *et al.* model only) and (iii) estimation method 3 – physical properties estimated at film temperature or surface temperature (for Polley *et al.* model only) plus the exclusion of removal term for all the models. In the original model proposed by Ebert and Panchal (1995), physical properties were estimated at the bulk temperature. Polley *et al.* (2002), in the critique of threshold fouling model mentioned that the use of film temperature may be more appropriate for the physical properties estimation. Therefore, physical properties estimation at film temperature was included as one of the estimation methods. It is also proposed to consider another method that is to exclude the removal term of the model due to the fact that the fluid shearing effect is considered to be very small where the flow regime for the flowing fluid is in the region of creeping or nearly laminar flow regime (Metals and Eckert, 1964).

Model parameters are estimated using least square technique to minimize the error between the predicted and experimental data. There are three model parameters that

are to be determined, α, γ and E. Values of E are fixed to the values obtained using Arrhenius plot where the E values obtained for a particular crude or crude blend is assumed to be the true activation energy of the crude or crude blend. Crittenden (2007) raised that the strong influence of velocity on the E value makes it impossible to evaluate the true activation energy and the term apparent activation energy is introduced to represent E value evaluated at certain crude velocity. Since the experiments in HLPS are conducted at a single crude velocity, the calculated values of E are assumed to be the true activation energy.

The other two parameters, α and γ are determined using least square technique by maximizing the coefficient of determination, R^2. The other assumptions used for the parameter estimation are:

1. Foulant thickness is considered negligible where its effect on crude velocity along the test section is very minimal

2. Bulk temperature of the crude varies linearly along the test section

Volumetric flowrate is maintained at a constant value throughout the experiment. Physical properties such as density, viscosity, thermal conductivity and mass specific heat capacity are extracted from process simulation software utilizing Advanced Peng-Robinson equation of state. For the estimation of wall shear stress, Fanning friction factor for laminar flow of Newtonian fluid in pipe represented by $16/Re$ is used. Constant β in $Re^{-\beta}$ term is assumed to be 0.66 which is a reasonable value for laminar flow conditions.

Based on the assumptions stated above, Solver function in Excel is used to perform least square procedure. The ultimate aim is to maximize the R^2 value based on the experimental data for initial fouling rate obtained at different surface temperatures. Based on Ebert and Panchal equation, Eq. (2.37) other than α and γ, the film temperature, T_f and physical properties need to be estimated An example of performing least square procedure using Ebert and Panchal (1995) equation is shown:

1. Film temperature, T_f is estimated using Eq. (2.9)

2. Physical properties for the Ebert and Panchal equation (1995) is estimated using the correlation established (temperature dependent) based on the properties extracted from simulation software and it is estimated either based on film, surface or bulk temperature. *Re* and τ_w are calculated based on the estimated physical properties.

3. Predicted values can then be obtained once physical properties and film temperature values have been obtained. α and γ values are estimated using Solver function by optimizing the objective function:

$$R^2 = 1 - \frac{\sum_i^n \left[\left(\frac{dRf}{dt} \right)_{\exp} - \left(\frac{dRf}{dt} \right)_{pred} \right]^2}{\sum_i^n \left[\left(\frac{dRf}{dt} \right)_{\exp} - \frac{1}{n} \sum_i^n \left(\frac{dRf}{dt} \right)_{\exp} \right]^2} \tag{4.2}$$

Apart from having a good R^2 value, the performance of the model prediction will be based on the following:

- The predicted trend should approach zero fouling rates as temperature decreases as shown in the experiment by Scarborough (1979)

- Applicability of the model in predicting fouling rates in the practical range of operating conditions

Ebert and Panchal (1995) estimated the model parameters for the experimental data by Scarborough (1979). The predicted trend by the model shows that fouling rates approaches zero as temperature decreases and this is expected to happen where the fouling rate should be zero when there is no fouling. Experiments by Scarborough were done at different crude velocities whilst in HLPS it is limited to one velocity only.

Applicability of the fouling model to predict the fouling rates is very appealing provided it could be used for a practical range of operating conditions (Ebert and Panchal, 1995). Practical range of operating condition is also a very

important issue to be considered. In the case of fouling experiments conducted in HLPS, the range for the applicability of the model prediction need to be determined. The upper range limit is defined as the boiling point for the test crude or crude blends where the boiling point is obtained from the prediction by a process simulation software utilizing Advanced Peng-Robinson equation of state. The boiling points for crudes and crude blends are tabulated in Appendix C. This is because the model is developed for prediction in single phase flow condition not two phase flow or boiling conditions. The mechanism for fouling under boiling conditions is known to be more complicated. The lower range limit is taken as the lowest possible temperature of the fluid which is the operational bulk temperature of 80^{o}C. In addition to that, Wax Appearing Temperature (WAT) or cloud point is also checked to see the possibility of wax appearing in the test crude and crude blends. This is to prevent other mechanisms of fouling process due to wax deposition to interfere with the chemical reaction fouling process. The WAT for all crude and crude blends are found to be less than the operational bulk temperature. So, operational bulk temperature is defined as the lower range limit for model prediction applicability. The list of WAT for all crude and crude blends is listed in Appendix D. The results for the models prediction are charted, tabulated and discussed. The results for Crude A are summarized in Table 4.7 and Figs. 4.10 – 4.12.

Table 4.7: Fouling model parameters and R^2 values for different models and estimation methods for Crude A

			Ebert Panchal	**Panchal *et al.***	**Polley *et al.***	**Nasr & Givi**
Estimation method 1	α	m^{2}K/Whr	1.9438	4.7187	2.0225	1.9433
	γ	m^{2}K/WhrPa	0.0020416	0.0020416	0	0.0000070
	R^2		**0.9404**	**0.9404**	**0.9456**	**0.9404**
Estimation method 2	α	m^{2}K/Whr	4.1909	9.1094	7.7124	5.0409
	γ	m^{2}K/WhrPa	0.0533040	0.0580250	0.0000541	0.0001002
	R^2		**0.9344**	**0.9319**	**0.9454**	**0.9373**
Estimation method 3	α	m^{2}K/Whr	3.5054	7.5084	4.0139	3.5054
	γ	m^{2}K/WhrPa	0	0	0	0
	R^2		**0.8726**	**0.8609**	**0.8283**	**0.8726**

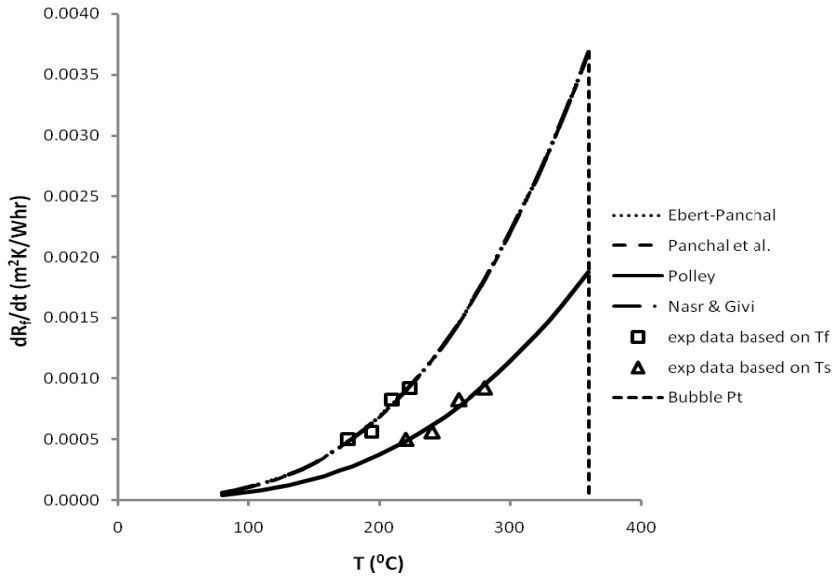

Fig. 4.10: Comparison of experimental and predicted data by the model estimated using estimation method 1 for Crude A

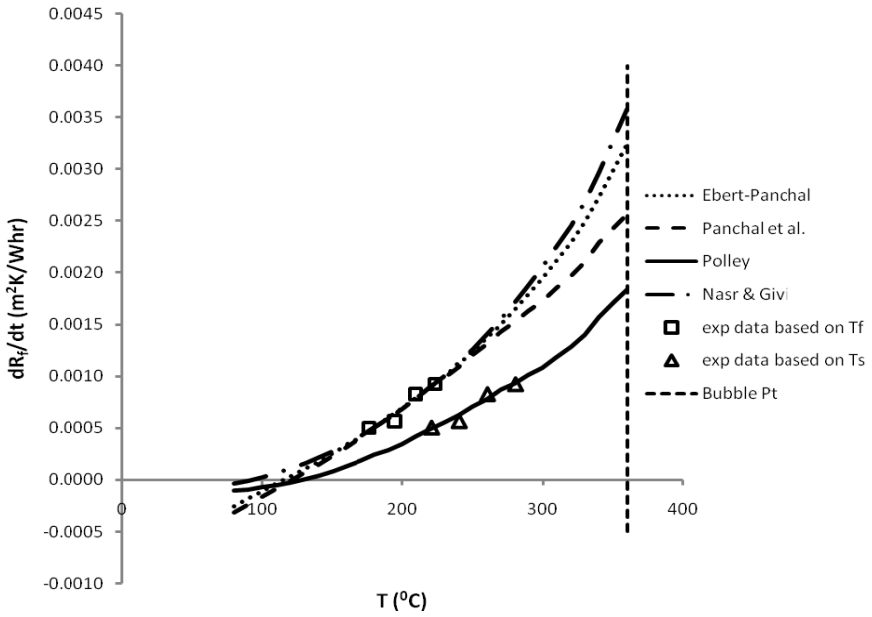

Fig. 4.11: Comparison of experimental and the predicted data by the model estimated using method 2 for Crude A

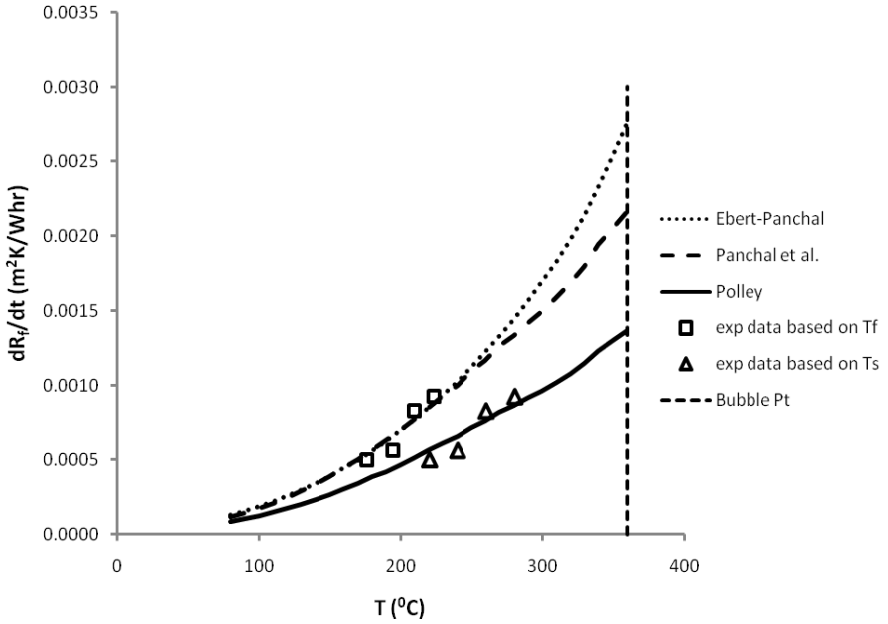

Fig. 4.12: Comparison of experimental and the predicted data by the model estimated using method 3 for Crude A

Since the model prediction for other crude oils and crude blends is observed to demonstrate almost similar trend as Crude A, the results for other crude oils and crude blends are shown in the following Table 4.8 – 4.13 and Figure 4.13 – 4.30 with the results are discussed later.

Table 4.8: Fouling model parameters and R^2 values for different models and estimation methods for Crude B

			Ebert Panchal	**Panchal *et al.***	**Polley *et al.***	**Nasr & Givi**
Estimation method 1	α	m^2K/Whr	1.3068	3.4398	0.6672	1.3068
	γ	$m^2K/WhrPa$	0	0	0	0
	R^2		**0.9139**	**0.9139**	**0.9327**	**0.9139**
Estimation method 2	α	m^2K/Whr	3.6075	6.7559	1.4247	5.1060
	γ	$m^2K/WhrPa$	0.0782188	0.0534764	0.0000019	0.0002611
	R^2		**0.9389**	**0.9355**	**0.7944**	**0.9316**
Estimation method 3	α	m^2K/Whr	2.8959	5.7882	1.3937	2.8959
	γ	$m^2K/WhrPa$	0	0	0	0
	R^2		**0.8296**	**0.8774**	**0.7936**	**0.8296**

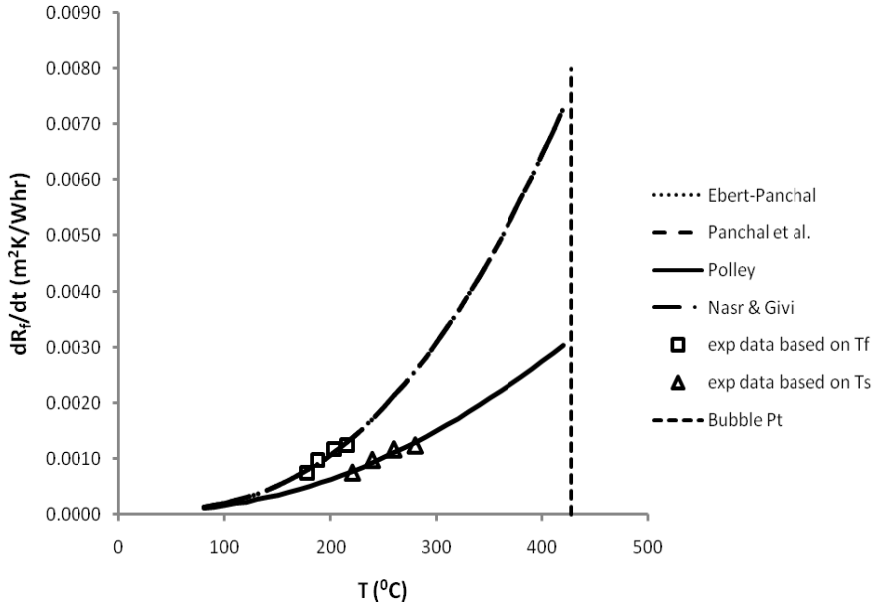

Fig. 4.13: Comparison of experimental and the predicted data by the model estimated using method 1 for Crude B

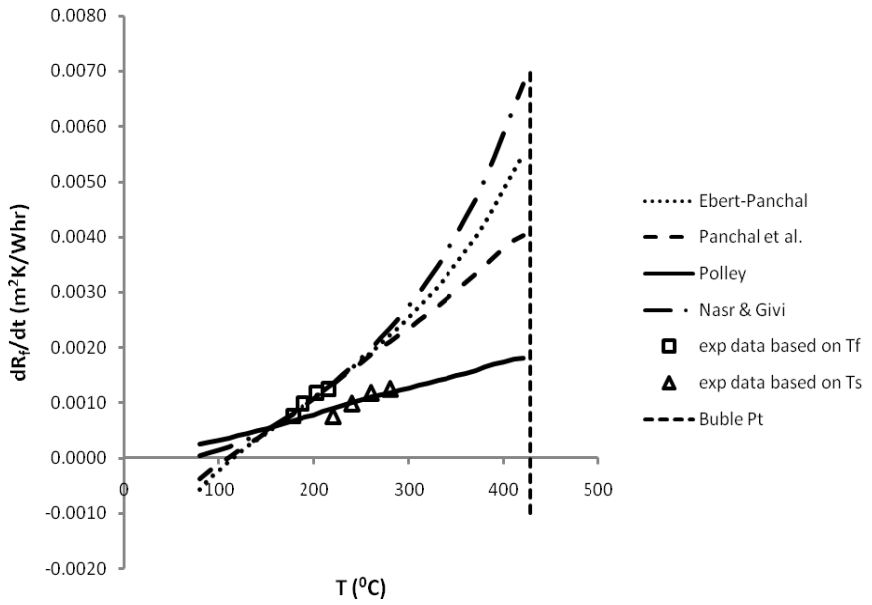

Fig. 4.14: Comparison of experimental and the predicted data by the model estimated using method 2 for Crude B

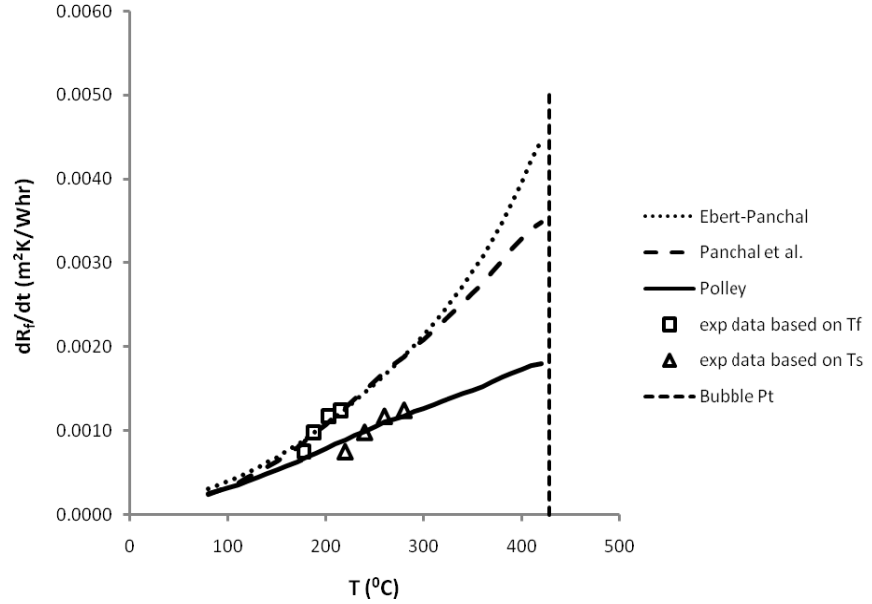

Fig. 4.15: Comparison of experimental and the predicted data by the model estimated using method 3 for Crude B

Table 4.9: Fouling model parameters and R^2 values for different models and estimation methods for Crude C

			Ebert Panchal	**Panchal *et al.***	**Polley *et al.***	**Nasr & Givi**
Estimation method 1	α	m^2K/Whr	0.9147	1.8419	0.6834	0.9147
	γ	$m^2K/WhrPa$	0	0	0	0
	R^2		**0.8961**	**0.8961**	**0.9161**	**0.8961**
Estimation method 2	α	m^2K/Whr	2.0853	3.3036	2.1749	2.6440
	γ	$m^2K/WhrPa$	0.1135468	0.0924401	0.0000421	0.0001305
	R^2		**0.9191**	**0.9149**	**0.8876**	**0.9245**
Estimation method 3	α	m^2K/Whr	1.8626	3.0109	1.3050	1.8626
	γ	$m^2K/WhrPa$	0	0	0	0
	R^2		**0.8814**	**0.8890**	**0.8300**	**0.8814**

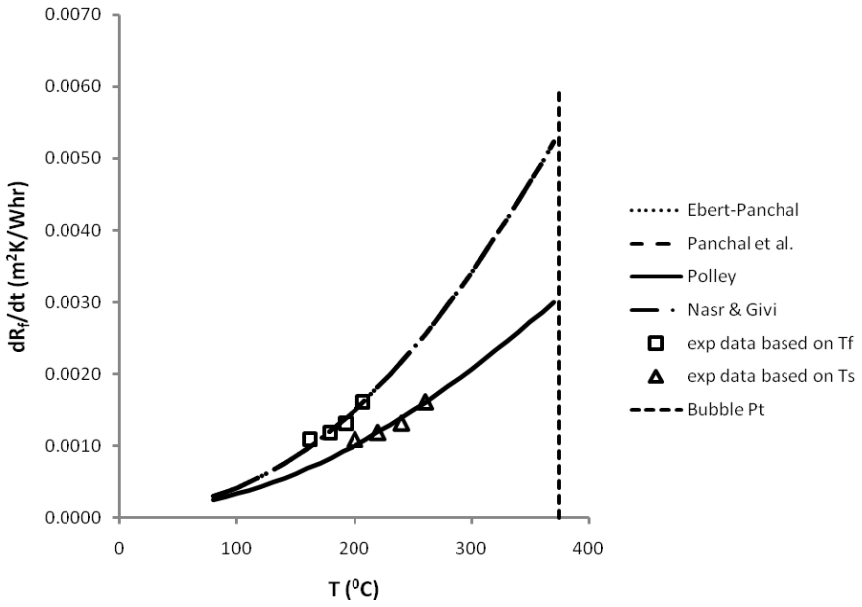

Fig. 4.16: Comparison of experimental and the predicted data by the model estimated using method 1 for Crude C

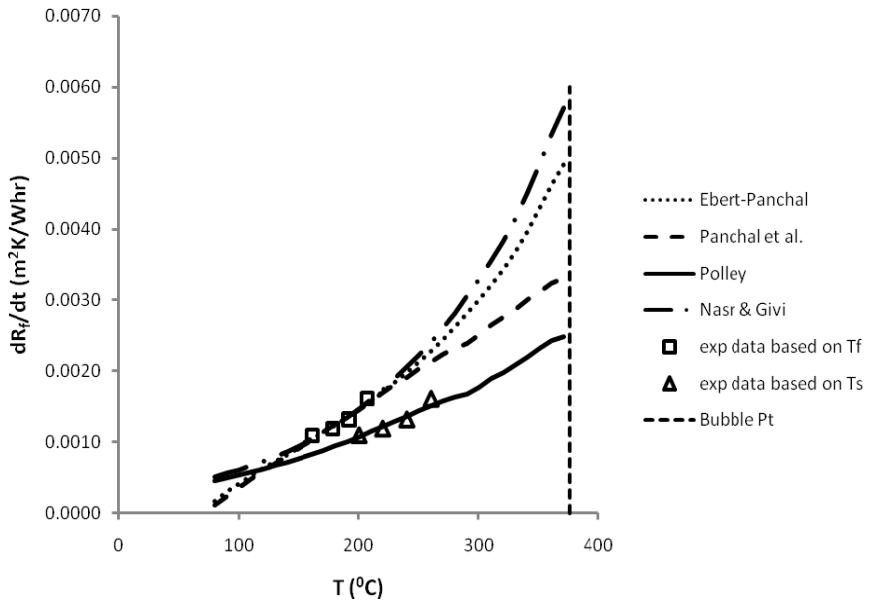

Fig. 4.17: Comparison of experimental and the predicted data by the model estimated using method 2 for Crude C

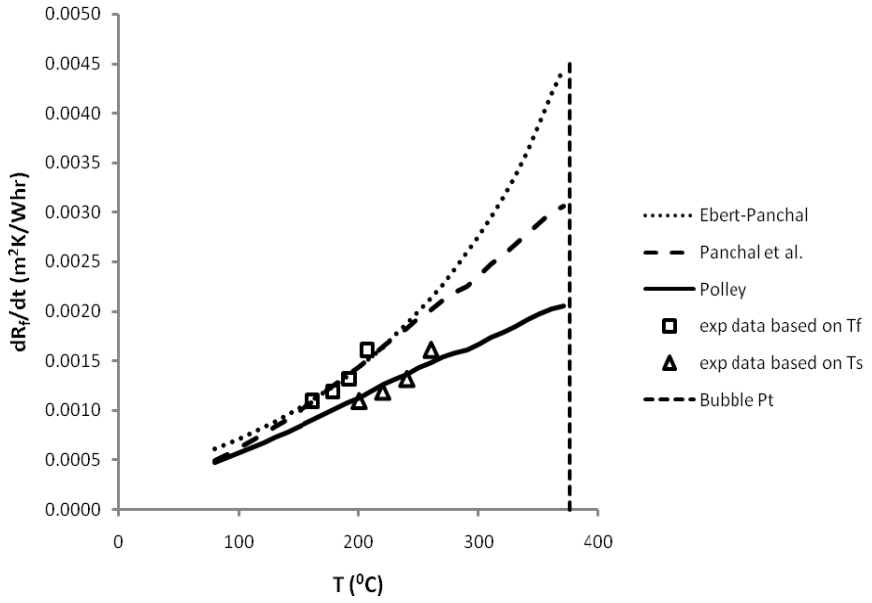

Fig. 4.18: Comparison of experimental and the predicted data by the model estimated using method 3 for Crude C

Table 4.10: Fouling model parameters and R^2 values for different models and estimation methods for Crude D

			Ebert Panchal	**Panchal *et al.***	**Polley *et al.***	**Nasr & Givi**
Estimation method 1	α	m^2K/Whr	0.8425	2.0427	1.0656	0.8378
	γ	$m^2K/WhrPa$	0.0035994	0.0035990	0.0000123	0.0000100
	R^2		**0.9776**	**0.9776**	**0.9648**	**0.9775**
Estimation method 2	α	m^2K/Whr	2.1639	4.1037	7.6227	3.4183
	γ	$m^2K/WhrPa$	0.1566651	0.1302627	0.0002959	0.0004633
	R^2		**0.9651**	**0.9651**	**0.8916**	**0.9708**
Estimation method 3	α	m^2K/Whr	1.6833	3.3185	2.0487	1.6833
	γ	$m^2K/WhrPa$	0	0	0	0
	R^2		**0.8210**	**0.8575**	**0.7483**	**0.8210**

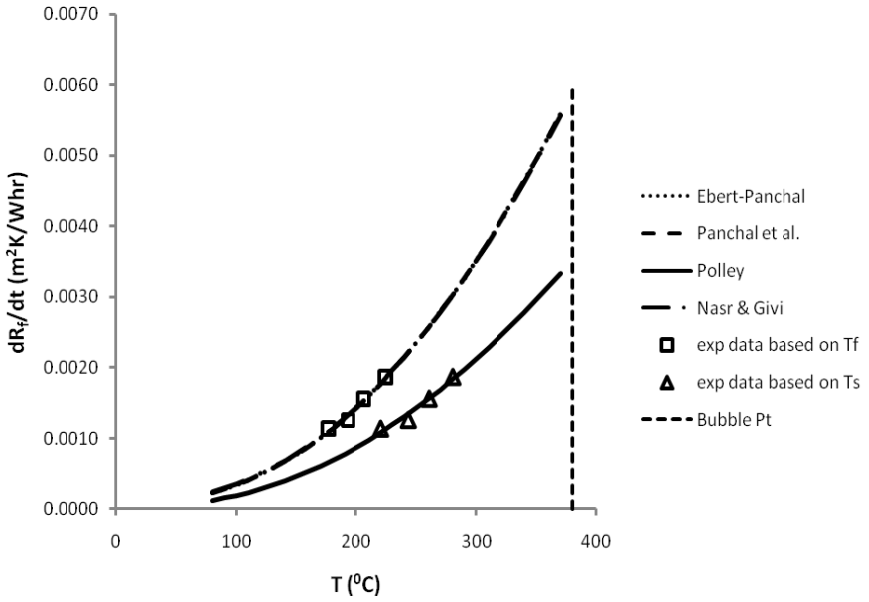

Fig. 4.19: Comparison of experimental and the predicted data by the model estimated using method 1 for Crude D

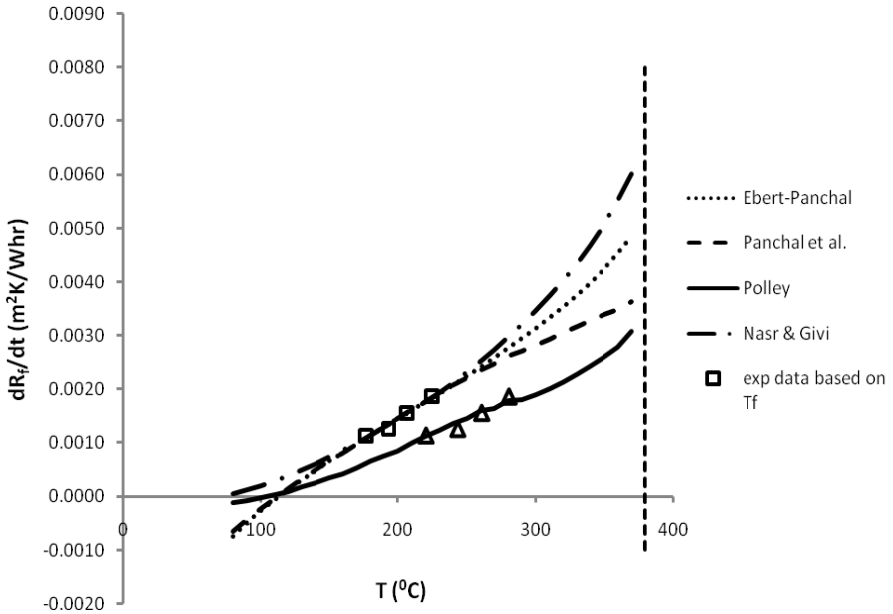

Fig. 4.20: Comparison of experimental and the predicted data by the model estimated using method 2 for Crude D

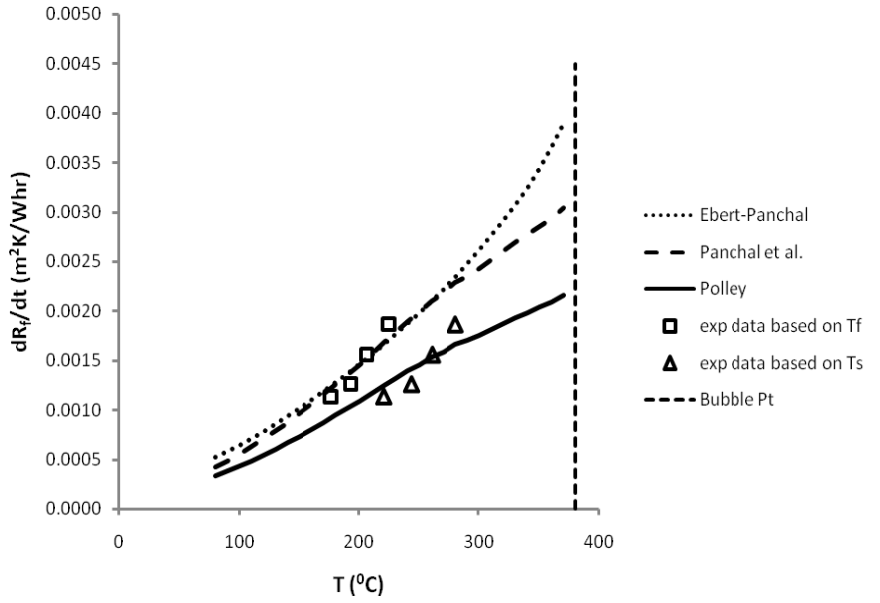

Fig. 4.21: Comparison of experimental and the predicted data by the model estimated using method 3 for Crude D

Table 4.11: Fouling model parameters and R^2 values for different models and estimation methods for A-B blend

			Ebert Panchal	**Panchal *et al.***	**Polley *et al.***	**Nasr & Givi**
Estimation method 1	α	m^2K/Whr	3.2668	8.3373	0.8560	3.1552
	γ	$m^2K/WhrPa$	0.0015954	0.0015935	0.0000007	0.0000002
	R^2		**0.9621**	**0.9621**	**0.9328**	**0.9609**
Estimation method 2	α	m^2K/Whr	8.2204	16.3822	1.7208	6.6120
	γ	$m^2K/WhrPa$	0.0361538	0.0302533	0	0.0000007
	R^2		**0.9524**	**0.9528**	**0.6300**	**0.8692**
Estimation method 3	α	m^2K/Whr	6.7163	13.8002	1.8519	6.7163
	γ	$m^2K/WhrPa$	0	0	0	0
	R^2		**0.8813**	**0.8999**	**0.7966**	**0.8813**

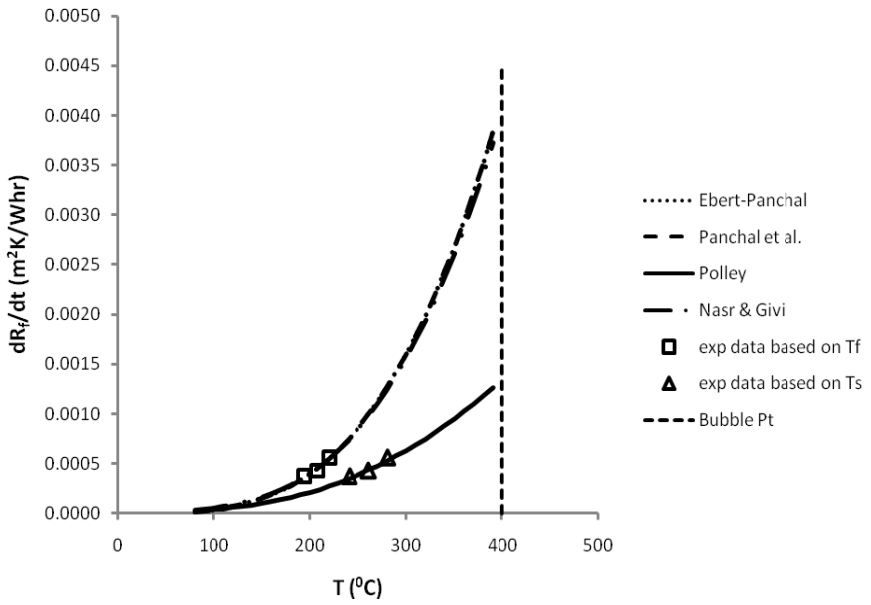

Fig. 4.22: Comparison of experimental and the predicted data by the model estimated using method 1 for A-B blend

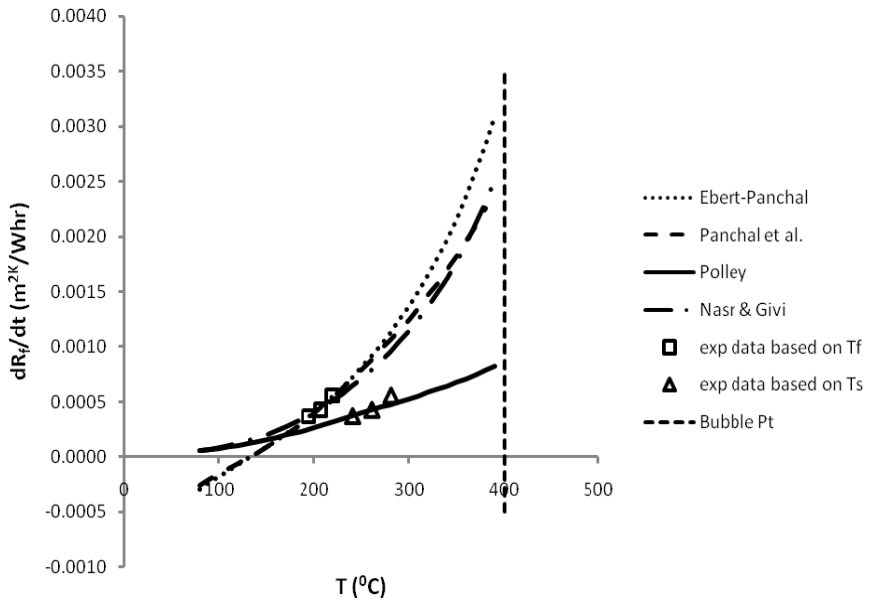

Fig. 4.23: Comparison of experimental and the predicted data by the model estimated using method 2 for A-B blend

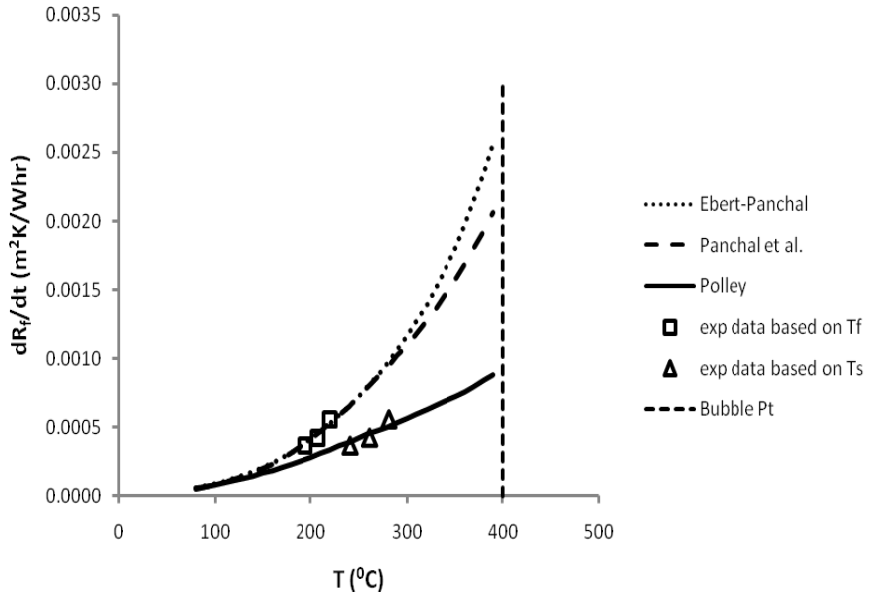

Fig. 4.24: Comparison of experimental and the predicted data by the model estimated using method 3 for A-B blend

Table 4.12: Fouling model parameters and R^2 values for different models and estimation methods for A-C blend

			Ebert Panchal	**Panchal *et al.***	**Polley *et al.***	**Nasr & Givi**
Estimation method 1	α	m^2K/Whr	0.7834	1.6854	1.0003	1.0003
	γ	$m^2K/WhrPa$	0.0032722	0.0032722	0.0000037	0.0001135
	R^2		**0.9851**	**0.9851**	**0.9502**	**0.9095**
Estimation method 2	α	m^2K/Whr	2.0781	3.6585	4.6031	2.8142
	γ	$m^2K/WhrPa$	0.1697457	0.1729296	0.0000602	0.0001688
	R^2		**0.9779**	**0.9753**	**0.9124**	**0.9810**
Estimation method 3	α	m^2K/Whr	1.6562	2.9044	2.0793	1.6562
	γ	$m^2K/WhrPa$	0	0	0	0
	R^2		**0.8680**	**0.8623**	**0.7494**	**0.8680**

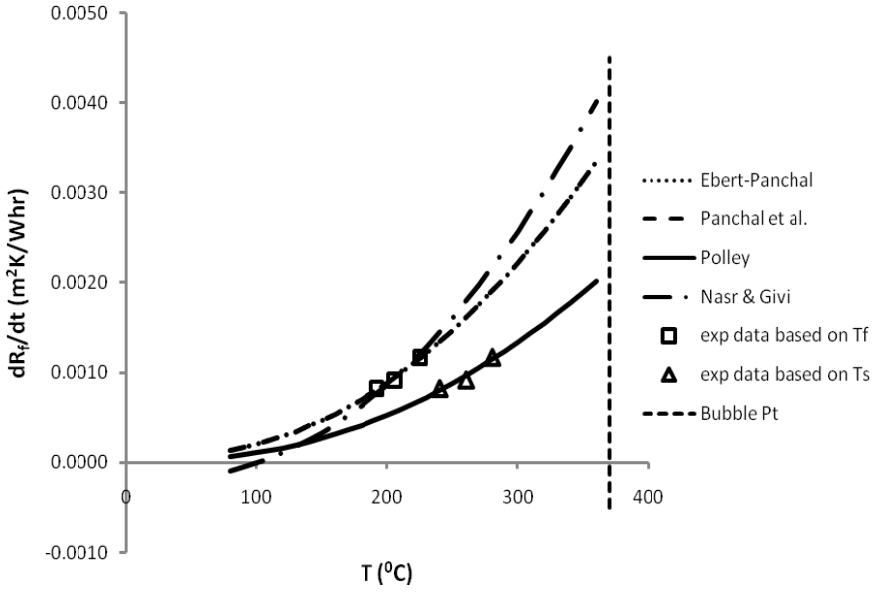

Fig. 4.25: Comparison of experimental and the predicted data by the model estimated using method 1 for A-C blend

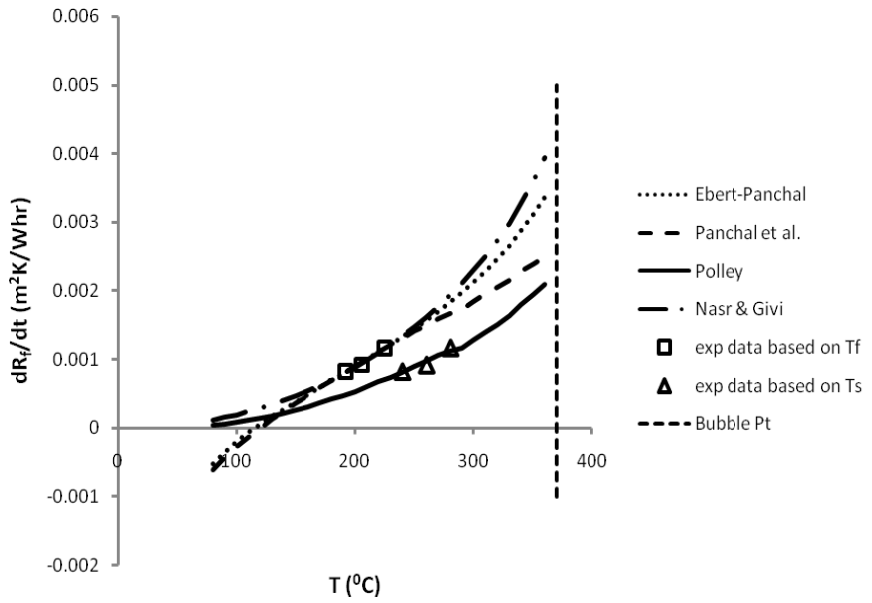

Fig. 4.26: Comparison of experimental and the predicted data by the model estimated using method 2 for A-C blend

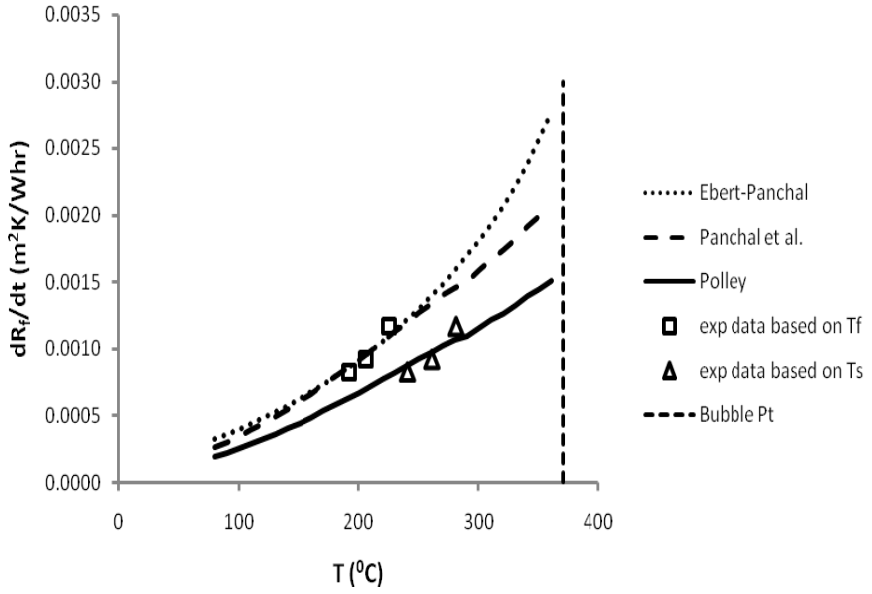

Fig. 4.27: Comparison of experimental and the predicted data by the model estimated using method 3 for A-C blend

Table 4.13: Fouling model parameters and R^2 values for different models and estimation methods for A-D blend

			Ebert Panchal	**Panchal *et al.***	**Polley *et al.***	**Nasr & Givi**
Estimation method 1	α	m^2K/Whr	1.4249	3.4591	0.8560	1.4281
	γ	$m^2K/WhrPa$	0	0	0.0000007	0.0000007
	R^2		**0.9712**	**0.9712**	**0.9339**	**0.9711**
Estimation method 2	α	m^2K/Whr	3.3976	6.7426	5.2042	4.1354
	γ	$m^2K/WhrPa$	0.0539579	0.0464025	0.0001016	0.0000980
	R^2		**0.9792**	**0.9796**	**0.9689**	**0.9766**
Estimation method 3	α	m^2K/Whr	2.8263	5.7450	1.7466	2.8263
	γ	$m^2K/WhrPa$	0	0	0	0
	R^2		**0.9081**	**0.9244**	**0.7943**	**0.9081**

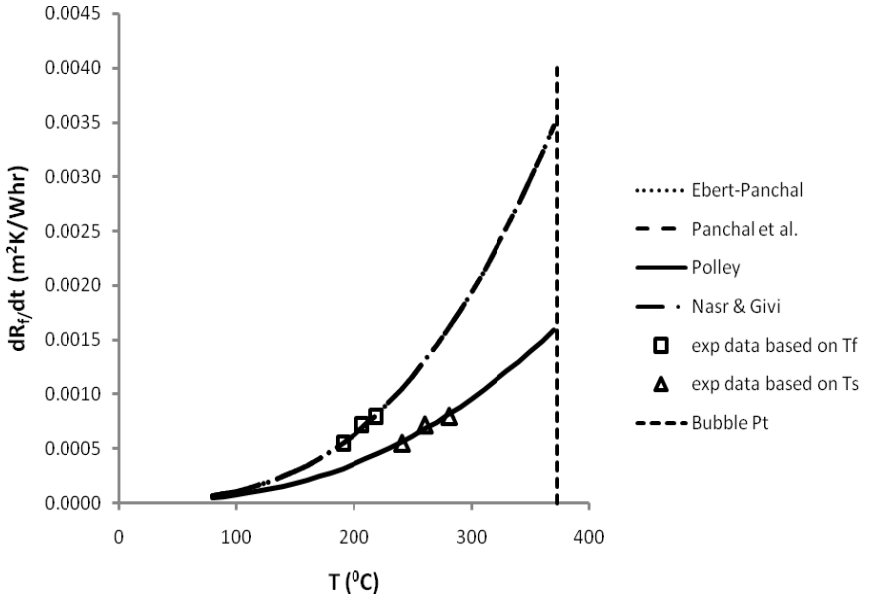

Fig. 4.28: Comparison of experimental and the predicted data by the model estimated using method 1 for A-D blend

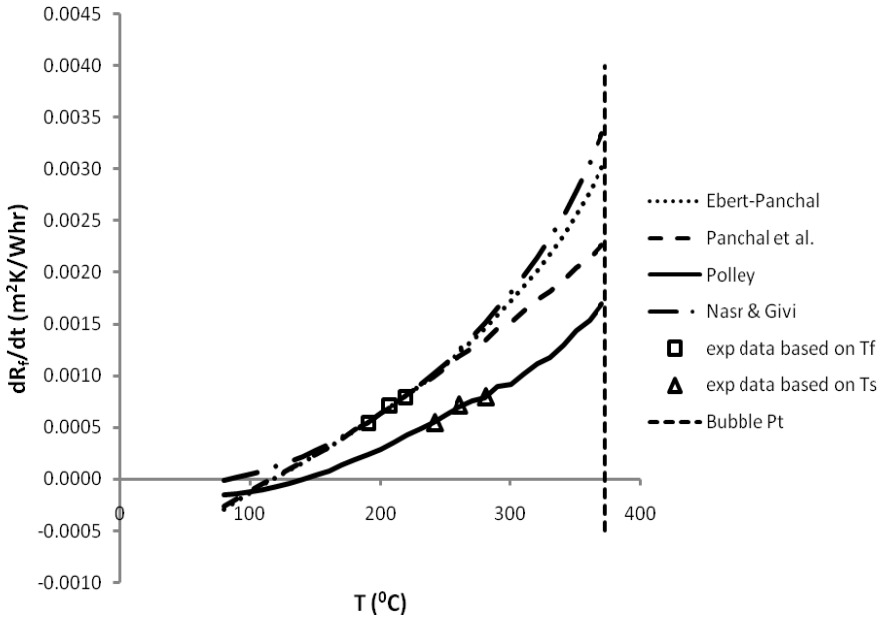

Fig. 4.29: Comparison of experimental and the predicted data by the model estimated using method 2 for A-D blend

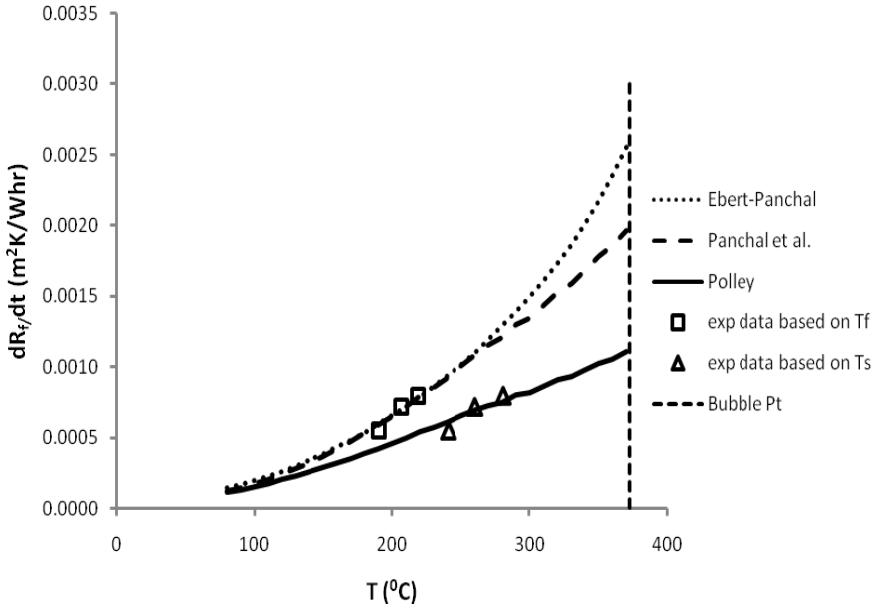

Fig. 4.30: Comparison of experimental and the predicted data by the model estimated using method 3 for A-D blend

It could be seen from Table 4.7 – 4.13 that the R^2 values for the model prediction using estimation method 1 for all threshold models generally give a better R^2 value of more than 0.9. This indicates that the estimation of the physical propeties for threshold models should be based on bulk temperature rather than surface temperature. Estimation method 3 that exclude the suppression term generally gives the worst R^2 value considering all threshold models and this indicates the need for inclusion of suppression term even though the suppression constant is estimated to be very small for all models. Furthermore, as mentioned earlier good model prediction also includes other criteria and this could be seen from the model prediction plot for all estimation method which is Figure 4.10 – 4.30. In term of the trend of model prediction at low temperature, estimation method 1 and 2 consistently shows the trend is approaching zero for almost all threshold models and this is expected to happen as demonstrated by Scarborough (1979) where fouling rates should approach zero as temperature decreases. On contrary, estimation method 3 shows that the trend is giving or approaching negative value for all threshold models considered and this is untrue as no fouling is represented by zero fouling rates and it could not reach negative value. For the practical operating range determined for each crude and crude blends, prediction in the defined range for estimation method 1 shows a very consistent prediction for all threshold models in comparison with other estimation method. It could also be seen that suppression constant is actually zero for some cases for estimation method 1 and 2 suggesting that the effect of flow velocity in suppressing fouling process is negligible due to low flow velocity for HLPS experiment.

In general, it is observed that the model prediction using estimation method 1 give a better prediction in comparison with model prediction using estimation methods 2 and 3. This is concluded based on (i) better R^2 values obtained during the model parameter estimation, (ii) fouling rates approaching zero at lower temperature without going to negative value and (iii) reasonably good and consistent prediction trend over the defined practical operating condition range. Again, this indicates that the physical properties of the flowing fluid should be evaluated at the bulk temperature rather than the film or surface temperatures. But the temperature dependent Arrhenius-like term of the model should be evaluated at the film or surface temperature depending on where the reaction is assumed to occur. From model applicabilty point of view, the

practical operating condition range defined is acceptable but the prediction accuracy beyond the experimental data points may still requires more experiments to be performed in that region.

4.3. Effect of blending with condensate on the fouling characteristics

Mixing typical paraffinic crudes or condensate and asphaltenic crudes can cause the asphaltenes to precipitate and subsequently increases the fouling rates. This may limit the amount of condensate that can be mixed with crude blend (ESDU, 2000b). Based on this statement, another investigation is done to determine the effect of mixing condensate with crude oil on the fouling characteristics. Since the previous practice in the refinery shows that fouling propensity significantly increase with the addition of condensate, an experiment for crude – condensate blend is performed to see the effect of blending to the fouling characteristics of the crude oil. Condensate alone is not being process in the refinery and it is decided not to test the fouling characteristics of condensate. However, only one crude – condensate blend is being tested to confirm the above statement with the fouling rates obtained being compared with the neat crude. Experiments were conducted using 50 – 50 vol% of Condensate E - Crude C blend. The fouling resistance versus time data for the experiments conducted at different surface temperatures is shown in Fig. 4.31.

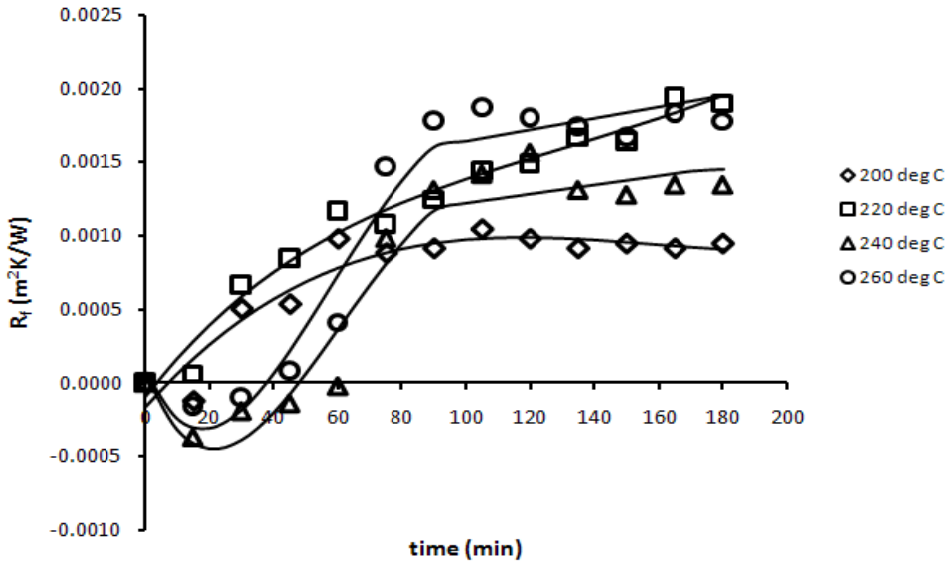

Fig. 4.31: R_f versus time graph for Condensate E – Crude C blend

The initial fouling rates data for each surface temperature are then determined based on the same procedure for the crude and crude blends and the results are summarized in Table 4.14.

Table 4.14: Initial fouling rates data for Condensate E – Crude C blend

Surface temperature (^oC)	**Initial Fouling Rates (m^2K/Whr) x 10^3**
200	1.2688
220	1.4194
240	1.5549
260	1.7699

Analysing the initial fouling rates for the tested surface temperature range, it shows that the fouling rates is higher than the fouling rates obtained for the crude and crude blends for the same temperature range. First observation on the experimental data shows that the condensate-crude oil blend has higher tendency to foul in comparison with the crude and crude blends.

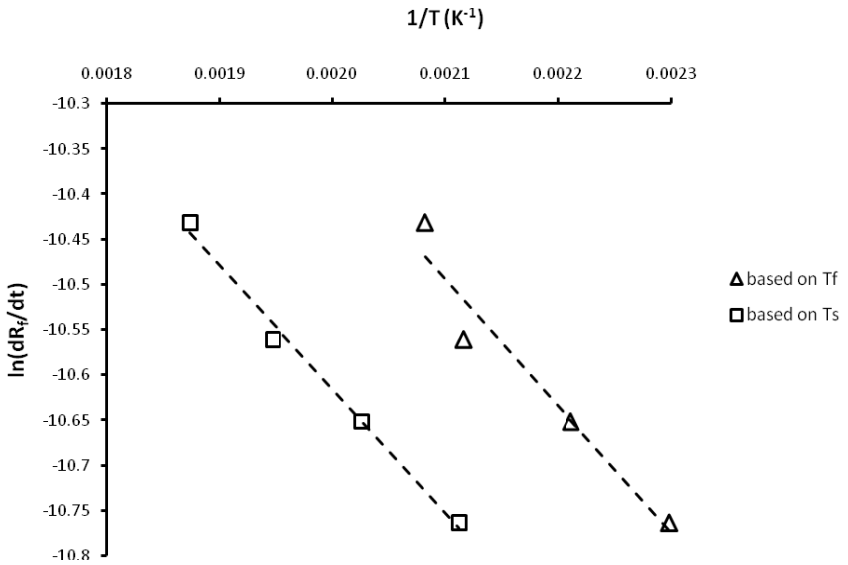

Fig. 4.32: Arrhenius plot for Condensate E – Crude C blend

Arrhenius plot performed gives *E* values of 11.67 and 11.39 kJmol^{-1} for the plot based on film and surface temperatures, respectively. Physical justification and interpretation of the Arrhenius equation is again reiterated where it says that lower *E* value contribute to the higher reaction rate due to less energy barrier to be surmounted for the molecules to react. If the *E* values obtained for condensate-crude oil blend to be compared with the *E* values obtained earlier for crude and crude blends, the value is the lowest. This agrees with the earlier statement regarding the addition of condensate to the crude oil where it will increase the fouling rates for the experiment conducted at a particular surface temperature.

In order to see the threshold models prediction capability on Condensate E –Crude C experimental data, the same procedure is performed for the experimental data where model prediction using estimation methods 1, 2 and 3 is applied. The results for model prediction are shown in Table 4.15 and Figs. 4.33 – 4.35.

Table 4.15: Fouling model parameters and R^2 values for different models and estimation methods for Condensate E – Crude C blend

			Ebert Panchal	**Panchal *et al.***	**Polley *et al.***	**Nasr & Givi**
Estimation method 1	α	m^2K/Whr	0.2217	0.4019	0.3317	0.2204
	γ	$m^2K/WhrPa$	0.0095844	0.0095844	0.0000249	0.0000063
	R^2		**0.9323**	**0.9323**	**0.9666**	**0.9323**
Estimation method 2	α	m^2K/Whr	0.4234	0.9799	0.9828	0.7194
	γ	$m^2K/WhrPa$	0.2952788	0.7080404	0.0000703	0.0004151
	R^2		**0.9243**	**0.9003**	**0.5385**	**0.9287**
Estimation method 3	α	m^2K/Whr	0.3358	0.6007	0.5182	0.3358
	γ	$m^2K/WhrPa$	0	0	0	0
	R^2		**0.7766**	**0.3937**	**0.5379**	**0.7766**

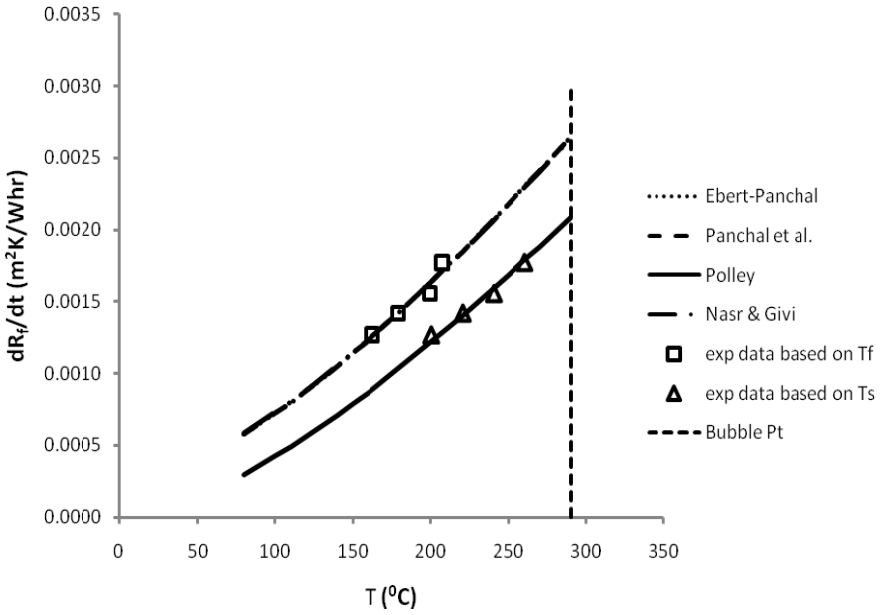

Fig. 4.33: Comparison of experimental and the predicted data by the model estimated using method 1 for Condensate E – Crude C blend

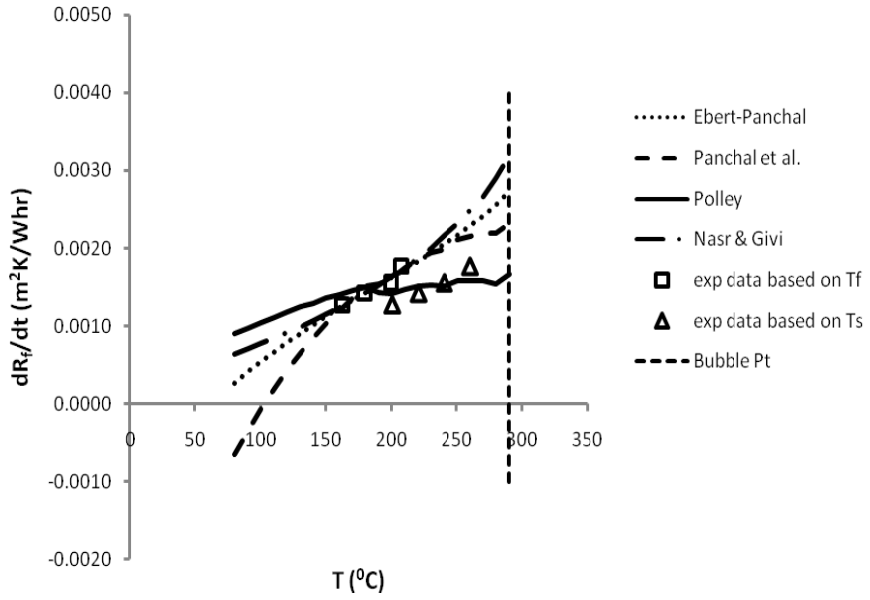

Fig. 4.34: Comparison of experimental and the predicted data by the model estimated using method 2 for Condensate E – Crude C blend

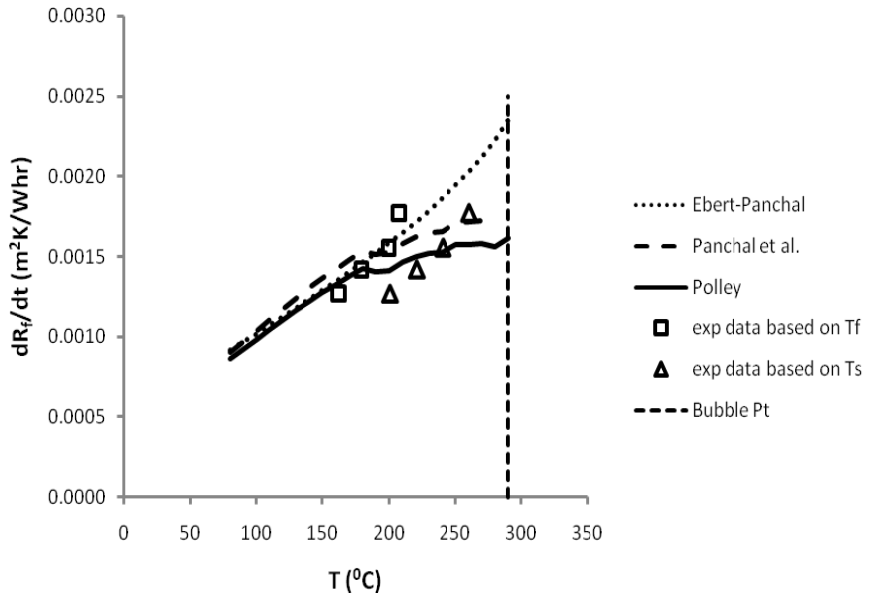

Fig. 4.35: Comparison of experimental and the predicted data by the model estimated using method 3 for Condensate E – Crude C blend

Based on the results, it is observed that the model prediction using estimation method 1 give a better prediction in terms of (i) model applicability over the practical operating range and (ii) prediction accuracy over the tested range of surface temperature. For model prediction using estimation method 2, Ebert and Panchal model and Panchal *et al.* models predict negative fouling rates value at the lower range and this is untrue. Panchal *et al.* and Polley *et al.* models using estimation methods 2 and 3 do not show a smooth prediction at the higher range. Model prediction using estimation method 3 give the lowest R^2 values and this indicates that the inclusion of removal term is required even the crude velocity and fluid shearing effect is very small.

4.4. Summary

In this chapter, experimental results obtained has been analyzed and discussed in detail based on the experiments performed to see the effect of surface temperature and addition of condensate to crude oil. Arrhenius equation was used to determine fouling propensity of the crude oils and crude blends. Four fouling threshold models with three different estimation methods were used to validate the experimental results from HLPS and the predicted values were compared with the experimental results.

CHAPTER 5

CONCLUSIONS AND RECOMMENDATIONS

The aim of the study was to determine the fouling characteristics and to compare the fouling propensity of different crude oils. The study has been performed using HLPS. Based on the results of the study, the following conclusions and recommendations are outlined.

5.1. Conclusions

1. Experiments in HLPS are able to demonstrate the differences in the fouling characteristics of crude oils, crude blends and condensate – crude oil blend. Each crude and crude blend gives different values of fouling rates indicating dissimilar tendency to foul but the trend is similar where the fouling rates increases with increasing surface temperature for each crude and crude blend.
2. *E* values calculated using Arrhenius plot for each crude and crude blend is a measure of how favorable the fouling reaction to proceed where lower *E* favors higher reaction rate. Crude ranking in terms of fouling propensity for the neat crude is in the order of Crude C > Crude D > Crude B > Crude A and this is suspected to be caused by the difference in crude properties related to fouling for each crude oil.
3. Blending Crude B, C and D to Crude A has caused the *E* value of A-C and A-D blend to be higher than Crude A whilst A-B blend resulted in lower *E* value compared to Crude A. This is suspected to be due to the alteration of crude properties because of blending and also due to different chemical class of the crude oils.

4. Addition of Condensate E to Crude C has resulted in the lowest *E* in comparison with other crudes and crude blends and this shows that Condensate E – Crude C blend has the highest fouling propensity among others.
5. Model prediction using estimation method 1 (physical properties estimated at inlet bulk temperature) give the better prediction in comparison with the model prediction using estimation methods 2 (physical properties estimated at film temperature or surface temperature) and 3 (physical properties estimated at film temperature or surface temperature plus the exclusion of removal term) for all crudes, crude blends and condensate – crude blend. This is based on (i) better R^2 values obtained during the model parameter estimation, (ii) fouling rates approaching zero at lower temperature without going to negative value and (iii) reasonably good and consistent prediction trend over the defined practical operating condition range
6. Physical properties for threshold models need to be estimated at the bulk temperature and the removal term for the models is required even though the crude velocity and the fluid shearing effect is very small for experiment in HLPS.
7. All threshold models (Ebert and Panchal, Panchal *et al.*, Polley *et al.* and Nasr and Givi) prediction using estimation method 1 give a reasonably good prediction where R^2 is more than 0.9 for all models.
8. Fouling characteristics data is developed for the selected Malaysian crude oils.

5.2. Recommendations

1. Since HLPS could only deliver a very low flowrates and therefore, low crude velocity, the study on the effect of crude velocity on the fouling process was not possible. So, bigger scale fouling rig where higher velocities can be achieved is required to enable the study on the effect of crude velocity which is believed to be one of the main factors that govern the fouling process.
2. To conduct more experiments in the lower and upper range of the practical operating condition range defined for each crude and crude blend so that a better threshold model prediction could be obtained, where the models cover a wider range of operating conditions.
3. To study the possibility of scaling up the fouling parameters obtained for the experiments in HLPS to bigger scale fouling rig or even the industrial heat exchangers.
4. To include the study of fouling under boiling conditions that could be another interesting fouling phenomenon that needs to be investigated. The threshold models can then be tested to determine their capabilities to represent the experimental data obtained for fouling under boiling conditions.

REFERENCES

1. Alcor Inc., "HLPS User's Manual," 1982.
2. API, "Draft for Technology Roadmap for Petroleum Industry," 2000.
3. API, "Petroleum Industry Technology Roadmap Workshop, Preliminary Results," *Energetics, Inc.*, Columbia, MD., 1999b.
4. API, "Technology Vision 2020: A Technology Vision for the U.S. Petroleum Refining Industry," *American Petroleum Institute (API)*, 1999a.
5. Asomaning, S., "Heat exchanger fouling by petroleum asphaltenes," Ph.D. dissertation, The University of British Columbia, 1997.
6. Asomaning, S., Panchal, C.B. and Liao, C.F., "Correlating field and laboratory data for crude oil fouling," *Heat Transfer Engineering*, 21(2), 17-23, 2000.
7. Atkins, G.T., "What to do about high coking rates." *Petro./Chem. Eng. in Petro. Management*, 34 (4), 170, 1962.
8. Bennet, C.A, Appleyard, S., Gough, M., Hohmann, R.P., Joshi, H.M., King, D.C., Lam, T.Y., Rudy, T.M. and Stomierowski, S.E., "Industry-recommended procedures for experimental crude oil preheat fouling research," *Heat Transfer Engineering*, Vol. 27, pp 28-35, 2006.
9. Bott, T.R., "Aspects of crystallization fouling," *Experimental Thermal and Fluid Science*, 14, 356-360, 1997.
10. Bott, T.R., "*Fouling of Heat Exchangers,"* Amsterdam, The Netherlands: Elsevier, 1995.
11. Bott, T.R., "Heat exchanger fouling. The challenge." *in Bohnet, M., Bott, T.R., Karabelas, A.J., Pilavachi, P.A., Semeria, R. and Vidil, R. eds Fouling Mechanisms - Theoretical and Practical Aspects*, Editions Europeenes Thermique et Industrie, Paris ed., 1992, 3-10.
12. Brons, G. and Rudy, T.M., "Fouling of whole crude oils on heated surfaces." *in Heat Exchanger Fouling - Fundamental Approaches and Technical Solutions*, Essen Germany: Publico Publications, 2002, 249-257.

13. Chilton, T.H. and Colburn, A.P., "Mass transfer (Absorption) coefficients. Prediction from data on heat transfer anf fluid friction," *Ind. Eng. Chem.,* 26, 1183, 1934.
14. Crittenden, B.D., "Chemical reaction fouling and heat exchanger efficiency," *Inst. Chem. Engrs. Course,* University of Leeds, 78, 1984.
15. Crittenden, B.D. and Kolaczkowski, S.T., "Energy savings through the accurate prediction of heat transfer fouling resistances," *in Energy for Industry,* 1979b, 257.
16. Crittenden, B.D. and Kolaczkowski, S.T., "Mass transfer and chemical kinetics in hydrocarbon fouling," *Proc. Conf. Fouling - Science or Art?,* Inst. Corr. Sci. and Tech./IChemE, 1979a, 169.
17. Crittenden, B.D., Kolaczkowski, S.T. and Downey, I.L., "Fouling of crude oil preheat exchangers," *Trans IChemE,* Vol. 70, pp 547-557, 1992.
18. Crittenden, B.D., Kolaczkowski, S.T. and Hout, S.A., "Modelling hydrocarbon fouling," *Chem. Eng. Res. Des.,* 65 (2), 171, 1987.
19. Crittenden, B.D., Kolaczkowski, S.T., Takemoto, T. and Philips, D.Z., "Crude oil fouling in a pilot-scale parallel tube apparatus," *in ECI 7th International Conference on Heat Exchanger Fouling and Cleaning: Challenges and Opportunities,* Tomar, Portugal, 2007, pp 14-22.
20. Dickakian, G., "Crude oil fouling control by a fouling analyser," *ASME HTD No. 108.* 1989, pp. 331-336.
21. Dickakian, G. and Seay, S., "Asphaltene precipitation: Primary crude exchanger fouling mechanism." *Oil and Gas Journal* Vol. 86 (No10), pp 47-50, 1988.
22. Eaton, P. and Lux, R., "Laboratory fouling test apparatus for hydrocarbon feedstocks," *ASME HTD,* 1984, pp 32-42.
23. Ebert, W. and Panchal, C.B., "Analysis of Exxon crude-oil slip stream coking data." *in Fouling Mitigation of Industrial Heat Exchange Equipment,* Begell House, NY, 1995, 451-460.
24. Epstein, N., "A model of the initial chemical reaction fouling rate for flow within a heated tube and its verification," *Proc. 10th Int. Heat Trans. Conf.,* Brighton: I.Chem.E., 1994, 225-229.
25. Epstein, N., "Thinking about heat transfer fouling: a 5 x matrix," *Heat Transfer Engineering,* 4, 43-56, 1983a.

26. ESDU, "Heat exchanger fouling in pre-heat train of a crude distillation unit, ESDU Data Item 00016," *ESDU International plc.*, London, 2000b.
27. ESDU, "Process Integration, ESDU Data Item 87030," *ESDU International plc.*, London, 2000a.
28. Fernandez-Baujin, J.M., and Solomon, S.M., "An industrial application of pyrolysis technology: Lummus SRT III module," *in Industrial and Laboratory Pyrolyses, ACS Symp. Ser. 32,* 1976, 345.
29. Fryer, P., "*Basic concepts in heat exchanger network modelling*," in Fouling Science and Technology, Kluwer, Norwell, MA, 1988, 495.
30. Jackman, A.P. and Arris, P, "Optimal control for pyrolytic reactors," *Proc. 4th Eur. Symp. on Chem. Reac. Eng.*, Pergamon, Oxford, 1971, 411.
31. Kern, D.O. and Seaton, R.E., "A theoretical analysis of thermal surface fouling," *Brit. Chem. Eng.*, 14 (No 5), 258, 1959.
32. Knudsen, J.G., Dahcheng, L. and Ebert, W.A, "The determination of the threshold fouling curve for a crude oil," *Understanding Heat Exchanger Fouling and Its Mitigation.*, Begell House, New York, 1999, pp 265-272.
33. Kuru, W.C., Panchal, C.B., Liao, C.F., Palen, J.W. and Ebert, W.A., "Development of high temperature, high pressure fouling unit," *in Proceedings of Understanding Heat Exchanger Fouling and Its Mitigation,* Lucca, Italy: Engineering Foundation Cenference, 1997.
34. Lambourn, G.A. and Durrieu, M., "Fouling in crude oil preheat trains," *in Heat Exchangers - Theory and Practice,* Hemisphere, New York, USA, 1983, pp 841-852.
35. Melo, L.F. and Bott, T.R., "Biofouling in water systems," *Experimental Thermal and Fluid Science*, 14, 375-381, 1997.
36. Metals, B. and Eckert, E.R.Q., "Forced, mixed and free convection region." *J. Heat Transfer,* 86, 295-296, 1964.
37. Muller-Steinhagen, H., "Fouling of heat exchangers surfaces." *Chemistry & Industry*, no. 5, pp. 171-175, 1995.
38. Muller-Steinhagen, H., *Heat exchanger fouling - Mitigation and cleaning technologies,* Publico Publications, 2000.
39. Mullin, J.W., *Crystallisation,* 2nd edition, London: Butterworths, 1972.

40. Nasr, M.R.J. and Givi, M.M., "Modeling of crude oil fouling in preheat exchangers of refinery distillation unit," *Applied Thermal Engineering*, pp 1572-1577, 2006.
41. Nelson, W.L., "Fouling of heat exchangers," *Ref. Nat. Gas. Manuf.*, 13 (7), 271, 1934.
42. Nijsing, R., "*Diffusional and kinetic phenomena associated with fouling. Considerations on the effect of hydrodynamic and thermal conditions,"* EURATOM Report EUR 543-e, 72 pages, 1964.
43. Oufer, L. "Fouling characteristics of organics fluids." Ph.D. dissertation, Oregon State University, 1990.
44. Panchal, C.B. and Watkinson, A.P., "Chemical reaction fouling model for single-phase heat transfer." *29th ASME/AIChE National Heat Transfer Conference*, Atlanta, 1993, 323-334.
45. Panchal, C.B., Kuru, W.C., Liao, C.F., Ebert, W.A. and Palen, J.W., "Threshold conditions for crude oil fouling," *Understanding Heat Exchanger Fouling and Its Mitigation*, Begell House, New York, 1999, pp 273-279.
46. Paterson, W.R. and Fryer, P.J., "A reaction engineering approach to the analysis of fouling," *Chem. Eng. Sci.*, Vol. 43, pp 1714-1717, 1988.
47. PetroSim, KBC Promatics, version 3.1.
48. Polley, G.T., Wilson, D.I., Yeap, B.L., and Pugh, S.J., "Evaluation of laboratory crude oil fouling data for application to refinery pre-heat trains," *Applied Thermal Engineering*, Vol. 22, 777-778, 2002.
49. Saleh, Z.S, Sheikholeslami, R. and Watkinson, A.P., "Fouling characteristics of a light Australian crude oil," *in 2003 ECI Conference on Heat Exchanger Fouling and Cleaning: Fundamentals and Applications*, Santa FE, New Mexico, USA, 2004, pp 226-233.
50. Saleh, Z.S., Sheikholeslami, R. and Watkinson, A.P., "Blending effect on fouling of four crude oils," *Proceedings of 6th International Conference on Heat Exchanger Fouling and Cleaning: Challenges and Opportunities*, Kloster Irsee, Germany, 2005, pp 37-46.
51. Scarborough, C.E., Cherrington, D.C., Diener, R. and Golan, L.P., "Coking of crude oil at high heat flux levels," *Chem. Eng. Proc.*, Vol. 75, 41-46, 1979.

52. Somerscales, E.F.C., "Fundamentals of corrosion fouling," *Experimental Thermal and Fluid Science*, 14, 335-355, 1997.
53. Srinivasan, M. and Watkinson, A.P., "Fouling of some Canadian crude oils," *in 2003 ECI Conference on Heat Exchanger Fouling and Cleaning: Fundamentals and Applications*, Santa FE, New Mexico, USA, 2004, pp 192-199.
54. Sundaram, K.M. and Froment, G.F., "Kinetics of coke deposition in the thermal cracking of propane," *Chem. Eng. Sci.*, 34, 635, 1979.
55. Taborek, J., Aoki, T., Palen, R.B. and Knudsen, J.G., "Predictive methods for fouling behaviour," *Chem. Eng. Prog.*, 68(7), 69-78, 1972.
56. Van Nostrand, W.L. JR., Leache, S.H. and Haluska, J.L., "Economic penalties associated with fouling of refinery heat transfer equipment," *in: Fouling of Heat Transfer Equipment*, 1981, B619-643.
57. Watkinson, A.P., "Chemical reaction fouling of organics fluids," *Chemical Engineering Technology* Vol. 15 (0), pp 82-90, 1992.
58. Watkinson, A.P., "Comparison of crude oil fouling using two different probes," *ECI Conference on Heat Exchanger Fouling and Cleaning: Fundamentals and Applications*, Santa Fe, New Mexico, USA, 2004.
59. Watkinson, A.P., "Critical review of organic fluid fouling," Argonne National Laboratory Report No. ANL/CNSV-TM-208, 1988.
60. Watkinson, A.P. and Wilson, D.I., "Chemical Reaction Fouling: A Review," *Experimental Thermal and Fluid Science*, 14, 356-360, 1997.
61. Watkinson, A.P. and Epstein, N., "Gas oil fouling in a sensible heat exchanger," *Chem. Eng. Prog. Sym. Ser. 65, No. 92*, 1969, 84-90.
62. Watkinson, A.P. and Epstein, N., "Particulate fouling of sensible heat exchangers," *Proc. International Heat Transfer Conf.*, 1970, pp12.
63. Wiehe, I.A., "A phase-separation kinetic model for coke formation," *I & EC Research*, Vol. 32 (No. 11), pp 2447-2454, 1993.
64. Wiehe, I.A., "Mitigation of plugging of a hydrotreater with the oil compatibility model," *Preprints of the International Conference on Petroleum Phase Behaviour and Fouling, AIChE*, 1999c, pp 404-411.
65. Wiehe, I.A., "Prevention of fouling by incompatible crudes with the oil compatibility model," *Preprints of the International Conference on Petroleum Phase Behaviour and Fouling, AIChE*, 1999b, pp 353-358.

66. Wiehe, I.A., "The oil compatibility model and crude oil incompatibility," *Preprints of the International Conference on Petroleum Phase Behaviour and Fouling, AIChE,* 1999a, pp 82-87.
67. Wiehe, I.A., "The role of phase equilibria in coke and sediment formation," Houston, Texas: AIChE Spring National Meeting, 1997b.
68. Wiehe, I.A., "Tutorial on the thermal reactivity of petroleum," ACS Div. Petroleum Chem. Meeting, San Francisco, 1997a.
69. Wiehe, I.A. and Kennedy, R.J., "Process for blending potentially incompatible petroleum oils," Patent US Patent 5,871,634, 1999.
70. Wilson, D.I. and Polley, G.T., "Mitigation of refinery preheat train fouling by nested optimization," *2001 AIChE Spring Meeting,* Houston, TX, 2001, 287-294.
71. Yeap, B.L., Wilson, D.I., Polley, G.T. and Pugh. S.J, "Retrofitting crude oil refinery heat exchanger networks to minimise fouling while maximising heat recovery," *ECI Conference on Heat Exchanger Fouling and Cleaning: Fundamentals and Applications,* Santa Fe, New Mexico, USA, 2004.

PUBLICATIONS

1. Rafeen, M.S., “Review of Ebert Panchal type fouling models and experimental results prediction for Malaysian crude oils”, *National Postgraduate Conference (NPC)*, Perak (2008)

2. Syamzari Rafeen, M., Johari, M., Ramasamy, M., “Analysis of the effect of temperature and blend ratio on crude oil fouling in Hot Liquid Process Simulator (HLPS)”, *National Postgraduate Conference (NPC)*, Perak (2009)

3. Deshannavar, U.B., Rafeen, M.S., Johari, M., Ramasamy, M., Subbarao, D., “Effect of blending on fouling on fouling characteristics of crude oil and condensate”, *The Proceeding of 3rd International Conference on Chemical & Bioprocess Engineering*, Sabah (2009)

4. Deshannavar, U.B., Rafeen, M.S., Ramasamy, M., Subbarao, D., “Crude oil fouling - A Review,” submitted to 24th Symposium of Malaysian Chemical Engineers / 1st International Conference on Process Engineering and Advanced Materials - 1st International Conference on Process Engineering and Advanced Materials, Kuala Lumpur (2010)

APPENDICES

APPENDIX A

Table A.1: Raw experimental data for Crude A tested at T_s = 220 ^{o}C (T_b = 80 ^{o}C, Crude flowrate = 3 ml/min)

Actual Time	Duration	A (Jacket)	B (Pump)	C (Line)	T_1	T_2	T_c (°C)							
	(min)	(°C)	(°C)	(°C)	(°C)	(°C)	Tube Profile (mm)							
1052	**12**						**0**	**10**	**20**	**30**	**38**	**40**	**50**	**60**
1104	15	90	78	60	80	148	154	184	206	221	221	221	200	151
1119	15	92	77	60	80	148	156	184	203	219	221	220	200	148
1134	15	84	78	61	79	147	156	186	208	220	221	220	200	149
1149	15	94	76	62	80	147	157	185	207	221	220	220	198	146
1204	15	84	77	63	80	146	156	185	207	219	221	218	197	148
1219	15	93	78	63	81	146	156	185	206	217	221	219	197	145
1234	15	85	78	62	81	146	153	184	208	219	221	220	197	142
1249	15	93	79	60	81	146	157	188	211	222	220	220	197	144
1304	15	93	79	60	81	146	157	188	211	222	220	220	197	144
1319	15	93	79	62	80	146	157	188	209	220	220	220	197	144
1334	15	88	98	61	80	146	157	188	209	220	220	221	199	148
1349	15	89	77	60	81	146	156	186	208	220	221	221	200	150
1404	15	88	79	61	81	146	156	186	208	220	221	221	200	150

Table A.2: Raw experimental dataA for Crude A tested at T_s = 240 ^{o}C (T_b = 80 ^{o}C, Crude flowrate = 3 ml/min)

Actual Time	Duration	A (Jacket)	B (Pump)	C (Line)	T_1	T_2	T_c (°C)							
	(min)	(°C)	(°C)	(°C)	(°C)	(°C)	Tube Profile (mm)							
1131	**15**						**0**	**10**	**20**	**30**	**38**	**40**	**50**	**60**
1146	15	82	76	69	80	176	175	206	229	241	240	238	215	163
1201	15	85	77	70	80	174	175	205	227	240	240	238	214	162
1216	15	92	77	70	80	173	175	206	228	240	241	240	216	162
1231	15	92	78	66	80	173	176	206	226	240	239	240	213	165
1246	15	88	78	67	80	174	177	207	229	241	241	240	215	163
1301	15	94	79	69	80	173	179	208	230	241	241	241	216	163
1316	15	91	79	68	79	173	177	205	227	240	241	240	215	166
1331	15	85	78	69	79	173	178	205	227	240	241	240	215	163
1346	15	87	78	68	81	172	179	207	227	240	240	239	216	161
1401	15	87	78	69	81	172	178	207	227	240	240	239	216	166
1416	15	86	80	66	81	171	178	207	227	240	240	240	216	166
1431	15	86	80	69	80	170	178	207	227	240	240	240	216	166
1446	15	91	78	68	79	169	178	207	227	240	240	239	216	166

Table A.3: Raw experimental data for Crude A tested at T_s = 260 ^{o}C (T_b = 80 ^{o}C, Crude flowrate = 3 ml/min)

Actual Time	Duration	A (Jacket)	B (Pump)	C (Line)	T_1	T_2	T_c (°C)							
	(min)	(°C)	(°C)	(°C)	(°C)	(°C)	Tube Profile (mm)							
914	**13**						**0**	**10**	**20**	**30**	**38**	**40**	**50**	**60**
927	15	88	76	58	81	192	187	222	247	258	260	260	238	181
942	15	93	77	58	80	190	188	222	248	260	260	260	238	182
957	15	87	78	55	80	189	188	223	247	260	260	260	238	185
1012	15	93	78	58	80	188	189	223	247	259	261	260	237	182
1027	15	94	79	58	80	187	193	225	250	261	261	261	238	183
1042	15	93	78	58	80	186	190	222	248	260	261	260	238	181
1057	15	94	78	58	80	185	190	222	248	259	260	258	235	180
1112	15	84	79	53	80	185	188	222	249	261	260	259	235	181
1127	15	84	78	52	81	185	188	222	248	260	261	260	235	180
1142	15	87	78	52	80	185	191	223	249	260	260	261	237	181
1157	15	92	80	52	80	184	190	221	248	260	260	261	235	176
1212	15	89	76	52	81	183	191	222	249	262	261	261	236	177
1227	15	86	80	53	81	183	191	222	249	262	261	261	236	177

Table A.4: Raw experimental data for Crude A tested at T_s = 280 ^{o}C (T_b = 80 ^{o}C, Crude flowrate = 3 ml/min)

Actual Time	Duration	A (Jacket)	B (Pump)	C (Line)	T_1	T_2	T_c (°C)							
	(min)	(°C)	(°C)	(°C)	(°C)	(°C)	Tube Profile (mm)							
1014	**13**						**0**	**10**	**20**	**30**	**38**	**40**	**50**	**60**
1027	15	102	75	54	81	205	199	237	261	276	281	280	258	196
1042	15	96	76	54	81	208	198	236	262	276	281	281	258	197
1057	15	96	78	54	80	206	199	234	261	278	282	280	258	193
1112	15	95	76	54	80	202	198	234	262	275	280	279	255	193
1127	15	83	78	52	81	199	200	235	263	280	279	282	257	189
1142	15	84	77	53	90	197	199	236	261	278	279	281	255	193
1157	15	88	78	53	79	195	196	232	258	275	281	277	249	186
1212	15	86	78	53	79	193	199	234	260	273	280	279	253	188
1227	15	88	80	53	79	192	200	234	259	275	280	280	254	188
1242	15	90	80	53	80	191	199	234	263	278	282	281	253	183
1257	15	92	80	53	80	187	199	235	263	278	281	279	246	183
1312	15	86	78	53	80	185	198	237	266	279	281	281	248	183
1327	15	90	79	53	80	182	198	238	266	279	281	280	249	184

Table A.5: Raw experimental data for Crude B tested at T_s = 220 ^{o}C (T_b = 80 ^{o}C, Crude flowrate = 3 ml/min)

Actual Time	Duration	A (Jacket)	B (Pump)	C (Line)	T_1	T_2	T_c (°C)							
	(min)	(°C)	(°C)	(°C)	(°C)	(°C)	Tube Profile (mm)							
1057	**16**						**0**	**10**	**20**	**30**	**38**	**40**	**50**	**60**
1113	15	95	79	67	80	155	168	193	213	221	220	219	193	139
1128	15	93	78	64	80	154	166	195	214	223	220	222	198	143
1143	15	88	80	62	80	154	165	192	211	221	220	219	196	141
1158	15	96	78	59	80	153	168	195	213	221	220	221	194	142
1213	15	98	79	60	80	152	167	195	213	222	220	217	197	142
1228	15	100	81	58	81	152	167	194	212	224	221	220	196	142
1243	15	94	80	58	80	151	167	194	213	222	221	220	194	142
1258	15	79	81	56	80	150	171	197	214	223	219	221	195	142
1313	15	81	81	55	81	149	168	194	212	220	220	218	194	140
1328	15	94	80	56	80	148	168	194	211	221	221	218	195	140
1343	15	106	82	54	81	148	168	195	214	223	221	220	195	142
1358	15	82	81	52	80	148	167	193	213	223	220	219	197	143
1413	15	92	83	56	80	147	168	194	212	220	221	220	196	143

Table A.6: Raw experimental data for Crude B tested at T_s = 240 ^{o}C (T_b = 80 ^{o}C, Crude flowrate = 3 ml/min)

Actual Time	Duration	A (Jacket)	B (Pump)	C (Line)	T_1	T_2	T_c (°C)							
	(min)	(°C)	(°C)	(°C)	(°C)	(°C)	Tube Profile (mm)							
1125	**15**						**0**	**10**	**20**	**30**	**38**	**40**	**50**	**60**
1140	15	103	82	68	79	153	165	202	225	238	240	237	210	157
1155	15	117	80	69	78	152	171	204	229	245	241	239	212	156
1210	15	98	81	73	80	151	169	203	229	239	241	234	209	163
1225	15	88	77	70	80	151	166	196	223	237	240	239	214	156
1240	15	92	80	70	80	150	163	197	223	237	240	239	211	154
1255	15	98	81	70	80	149	164	197	226	240	240	239	213	153
1310	15	109	83	72	80	149	167	204	228	238	241	240	214	153
1325	15	100	81	72	80	149	163	208	232	238	241	240	214	155
1340	15	88	84	71	80	148	173	208	233	240	240	240	214	154
1355	15	93	81	73	80	148	174	210	235	240	239	240	214	153
1410	15	90	81	72	80	147	174	210	235	240	239	240	214	153
1425	15	97	83	70	81	147	175	210	235	240	239	240	213	154
1440	15	100	81	73	80	146	174	210	235	240	240	241	214	154

Table A.7: Raw experimental data for Crude B tested at T_s = 260 ^{o}C (T_b = 80 ^{o}C, Crude flowrate = 3 ml/min)

Actual Time	Duration	A (Jacket)	B (Pump)	C (Line)	T_1	T_2	T_c (°C)							
	(min)	(°C)	(°C)	(°C)	(°C)	(°C)	Tube Profile (mm)							
1015	**13**						**0**	**10**	**20**	**30**	**38**	**40**	**50**	**60**
1028	15	96	78	59	81	171	181	216	243	260	261	260	233	179
1043	15	83	77	59	80	170	182	217	243	259	261	259	235	175
1053	15	92	77	60	80	168	182	218	247	261	260	261	236	175
1113	15	89	78	58	79	166	180	218	245	258	260	256	229	175
1128	15	88	78	59	80	165	186	221	252	265	260	261	233	176
1143	15	85	78	59	80	164	186	222	250	265	261	263	233	174
1158	15	84	79	60	81	163	183	221	248	262	260	259	233	173
1213	15	84	79	57	79	161	185	222	252	263	259	259	233	173
1228	15	85	79	59	80	161	186	221	250	262	261	260	228	170
1243	15	97	80	57	80	160	187	223	249	262	261	258	228	172
1258	15	94	78	57	81	159	186	223	247	261	258	260	231	172
1313	15	92	80	59	80	158	187	224	251	263	260	259	231	170
1328	15	92	80	59	80	158	186	224	251	263	261	259	231	171

Table A.8: Raw experimental data for Crude B tested at T_s = 280 ^{o}C (T_b = 80 ^{o}C, Crude flowrate = 3 ml/min)

Actual Time	Duration	A (Jacket)	B (Pump)	C (Line)	T_1	T_2	T_c (°C)							
	(min)	(°C)	(°C)	(°C)	(°C)	(°C)	Tube Profile (mm)							
913	**15**						**0**	**10**	**20**	**30**	**38**	**40**	**50**	**60**
928	15	93	79	68	80	174	197	236	264	279	280	276	242	179
943	15	86	81	65	81	174	198	236	263	280	280	278	247	180
958	15	83	81	65	80	173	201	238	268	283	281	279	248	180
1013	15	79	80	59	81	171	204	240	267	282	280	282	251	182
1028	15	79	80	59	80	170	205	238	267	280	281	278	246	180
1043	15	92	82	57	81	169	205	240	267	282	281	279	248	180
1058	15	94	82	58	80	168	203	238	266	280	280	279	242	178
1113	15	93	82	58	80	167	203	242	268	283	280	279	243	180
1128	15	90	83	55	80	166	205	241	268	281	280	279	245	178
1143	15	88	81	52	80	165	200	241	268	280	280	279	246	180
1158	15	84	83	54	81	165	208	245	270	282	280	281	246	179
1213	15	80	82	54	80	165	208	245	271	280	280	281	247	180
1228	15	99	82	53	81	164	209	245	271	283	280	277	242	177

Table A.9: Raw experimental data for Crude C tested at T_s = 220 ^{o}C (T_b = 80 ^{o}C, Crude flowrate = 3 ml/min)

Actual Time	Duration	A (Jacket)	B (Pump)	C (Line)	T_1	T_2	T_c (°C)							
	(min)	(°C)	(°C)	(°C)	(°C)	(°C)	Tube Profile (mm)							
1056	**9**						**0**	**10**	**20**	**30**	**38**	**40**	**50**	**60**
1104	15	96	68	64	80	156	160	190	208	220	221	218	195	144
1119	15	88	69	48	80	155	159	183	201	218	220	218	199	150
1134	15	75	68	47	85	159	167	186	203	216	220	218	199	151
1149	15	73	69	46	86	159	168	186	204	218	220	218	199	150
1204	15	87	68	46	87	157	169	186	204	217	220	218	199	151
1219	15	80	67	44	86	156	169	188	205	218	220	219	199	151
1234	15	82	69	44	86	155	169	188	205	218	221	219	199	151
1249	15	77	68	44	84	153	168	188	205	218	220	218	199	150
1304	15	82	69	44	84	152	168	188	204	217	220	218	198	150
1319	15	77	69	42	82	152	165	188	205	217	220	218	198	150
1334	15	81	68	43	82	152	164	188	204	217	220	218	198	150
1349	15	82	69	46	80	151	164	188	205	218	220	218	199	151
1404	15	83	70	43	80	150	164	187	205	217	220	218	198	150

Table A.10: Raw experimental data for Crude C tested at T_s = 240 ^{o}C (T_b = 80 ^{o}C, Crude flowrate = 3 ml/min)

Actual Time	Duration	A (Jacket)	B (Pump)	C (Line)	T_1	T_2	T_c (°C)							
	(min)	(°C)	(°C)	(°C)	(°C)	(°C)	Tube Profile (mm)							
941	**14**						**0**	**10**	**20**	**30**	**38**	**40**	**50**	**60**
955	15	105	66	68	80	167	172	203	226	237	241	234	207	160
1010	15	109	67	71	80	170	178	207	230	239	240	237	211	162
1025	15	101	68	68	80	169	178	208	230	239	240	238	210	162
1040	15	89	69	69	80	166	177	207	230	238	240	237	209	161
1055	15	93	68	69	81	165	176	207	229	237	240	236	209	161
1110	15	90	68	68	81	165	176	207	229	237	241	236	209	161
1125	15	91	67	65	80	164	176	207	229	238	240	237	210	161
1140	15	97	69	67	80	164	176	206	229	237	241	237	209	161
1155	15	96	70	64	80	164	176	206	228	237	240	236	209	160
1210	15	101	69	64	81	164	175	206	228	237	240	236	209	160
1225	15	96	68	65	80	163	175	206	228	237	240	236	209	160
1240	15	104	70	63	80	163	175	205	228	237	240	236	209	160
1255	15	100	69	62	80	163	175	205	228	237	240	236	209	160

Table A.11: Raw experimental data for Crude C tested at T_s = 260 ^{o}C (T_b = 80 ^{o}C, Crude flowrate = 3 ml/min)

Actual Time	Duration	A (Jacket)	B (Pump)	C (Line)	T_1	T_2	T_c (°C)							
	(min)	(°C)	(°C)	(°C)	(°C)	(°C)	Tube Profile (mm)							
1114	**20**						**0**	**10**	**20**	**30**	**38**	**40**	**50**	**60**
1125	15	97	66	63	80	183	184	221	247	257	261	257	233	177
1140	15	89	67	63	80	185	186	225	249	259	260	258	235	181
1155	15	94	67	64	80	184	185	224	248	258	261	257	232	180
1210	15	92	67	64	80	183	186	224	248	258	261	257	233	181
1225	15	94	67	63	80	181	186	224	248	258	260	257	233	180
178	15	87	68	63	81	178	186	224	250	259	260	257	233	180
1255	15	96	66	61	80	175	186	225	249	259	261	257	232	180
1310	15	89	67	60	81	175	186	225	249	259	261	257	232	179
1325	15	99	67	60	80	174	186	225	250	259	260	258	232	179
1340	15	97	68	61	80	174	186	224	249	258	260	258	232	179
1355	15	107	69	60	80	174	185	223	248	258	260	257	231	178
1410	15	102	69	61	81	174	185	223	248	259	261	258	232	178
1425	15	101	69	60	81	174	185	222	248	258	260	258	232	179

Table A.12: Raw experimental data for Crude C tested at T_s = 280 ^{o}C (T_b = 80 ^{o}C, Crude flowrate = 3 ml/min)

Actual Time	Duration	A (Jacket)	B (Pump)	C (Line)	T_1	T_2	T_c (°C)							
	(min)	(°C)	(°C)	(°C)	(°C)	(°C)	Tube Profile (mm)							
1028	**14**						**0**	**10**	**20**	**30**	**38**	**40**	**50**	**60**
1042	15	82	76	73	80	197	192	232	261	276	282	280	254	198
1057	15	96	76	74	80	195	197	236	265	280	281	280	256	196
1112	15	96	75	74	81	192	194	234	265	280	280	280	256	197
1127	15	84	76	73	80	190	194	232	263	278	281	280	256	194
1142	15	85	76	72	80	191	196	234	263	279	281	281	253	193
1157	15	99	77	72	80	191	195	234	263	280	280	279	252	192
1212	15	100	79	73	80	191	196	234	266	280	280	280	252	192
1227	15	100	78	73	80	191	196	232	260	277	281	277	249	192
1242	15	100	79	74	81	191	198	236	265	279	281	279	253	195
1257	15	100	78	76	79	192	197	233	265	281	282	281	253	193
1312	15	100	80	76	79	191	195	233	262	279	281	278	253	198
1327	15	98	77	74	81	190	199	236	266	277	280	281	256	198
1342	15	96	78	72	81	190	199	236	266	277	280	281	256	198

Table A.13: Raw experimental data for Crude D tested at T_s = 220 ^{o}C (T_b = 80 ^{o}C, Crude flowrate = 3 ml/min)

Actual Time	Duration	A (Jacket)	B (Pump)	C (Line)	T_1	T_2	T_c (°C)							
	(min)	(°C)	(°C)	(°C)	(°C)	(°C)	Tube Profile (mm)							
1118	**16**						**0**	**10**	**20**	**30**	**38**	**40**	**50**	**60**
1134	15	91	57	80	80	153	163	194	214	222	221	221	198	150
1149	15	110	80	72	80	151	164	193	212	222	220	221	198	151
1204	15	103	81	75	79	149	164	192	212	222	220	218	196	148
1219	15	103	73	79	80	148	164	190	210	220	220	219	196	144
1234	15	95	81	76	80	148	163	192	210	220	220	221	196	147
1249	15	92	82	77	80	148	165	194	213	221	221	220	196	145
1304	15	103	84	73	81	148	162	192	210	219	221	220	196	144
1319	15	108	84	74	80	148	162	192	210	219	221	220	196	144
1334	15	89	83	77	80	148	165	193	212	220	221	218	194	146
1349	15	92	84	72	80	147	165	194	213	222	220	220	195	142
1404	15	103	83	75	80	147	165	195	214	222	220	222	198	147
1419	15	95	84	74	80	147	165	195	214	222	221	220	196	147
1434	15	104	86	74	79	147	164	191	211	220	220	216	192	143

Table A.14: Raw experimental data for Crude D tested at T_s = 240 ^{o}C (T_b = 80 ^{o}C, Crude flowrate = 3 ml/min)

Actual Time	Duration	A (Jacket)	B (Pump)	C (Line)	T_1	T_2	T_c (°C)							
	(min)	(°C)	(°C)	(°C)	(°C)	(°C)	Tube Profile (mm)							
1229	**13**						**0**	**10**	**20**	**30**	**38**	**40**	**50**	**60**
1242	15	122	79	64	79	166	177	208	231	241	241	241	216	161
1257	15	105	79	67	80	169	178	209	232	241	243	242	218	162
1312	15	86	82	66	79	167	181	213	234	244	243	245	220	166
1327	15	87	73	65	79	166	178	211	234	245	245	247	221	165
1342	15	97	75	67	80	166	177	207	230	244	247	245	222	165
1357	15	106	83	67	80	165	179	210	235	245	247	248	223	168
1412	15	103	82	67	80	167	181	213	238	250	249	250	224	167
1427	15	94	83	67	81	167	181	214	238	250	251	250	225	169
1442	15	101	82	66	80	159	176	208	229	237	240	239	211	156
1457	15	95	82	63	81	155	176	208	230	239	240	239	210	155
1512	15	104	80	66	80	154	176	209	231	240	240	239	211	155
1527	15	109	83	64	80	152	175	209	232	241	239	238	210	154
1542	15	107	83	67	81	153	176	209	232	242	240	238	210	154

Table A.15: Raw experimental data for Crude D tested at T_s = 260 ^{o}C (T_b = 80 ^{o}C, Crude flowrate = 3 ml/min)

Actual Time	Duration	A (Jacket)	B (Pump)	C (Line)	T_1	T_2	T_c (°C)							
	(min)	(°C)	(°C)	(°C)	(°C)	(°C)	Tube Profile (mm)							
1237	**13**						**0**	**10**	**20**	**30**	**38**	**40**	**50**	**60**
1250	15	124	80	71	80	183	186	220	243	255	261	259	235	183
1305	15	115	74	71	79	184	188	223	245	256	261	259	236	184
1320	15	94	80	70	79	181	187	222	245	256	261	260	236	180
1335	15	87	80	74	79	179	184	220	245	256	261	260	237	180
1350	15	89	81	74	80	176	184	218	244	255	261	260	233	178
1405	15	103	82	74	80	172	186	220	246	259	261	260	234	175
1420	15	104	82	72	80	172	185	219	244	256	260	259	231	176
1435	15	107	81	75	80	172	186	222	245	259	261	261	235	178
1450	15	104	84	73	81	172	188	224	249	260	261	260	233	179
1505	15	98	83	72	80	172	189	224	249	259	260	259	234	176
1520	15	111	85	72	81	172	190	226	249	261	261	260	233	175
1535	15	98	83	72	81	171	188	222	248	259	261	260	232	175
1550	15	90	80	73	81	169	188	223	247	258	260	258	231	173

Table A.16: Raw experimental data for Crude D tested at T_s = 280 ^{o}C (T_b = 80 ^{o}C, Crude flowrate = 3 ml/min)

Actual Time	Duration	A (Jacket)	B (Pump)	C (Line)	T_1	T_2	T_c (°C)							
	(min)	(°C)	(°C)	(°C)	(°C)	(°C)	Tube Profile (mm)							
1042	**13**						**0**	**10**	**20**	**30**	**38**	**40**	**50**	**60**
1055	15	120	79	66	80	212	184	231	255	273	281	281	260	202
1110	15	92	79	65	78	212	181	229	254	272	279	281	260	202
1125	15	92	80	66	81	212	186	232	257	272	281	280	260	203
1140	15	87	82	68	80	210	181	232	258	274	281	281	254	200
1155	15	86	69	68	80	200	185	230	264	278	280	281	255	196
1210	15	87	75	66	80	198	176	228	259	277	281	280	254	195
1225	15	89	67	66	80	198	180	228	261	276	280	281	252	194
1240	15	95	74	69	81	196	182	229	263	278	280	280	252	194
1255	15	87	58	69	81	196	183	232	265	281	280	280	250	194
1310	15	88	61	65	80	194	181	233	264	280	281	280	251	193
1325	15	88	85	67	80	194	184	232	263	280	281	280	250	192
1340	15	114	85	67	80	194	183	233	263	280	281	281	252	192
1355	15	93	80	66	80	193	181	230	265	280	280	281	252	191

Table A.17: Raw experimental data for A-B blend tested at T_s = 240 ^{o}C (T_b = 80 ^{o}C, Crude flowrate = 3 ml/min)

Actual Time	Duration	A (Jacket)	B (Pump)	C (Line)	T_1	T_2	T_c (°C)							
	(min)	(°C)	(°C)	(°C)	(°C)	(°C)	Tube Profile (mm)							
1134	**15**						**0**	**10**	**20**	**30**	**38**	**40**	**50**	**60**
1149	15	83	77	67	80	172	174	204	227	240	241	239	214	160
1204	15	83	76	68	80	172	176	204	229	240	240	240	215	162
1219	15	84	77	68	80	172	177	206	228	240	240	240	215	158
1234	15	83	79	68	80	171	179	210	231	244	240	240	214	156
1249	15	94	79	66	80	170	179	209	231	241	240	240	208	156
1304	15	87	77	67	80	171	181	210	234	244	241	241	214	162
1319	15	89	79	68	80	170	178	207	229	241	240	240	214	156
1334	15	85	78	68	81	170	177	209	231	242	240	239	211	157
1349	15	89	80	69	81	170	178	208	231	242	241	239	212	157
1404	15	91	80	70	81	170	180	210	232	243	241	241	212	156
1419	15	86	80	67	80	169	177	207	230	240	240	237	209	159
1434	15	88	80	69	80	168	177	208	231	242	241	240	212	158
1449	15	86	79	66	80	168	177	208	231	242	241	240	212	158

Table A.18: Raw experimental data for A-B blend tested at T_s = 260 ^{o}C (T_b = 80 ^{o}C, Crude flowrate = 3 ml/min)

Actual Time	Duration	A (Jacket)	B (Pump)	C (Line)	T_1	T_2	T_c (°C)							
	(min)	(°C)	(°C)	(°C)	(°C)	(°C)	Tube Profile (mm)							
1212	**13**						**0**	**10**	**20**	**30**	**38**	**40**	**50**	**60**
1225	15	81	77	78	80	180	185	212	241	256	261	261	238	171
1240	15	96	77	73	80	180	192	223	248	260	260	260	233	167
1255	15	91	78	76	81	180	192	223	248	260	260	260	232	172
1310	15	83	79	78	80	179	193	222	247	259	260	259	232	170
1325	15	96	78	77	80	179	193	223	249	261	261	260	235	180
1340	15	89	80	78	80	179	194	226	249	261	260	259	232	168
1355	15	100	77	76	80	178	193	225	250	262	261	259	231	170
1410	15	98	79	77	80	178	193	226	250	262	261	260	232	170
1425	15	95	77	76	80	177	197	228	254	265	261	260	232	167
1440	15	100	79	73	79	177	197	227	252	264	261	261	232	170
1455	15	84	81	75	79	176	195	227	252	263	261	260	231	167
1510	15	85	80	74	79	175	195	227	252	263	261	260	231	167
1525	15	97	80	78	80	175	196	227	254	263	260	261	232	168

Table A.19: Raw experimental data for A-B blend tested at T_s = 280 ^{o}C (T_b = 80 ^{o}C, Crude flowrate = 3 ml/min)

Actual Time	Duration	A (Jacket)	B (Pump)	C (Line)	T_1	T_2	T_c (°C)							
	(min)	(°C)	(°C)	(°C)	(°C)	(°C)	Tube Profile (mm)							
1046	**14**						**0**	**10**	**20**	**30**	**38**	**40**	**50**	**60**
1100	15	97	75	74	80	187	197	236	266	281	281	280	255	194
1115	15	85	76	73	80	189	198	235	264	279	281	281	254	195
1130	15	82	77	74	80	188	200	236	263	279	280	280	252	190
1145	15	100	76	77	81	186	198	235	261	279	281	278	250	187
1200	15	100	77	77	81	185	198	236	264	279	281	279	249	189
1215	15	97	78	78	80	184	200	234	263	280	281	280	250	190
1230	15	92	79	73	79	183	202	238	266	282	280	281	250	192
1245	15	91	79	73	80	181	201	238	267	282	281	280	248	188
1300	15	89	78	74	79	181	199	236	265	281	281	280	248	193
1315	15	92	79	76	80	180	202	237	268	281	280	280	247	189
1330	15	94	81	73	80	179	202	240	268	284	280	277	249	184
1345	15	95	79	73	80	178	202	239	268	283	280	277	246	187
1400	15	98	79	75	79	177	201	239	269	285	281	280	248	187

Table A.20: Raw experimental data for A-C blend tested at T_s = 240 ^{o}C (T_b = 80 ^{o}C, Crude flowrate = 3 ml/min)

Actual Time	Duration	A (Jacket)	B (Pump)	C (Line)	T_1	T_2	T_c (°C)							
	(min)	(°C)	(°C)	(°C)	(°C)	(°C)	Tube Profile (mm)							
1006	**13**						**0**	**10**	**20**	**30**	**38**	**40**	**50**	**60**
1019	15	106	66	70	80	168	176	205	228	240	240	240	214	160
1034	15	99	70	69	80	167	175	207	230	242	240	240	216	161
1049	15	88	68	70	80	166	174	203	227	240	241	239	212	160
1104	15	86	70	70	80	165	174	204	229	242	241	239	214	161
1119	15	92	69	70	80	164	173	203	227	240	241	239	210	157
1134	15	90	68	71	81	163	173	204	227	240	240	239	212	161
1149	15	88	70	70	81	162	173	204	228	241	240	240	213	160
1204	15	89	70	68	80	162	174	202	226	240	240	238	214	156
1219	15	84	68	68	80	162	175	205	228	240	241	239	211	157
1234	15	94	49	70	80	162	174	206	229	241	240	240	216	161
1249	15	95	69	68	80	162	175	206	229	240	241	240	210	161
1304	15	99	72	70	81	162	175	204	228	241	241	240	213	157
1319	15	100	69	68	80	162	177	207	228	241	240	240	213	158

Table A.21: Raw experimental data for A-C blend tested at T_s = 260 ^{o}C (T_b = 80 ^{o}C, Crude flowrate = 3 ml/min)

Actual Time	Duration	A (Jacket)	B (Pump)	C (Line)	T_1	T_2	T_c (°C)							
	(min)	(°C)	(°C)	(°C)	(°C)	(°C)	Tube Profile (mm)							
1022	**11**						**0**	**10**	**20**	**30**	**38**	**40**	**50**	**60**
1033	15	105	76	71	81	178	196	224	248	261	260	258	230	170
1048	15	98	78	70	81	182	197	227	251	265	261	259	233	167
1103	15	99	77	71	80	180	194	225	250	264	261	259	226	165
1118	15	86	78	71	80	179	193	227	253	267	261	258	225	163
1133	15	93	79	71	80	176	195	227	253	265	260	257	222	159
1148	15	86	77	69	81	176	194	228	255	267	260	257	223	158
1203	15	92	78	70	80	176	197	230	258	268	260	258	221	159
1218	15	92	79	68	81	176	197	232	260	269	261	259	224	162
1233	15	88	79	68	81	175	198	235	261	270	260	258	222	162
1248	15	89	80	69	81	173	199	236	262	269	260	257	219	159
1303	15	90	78	68	81	172	200	238	263	269	260	258	222	159
1318	15	90	80	70	81	170	202	239	265	271	261	258	219	155
1313	15	88	79	70	81	168	209	245	268	275	261	256	220	155

Table A.22: Raw experimental data for A-C blend tested at T_s = 280 ^{o}C (T_b = 80 ^{o}C, Crude flowrate = 3 ml/min)

Actual Time	Duration	A (Jacket)	B (Pump)	C (Line)	T_1	T_2	T_c (°C)							
	(min)	(°C)	(°C)	(°C)	(°C)	(°C)	Tube Profile (mm)							
956	**16**						**0**	**10**	**20**	**30**	**38**	**40**	**50**	**60**
1012	15	81	70	70	80	212	205	239	265	278	281	280	256	192
1027	15	87	70	71	80	208	204	240	266	278	280	280	256	196
1042	15	99	69	69	80	206	202	239	265	277	281	280	256	194
1057	15	99	71	68	80	204	201	238	265	277	281	280	254	195
1112	15	83	71	70	80	203	202	238	263	276	281	280	255	193
1127	15	88	60	70	81	203	202	239	265	277	281	281	258	190
1142	15	89	98	64	79	202	198	237	263	276	280	280	258	193
1157	15	93	71	68	81	201	201	237	263	277	281	281	257	192
1212	15	89	73	68	81	200	200	238	264	277	280	281	255	192
1227	15	85	73	68	80	200	198	236	262	276	281	280	256	192
1242	15	92	72	69	79	199	200	237	265	278	280	281	254	191
1257	15	94	67	70	79	198	200	236	265	279	280	281	256	194
1312	15	93	63	70	79	197	201	239	266	278	281	281	255	192

Table A.23: Raw experimental data for A-D blend tested at T_s = 240 ^{o}C (T_b = 80 ^{o}C, Crude flowrate = 3 ml/min)

Actual Time	Duration	A (Jacket)	B (Pump)	C (Line)	T_1	T_2	T_c (°C)							
	(min)	(°C)	(°C)	(°C)	(°C)	(°C)	Tube Profile (mm)							
939	**13**						**0**	**10**	**20**	**30**	**38**	**40**	**50**	**60**
952	15	105	67	81	79	159	179	206	226	237	241	238	212	159
1007	15	82	75	81	78	159	180	208	228	239	241	239	213	159
1022	15	82	75	79	80	160	181	209	230	240	241	240	214	159
1037	15	86	77	78	80	159	181	208	228	239	241	240	214	159
1052	15	88	76	80	80	158	181	208	229	239	241	240	214	158
1107	15	97	76	80	81	158	182	210	230	241	241	240	214	159
1122	15	101	76	78	81	157	181	208	229	239	241	240	212	158
1137	15	101	79	79	81	157	182	209	229	240	241	240	212	158
1152	15	102	78	80	80	157	183	209	228	240	241	240	213	157
1207	15	103	77	77	81	157	183	209	228	239	241	240	212	157
1222	15	90	80	79	81	157	182	208	229	239	241	240	212	156
1237	15	97	78	78	81	157	183	210	230	240	241	240	211	156
1252	15	86	78	77	81	157	185	213	236	248	241	242	216	160

Table A.24: Raw experimental data for A-D blend tested at T_s = 260 ^{o}C (T_b = 80 ^{o}C, Crude flowrate = 3 ml/min)

Actual Time	Duration	A (Jacket)	B (Pump)	C (Line)	T_1	T_2	T_c (°C)							
	(min)	(°C)	(°C)	(°C)	(°C)	(°C)	Tube Profile (mm)							
945	**20**						**0**	**10**	**20**	**30**	**38**	**40**	**50**	**60**
1005	15	100	77	62	80	179	190	224	248	262	260	261	236	178
1020	15	85	78	64	81	178	193	225	247	260	260	259	237	178
1035	15	82	77	65	80	177	193	227	250	261	260	262	238	180
1050	15	99	78	63	81	177	192	224	249	259	260	260	233	175
1105	15	99	79	63	80	176	192	224	250	258	260	260	232	176
1120	15	87	79	65	80	176	192	226	250	261	260	261	235	179
1135	15	87	80	68	80	176	194	226	250	261	261	261	233	179
1150	15	91	78	65	80	176	193	223	248	260	260	260	233	177
1205	15	88	78	68	81	176	193	223	248	261	261	259	233	178
1220	15	93	78	68	81	176	193	225	249	261	261	261	235	179
1235	15	100	80	65	80	175	192	225	248	259	261	260	233	176
1250	15	102	78	68	80	175	191	224	248	259	260	259	232	176
1305	15	102	80	68	80	175	191	223	246	259	260	261	240	177

Table A.25: Raw experimental data for A-D blend tested at T_s = 280 ^{o}C (T_b = 80 ^{o}C, Crude flowrate = 3 ml/min)

Actual Time	Duration	A (Jacket)	B (Pump)	C (Line)	T_1	T_2	T_c (°C)							
	(min)	(°C)	(°C)	(°C)	(°C)	(°C)	Tube Profile (mm)							
1002	**15**						**0**	**10**	**20**	**30**	**38**	**40**	**50**	**60**
1017	15	87	75	82	81	186	214	246	267	279	281	280	251	190
1032	15	83	76	75	80	184	213	243	266	281	281	281	258	194
1047	15	96	76	77	81	183	210	242	265	278	281	278	250	189
1102	15	88	76	79	80	182	211	241	266	280	280	280	252	190
1117	15	91	78	73	80	182	208	240	264	278	281	278	251	185
1132	15	83	78	80	79	180	207	241	264	280	280	278	249	187
1147	15	86	79	83	80	180	204	237	262	279	281	280	250	187
1202	15	88	80	73	80	179	208	240	265	281	281	280	249	188
1217	15	96	80	69	81	179	205	236	261	278	282	280	248	187
1232	15	97	78	73	79	177	198	230	256	273	281	279	247	182
1247	15	96	78	70	79	176	206	237	262	280	280	279	248	186
1302	15	106	78	73	79	175	206	237	262	280	281	279	249	188
1317	15	100	77	77	79	176	205	237	262	280	280	279	250	182

Table A.26: Raw experimental data for Condensate E – Crude C blend tested at T_s = 200 ^{o}C (T_b = 80 ^{o}C, Crude flowrate = 3 ml/min)

Actual Time	Duration	A (Jacket)	B (Pump)	C (Line)	T_1	T_2	T_c (°C)							
	(min)	(°C)	(°C)	(°C)	(°C)	(°C)	Tube Profile (mm)							
949	**10**						**0**	**10**	**20**	**30**	**38**	**40**	**50**	**60**
1000	15	103	65	70	80	138	147	174	192	199	200	198	178	132
1015	15	113	67	72	80	138	146	173	191	197	201	197	178	133
1030	15	95	66	72	80	136	146	173	191	198	200	196	176	132
1045	15	93	65	72	80	136	146	173	191	198	200	197	176	133
1100	15	96	65	72	80	135	146	174	191	198	201	196	177	133
1115	15	88	65	72	80	135	146	173	191	197	200	197	176	132
1130	15	89	65	72	80	135	147	173	191	197	201	196	177	132
1145	15	88	67	72	80	135	147	174	192	198	201	197	177	133
1200	15	90	69	73	80	135	147	174	192	198	200	197	176	133
1215	15	91	68	72	80	135	147	174	192	197	200	196	176	133
1230	15	97	68	72	80	135	147	174	192	198	200	196	176	133
1245	15	91	70	72	80	135	147	173	192	198	200	196	176	133
1300	15	95	69	72	80	135	147	173	192	198	200	197	176	133

Table A.27: Raw experimental data for Condensate E – Crude C blend tested at T_s = 220 ^{o}C (T_b = 80 ^{o}C, Crude flowrate = 3 ml/min)

Actual Time	Duration	A (Jacket)	B (Pump)	C (Line)	T_1	T_2	T_c (°C)							
	(min)	(°C)	(°C)	(°C)	(°C)	(°C)	Tube Profile (mm)							
1056	**9**						**0**	**10**	**20**	**30**	**38**	**40**	**50**	**60**
933	15	109	69	70	80	162	168	194	211	219	221	219	198	153
948	15	101	65	73	80	161	165	193	210	218	221	217	196	153
1003	15	89	63	71	80	159	165	195	213	219	220	219	197	153
1018	15	87	64	72	80	158	165	194	213	219	220	218	197	152
1033	15	91	65	73	80	157	165	195	215	219	221	218	197	152
1048	15	91	65	71	80	157	165	195	214	218	220	218	196	152
1103	15	89	66	70	80	156	165	194	213	218	220	217	196	152
1118	15	90	68	71	80	155	165	194	213	218	220	216	195	151
1133	15	91	68	70	80	155	165	195	213	218	221	216	195	151
1148	15	92	68	71	80	154	164	194	212	218	221	216	194	151
1203	15	94	68	71	80	154	164	194	212	218	220	216	194	150
1218	15	89	66	71	80	153	164	194	213	218	220	217	194	150
1233	15	92	68	72	80	153	163	193	212	218	221	216	194	150

Table A.28: Raw experimental data for Condensate E – Crude C blend tested at T_s = 240 ^{o}C (T_b = 80 ^{o}C, Crude flowrate = 3 ml/min)

Actual Time	Duration	A (Jacket)	B (Pump)	C (Line)	T_1	T_2	T_c (°C)							
	(min)	(°C)	(°C)	(°C)	(°C)	(°C)	Tube Profile (mm)							
952	**9**						**0**	**10**	**20**	**30**	**38**	**40**	**50**	**60**
1005	15	111	63	66	80	196	165	198	216	239	241	239	225	175
1020	15	100	65	67	80	199	165	199	216	238	240	239	224	175
1035	15	104	67	66	80	197	164	198	216	238	241	238	222	175
1050	15	90	67	67	80	196	164	198	215	237	240	238	221	173
1105	15	96	67	66	80	195	164	198	215	237	240	238	221	173
1120	15	100	66	66	80	187	165	198	215	237	241	238	220	173
1135	15	89	67	67	80	185	166	199	218	237	240	238	220	173
1150	15	91	68	66	80	184	167	199	218	236	240	238	219	172
1205	15	92	67	66	80	183	166	199	218	236	240	238	219	172
1220	15	96	67	67	80	185	167	200	219	236	240	238	219	172
1235	15	89	67	66	80	185	167	200	219	236	240	237	218	172
1250	15	101	68	68	80	185	168	200	220	237	241	237	219	172
1305	15	91	68	66	80	185	168	200	220	237	241	238	218	172

Table A.29: Raw experimental data for Condensate E – Crude C blend tested at T_s = 260 ^{o}C (T_b = 80 ^{o}C, Crude flowrate = 3 ml/min)

Actual Time	**Duration**	**A (Jacket)**	**B (Pump)**	**C (Line)**	T_1	T_2	T_c (°C)							
	(min)	**(°C)**	**(°C)**	**(°C)**	**(°C)**	**(°C)**	**Tube Profile (mm)**							
1114	**9**						**0**	**10**	**20**	**30**	**38**	**40**	**50**	**60**
1125	15	97	66	63	80	183	184	221	247	257	261	257	233	177
1140	15	89	67	63	80	185	186	225	249	259	260	258	235	181
1155	15	94	67	64	80	184	185	224	248	258	261	257	232	180
1210	15	92	67	64	80	183	186	224	248	258	261	257	233	181
1225	15	94	67	63	80	181	186	224	248	258	260	257	233	180
1240	15	87	68	63	81	176	186	224	250	259	260	257	233	180
1255	15	96	66	61	80	174	186	225	249	259	261	257	232	180
1310	15	89	67	60	81	174	186	225	249	259	261	257	232	179
1325	15	99	67	60	80	174	186	225	250	259	260	258	232	179
1340	15	97	68	61	80	174	186	224	249	258	260	258	232	179
1355	15	107	69	60	80	174	185	223	248	258	260	257	231	178
1410	15	102	69	61	81	174	185	223	248	259	261	258	232	178
1425	15	101	69	60	**81**	174	185	222	248	258	260	258	232	179

APPENDIX B

Table B.30: R_f versus time data for Crude A

time (min)	R_f (m^{2}K/Wmin)			
	T_s = 220 ^{o}C	T_s = 240 ^{o}C	T_s = 260 ^{o}C	T_s = 280 ^{o}C
0	0.0000000	0.0000000	0.0000000	0.0000000
15	-0.0001495	0.0002447	0.0002780	-0.0003437
30	0.0002022	0.0005437	0.0004206	-0.0001588
45	0.0002384	0.0004164	0.0005502	0.0002209
60	0.0004326	0.0004066	0.0008401	0.0008118
75	0.0005256	0.0006528	0.0008805	0.0014946
90	0.0006299	0.0004261	0.0009217	0.0009139
105	0.0008645	0.0004261	0.0009860	0.0012992
120	0.0008645	0.0007511	0.0010436	0.0014895
135	0.0006124	0.0007511	0.0010504	0.0018336
150	0.0006894	0.0009531	0.0011261	0.0023263
165	0.0008124	0.0010675	0.0014463	0.0028201
180	0.0008124	0.0011632	0.0014463	0.0033654

Table B.31: R_f versus time data for Crude B

time (min)	R_f (m^{2}K/Wmin)			
	T_s = 220 ^{o}C	T_s = 240 ^{o}C	T_s = 260 ^{o}C	T_s = 280 ^{o}C
0	0.0000000	0.0000000	0.0000000	0.0000000
15	0.0005376	0.0005575	0.0001397	0.0002226
30	0.0002408	0.0007807	0.0007412	0.0005746
45	0.0006040	0.0006378	0.0007641	0.0012311
60	0.0008600	0.0008899	0.0016087	0.0011307
75	0.0010438	0.0013945	0.0018918	0.0016190
90	0.0011233	0.0016397	0.0020380	0.0015163
105	0.0015150	0.0018359	0.0024088	0.0019566
120	0.0016528	0.0022128	0.0024106	0.0021929
135	0.0018604	0.0022875	0.0026552	0.0024546
150	0.0021963	0.0026264	0.0030435	0.0027899
165	0.0019849	0.0027853	0.0033574	0.0026519
180	0.0022304	0.0030270	0.0033790	0.0029438

Table B.32: R_f versus time data for Crude C

time (min)	R_f (m^{2}K/Wmin)			
	T_s = 220 ^{o}C	T_s = 240 ^{o}C	T_s = 260 ^{o}C	T_s = 280 ^{o}C
0	0.0000000	0.0000000	0.0000000	0.0000000
15	-0.0000629	-0.0002654	-0.0001522	0.0004698
30	-0.0004608	-0.0000585	-0.0000931	0.0009262
45	-0.0003021	0.0004535	0.0000821	0.0010976
60	0.0002545	0.0006851	0.0003926	0.0009584
75	0.0005232	0.0007052	0.0010327	0.0009127
90	0.0008062	0.0008690	0.0015099	0.0009736
105	0.0010573	0.0008287	0.0015908	0.0007301
120	0.0012528	0.0007682	0.0017191	0.0010498
135	0.0010428	0.0008573	0.0016651	0.0008086
150	0.0010186	0.0009823	0.0015931	0.0008234
165	0.0011244	0.0009619	0.0017485	0.0012531
180	0.0013154	0.0009619	0.0016939	0.0012531

Table B.33: R_f versus time data for Crude D

time (min)	R_f (m^{2}K/Wmin)			
	T_s = 220 ^{o}C	T_s = 240 ^{o}C	T_s = 260 ^{o}C	T_s = 280 ^{o}C
0	0.0000000	0.0000000	0.0000000	0.0000000
15	0.0004318	-0.0003898	-0.0001018	-0.0001321
30	0.0007124	0.0002033	0.0003845	0.0000417
45	0.0010013	0.0004909	0.0007081	0.0002072
60	0.0011021	0.0004222	0.0011779	0.0015321
75	0.0012534	0.0009000	0.0021204	0.0016720
90	0.0012129	0.0007798	0.0019164	0.0016576
105	0.0010769	0.0009527	0.0021760	0.0020420
120	0.0010769	0.0013829	0.0023401	0.0021306
135	0.0015267	0.0025936	0.0022131	0.0023836
150	0.0017059	0.0028317	0.0023963	0.0023389
165	0.0016291	0.0033871	0.0024566	0.0023985
180	0.0010331	0.0032849	0.0027944	0.0025168

Table B.34: R_f versus time data for A-B blend

time (min)	R_f (m^{2}K/Wmin)		
	T_s = 240 °C	T_s = 260 °C	T_s = 280 °C
0	0.0000000	0.0000000	0.0000000
15	0.0000548	0.0002517	-0.0004028
30	0.0000731	0.0003009	-0.0003041
45	0.0004384	0.0003393	-0.0000013
60	0.0004385	0.0005088	0.0002339
75	0.0005308	0.0004749	0.0003353
90	0.0004758	0.0006686	0.0005820
105	0.0005661	0.0007199	0.0010062
120	0.0005849	0.0010566	0.0008435
135	0.0006983	0.0009303	0.0011438
150	0.0005141	0.0010615	0.0014198
165	0.0009162	0.0012479	0.0015303
180	0.0009162	0.0013802	0.0017927

Table B.35: R_f versus time data for A-C blend

time (min)	R_f (m^{2}K/Wmin)		
	T_s = 240 °C	T_s = 260 °C	T_s = 280 °C
0	0.0000000	0.0000000	0.0000000
15	0.0003527	-0.0004392	0.0004618
30	0.0003004	-0.0003521	0.0006703
45	0.0006451	-0.0000771	0.0008720
60	0.0006757	0.0003421	0.0009685
75	0.0010256	0.0005272	0.0011208
90	0.0013337	0.0005358	0.0010656
105	0.0011106	0.0007941	0.0013086
120	0.0011932	0.0010061	0.0014262
135	0.0013584	0.0013520	0.0013239
150	0.0012345	0.0016887	0.0014657
165	0.0013546	0.0021758	0.0016273
180	0.0012964	0.0028604	0.0018059

Table B.36: R_f versus time data for A-D blend

time (min)	R_f (m^{2}K/Wmin)		
	T_s = 240 ^{o}C	T_s = 260 ^{o}C	T_s = 280 ^{o}C
0	0.0000000	0.0000000	0.0000000
15	0.0000637	0.0001997	0.0003742
30	0.0001656	0.0004830	0.0003698
45	0.0003224	0.0003310	0.0005562
60	0.0005922	0.0004229	0.0004399
75	0.0008201	0.0005820	0.0007293
90	0.0009245	0.0005643	0.0007625
105	0.0009693	0.0004229	0.0010743
120	0.0008470	0.0005186	0.0009732
135	0.0009245	0.0006436	0.0008599
150	0.0009245	0.0006473	0.0014067
165	0.0009917	0.0005758	0.0016468
180	0.0015289	0.0007009	0.0014417

Table B.37: R_f versus time data for Condensate E – Crude C blend

time (min)	R_f (m^{2}K/Wmin)			
	T_s = 200 ^{o}C	T_s = 220 ^{o}C	T_s = 240 ^{o}C	T_s = 260 ^{o}C
0	0.0000000	0.0000000	0.0000000	0.0000000
15	-0.0001231	0.0000555	-0.0003694	-0.0001574
30	0.0005033	0.0006679	-0.0001915	-0.0000966
45	0.0005351	0.0008485	-0.0001388	0.0000867
60	0.0009796	0.0011730	-0.0000229	0.0004114
75	0.0008822	0.0010803	0.0009820	0.0014691
90	0.0009147	0.0012477	0.0013083	0.0017803
105	0.0010444	0.0014434	0.0014160	0.0018707
120	0.0009796	0.0014910	0.0015605	0.0017993
135	0.0009147	0.0016685	0.0013083	0.0017423
150	0.0009471	0.0016444	0.0012742	0.0016663
165	0.0009147	0.0019487	0.0013423	0.0018323
180	0.0009471	0.0018998	0.0013423	0.0017747

APPENDIX C

Table C.38: Boiling points for crudes and crude blends

Crude/Blend	Blend ratio (vol%)	Boiling point @ Operating pressure of 35 bar (^{o}C)
A	100	360
B	100	427.5
C	100	375
D	100	380
A-B	40-60	400
A-C	40-60	370
A-D	40-60	372.5

APPENDIX D

Table D.39: WAT for crudes and crude blends

Crude / Blend	Could Point / WAT (^{o}C)
Crude A (100 vol %)	21.24
Crude C (100 vol %)	17.26
Crude B (100 vol %)	11.27
Crude D (100 vol %)	13.76
A - C Blend (40 - 60 vol%)	18.96
A - B Blend (40 - 60 vol%)	15.38
A - D Blend (40 - 60 vol%)	16.93
C - E Blend (50 - 50 vol%)	1.93